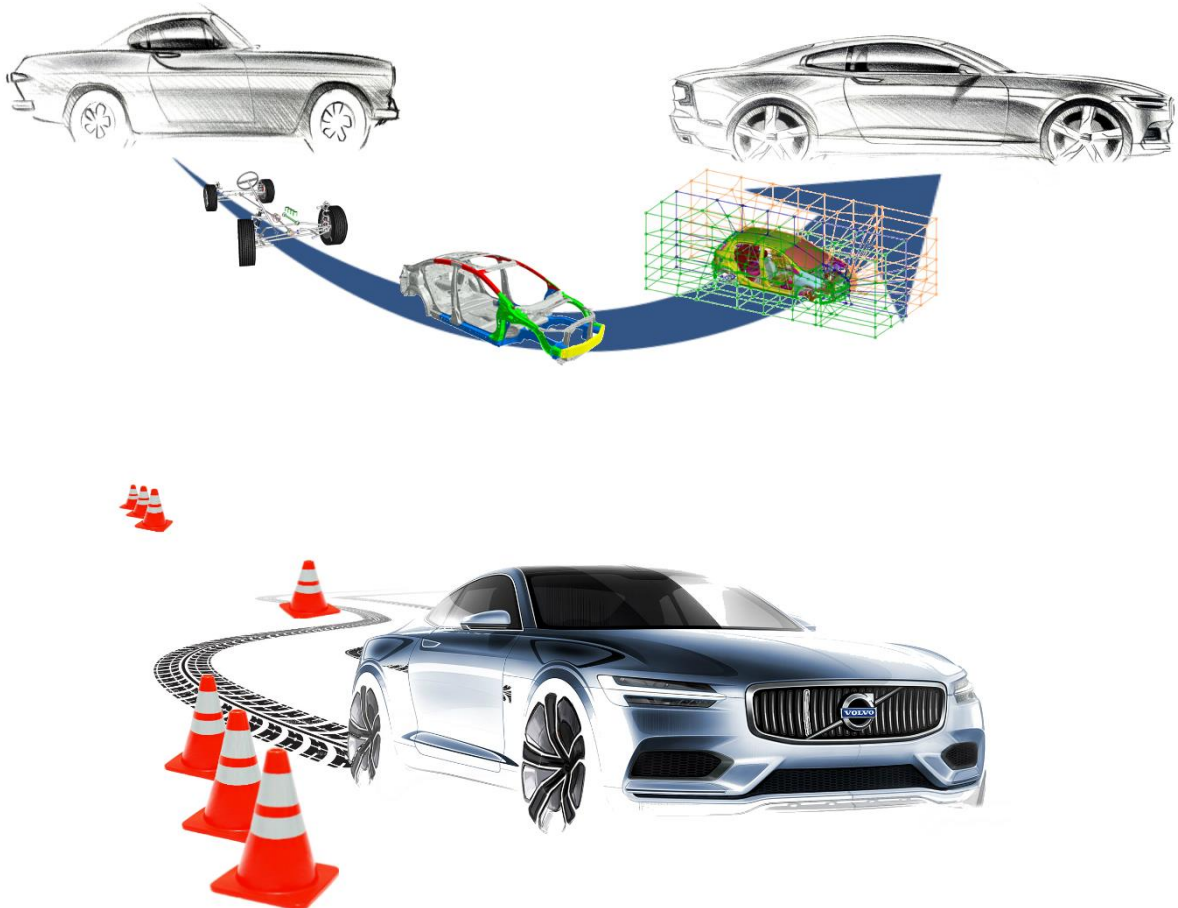




*Technical University of Crete  
School of Production Engineering & Management*

# **EMPLOYING OPTIMIZATION IN CAE VEHICLE DYNAMICS**



*Alexandros Leledakis  
December 2014*



# ACKNOWLEDGEMENTS

This thesis study was performed between March and October 2014 at Volvo Cars in Goteborg of Sweden, where I had the chance to work inside Volvo's Research and Development Centre (in the Active Safety CAE department).

I would like to thank my Volvo Cars supervisor **Diomidis Katzourakis**, CAE Active Safety Assignment Leader, for his constant guidance during this thesis. He always provided knowledge and ideas during all phases of the thesis; planning, modelling, setup of experiments, etc. .

It is with immense gratitude that I acknowledge the support and help of my academic supervisor **Nikolaos Tsourveloudis**, Professor and Dean of the school of Production engineering and management at Technical University of Crete, for his trust and guidance throughout my studies.

The MSc thesis of **Stavros Angelis and Matthias Tidlund** served as-foundation of the current thesis: I would also like to thank **Mathias Lidberg**, Associate Professor in Vehicle Dynamics, Chalmers University of Technology.

Field tests would have been impossible without the help of **Per Hesselund**, who installed the steering robot in the vehicle for our DLC verification testing session, conducted each test and guided me through the procedure of instrumenting a vehicle and performing a test.

I share the credit of my work with **Lukas Wikander** and **Josip Zekic**, who helped with the setup of the Vehicle for the steering torque interventions test as well as **Henrik Weiefors**, from Sentient, for his support regarding the Control EPAS functionality.

I would also like to thank **Georgios Minos**, manager of CAE Active Safety. Additionally I would like to express my gratitude to **Bo Svanberg** and **Mats Petersson**, from Volvo's Safety centre, for all the support and trust during the setup, testing and evaluation phase of the developed Driver Behaviour Model.

Finally, I am particularly grateful for the support of my family.

Chania

17 October 2014  
Leledakis Alexandros



# CONTENTS

<b>ACKNOWLEDGEMENTS</b> .....	<b>1</b>
<b>1 INTRODUCTION</b> .....	<b>6</b>
<b>2 LITERATURE STUDY</b> .....	<b>7</b>
<b>2.1 VEHICLE OVERVIEW</b> .....	<b>7</b>
<b>2.2 SUSPENSIONS</b> .....	<b>8</b>
<b>2.3 STEERING SYSTEM</b> .....	<b>10</b>
2.3.1 Caster angle.....	12
2.3.2 Steering ratio.....	13
2.3.3 Power Assisted Steering.....	13
<b>2.4 TIRE MODELS</b> .....	<b>14</b>
2.4.1 Slip Angle.....	14
2.4.2 Camber.....	14
2.4.3 Lateral force load dependency.....	16
2.4.1 Transient Tires.....	17
2.4.2 Pneumatic Trail.....	17
2.4.3 Linear Tire Model.....	18
2.4.4 Pacejka's Magic Formula.....	19
<b>2.5 VEHICLE DYNAMIC MODELS</b> .....	<b>23</b>
2.5.1 Point Mass Model.....	24
2.5.2 Single Track Model.....	24
2.5.3 Two Track Model.....	25
<b>2.6 SAFETY SYSTEMS</b> .....	<b>27</b>
2.6.1 Electronic Stability Control (ESC).....	27
2.6.2 Lane Keeping Aid (LKA).....	29
<b>2.7 DRIVER BEHAVIOUR MODELS</b> .....	<b>30</b>
<b>3 DOUBLE LANE CHANGE OPTIMIZATION</b> .....	<b>32</b>
<b>3.1 INTRODUCTION-PROBLEM DEFINITION</b> .....	<b>32</b>
<b>3.2 OPTIMAL STEERING INPUT GENERATION</b> .....	<b>33</b>
3.2.1 Optimization Method.....	33
3.2.2 Path constraints.....	34
3.2.3 Complexity built-up hierarchy.....	34
3.2.4 Parameterization.....	41
<b>3.3 DLC OPTIMIZATION RESULTS</b> .....	<b>43</b>
3.3.1 Sensitivity analysis.....	43
3.3.2 Four optimization cases.....	44
<b>3.4 DISCUSSION</b> .....	<b>47</b>
3.4.1 Real vehicle testing and validation.....	48
3.4.2 Future work.....	48
3.4.3 Rationale of this work and vision.....	48
<b>4 LANE KEEPING AID OPTIMIZATION</b> .....	<b>49</b>
<b>4.1 PROBLEM STATEMENT</b> .....	<b>49</b>
<b>4.2 METHODOLOGY</b> .....	<b>50</b>
4.2.1 Car setup.....	50
4.2.2 Preliminary Testing.....	52
4.2.3 Physical Testing.....	52
4.2.4 Test Data Post-processing.....	54
4.2.5 Driver Behaviour Model.....	58

<b>4.3 OPTIMIZATION RESULTS.....</b>	<b>60</b>
<b>4.4 DISCUSSION .....</b>	<b>62</b>
<b>5 REFERENCES.....</b>	<b>63</b>
<b>6 APPENDICES.....</b>	<b>1</b>
<b>6.1 ISO 3888 DESCRIPTION.....</b>	<b>1</b>
<b>6.2 TEST VEHICLE SPECIFICATIONS .....</b>	<b>2</b>
<b>6.3 DLC STEERING ROBOT TESTS.....</b>	<b>3</b>
<b>6.4 LANE KEEPING AID TESTS.....</b>	<b>15</b>

## LIST OF ABBREVIATIONS AND ACRONYMS

<i>Symbol</i>	<i>Description</i>	<i>Symbol</i>	<i>Description</i>
F	Force	m	Mass
T	Torque	CoG	Centre of gravity
M	Yaw torque	C/L	Centreline
I	Moment of inertia	$t_w$	track width
Y	Global lateral coordinate	b	Distance of rear axle from CoG
X	Global longitudinal coordinate	f	Distance of front axle from CoG
$\psi$	Yaw angle	$W_j$	Distance from CoG to side
$\varphi$	Roll angle	e	Roll centre height
$\theta$	Pitch angle	$h_e$	CoG height over roll axis
x	Local longitudinal coordinate	L	Wheelbase
Y	Local lateral coordinate	K	Roll stiffness
z	Local and global vertical coordinate	r	Wheel radius
v	Local velocity	$C_\alpha$	Cornering stiffness
$a_y$	Lateral acceleration	$\epsilon, \gamma$	Camber angle
$a_x$	Longitudinal acceleration	$C_\gamma$	Camber stiffness
$\omega$	Rotational speed	$\tau$	Relaxation time constant
B	Magic formula stiffness factor	$L_{relax}$	Relaxation length
C	Magic formula shape factor	R	Turn radius
D	Magic formula peak factor	$a_{tr}$	Smoothness for track boundaries.
E	Magic formula curvature factor	$a_g$	Smoothness for the guessed trajectory
$\mu$	Friction coefficient	$a_{DSTC}$	Smoothness for DSTC implementation
$\alpha$	Slip angle (For the tires)	$T_{if}$	Torque increase factor for DSTC implementation
$\kappa$	Longitudinal slip	$\rho$	Front-to-back brake proportioning
$s_x, s_y, s$	Tire slip in x, y axis, resultant tire slip	$\xi$	weighting factor for the slip angle contribution
$\beta$	Sideslip angle	$A_w$	Effective area of the disc brake
$K_{us}$	Understeer gradient	$P_{bij}$	Brake pressure
$A_{tr}, B_{tr}, C_{tr}$	Width of the track in specified sections	$\alpha_{const}$	ESC constant
J	Objective function	$\theta_{sw}$	Steering wheel angle
$W_{t_f}, W_\psi, W_\delta$	Weighting factor for the energy terms of the objective function	$\theta_{clmn}$	Steering column angle
t	Time	$e_{ss}$	steady state error
$\delta$	Steering angle	$T_d$	Torsion bar torque
n	Number of collocation points	$t_{stiff}$	Steering column torsional stiffness

<i>Index</i>	<i>Description</i>	<i>Index</i>	<i>Description</i>
i	Front and Rear	x	Longitudinal direction
j	Left and Right	y	Lateral direction
r	right	z	Vertical direction
l	left		
f	front	e	error
r	rear	d	desired
		ss	Steady state
init	Initial value	eff	effective
f	final		
g	Initial guess value	I	inertial
		d	damper
		s	spring

<i>Abbreviations</i>	<i>Description</i>
DLC	Double Lane Change
CAN	Controller Area Network
ESC	Electronic Stability Control
DSTC	Dynamic Stability Traction Control
RMS	Root Mean Square
EPAS	Electric Power Assisted Steering
HPAS	Hydraulic Power Assisted Steering
LKA	Lane Keeping Aid
LDW	Lane Departure Warning
CAE	Computer Aided Engineering
NMS	Neuromuscular
CNS	Central-nervous-System
VDM	Vehicle Dynamics Model
STM	Single Track Model
DOF	Degree of Freedom
GA	Genetic Algorithm
K&C	Kinematics and Compliance
FFT	Fast Fourier transform

# 1 INTRODUCTION

The use of Computer Aided Engineering (CAE) tools from the Conceptual Design stage can lead to reduced production time and cost, while it can also help attribute leaders to more efficiently achieve the desired vehicle specifications.

CAE tools can facilitate engineers to design, modify, calibrate and optimize their designs in an early development phase. Therefore, physical testing during the development process of a new vehicle can be reduced; methods can be developed, which can facilitate physical testing scenarios in virtual environments using simulation software.

Automotive industry is aiming towards vehicle verification using Simulation software rather than physical prototype testing. This thesis aims to develop CAE methods for Vehicle dynamics related to active safety features.

**Chapter 2** contains the outline of the literature study related to the problems described in the following paragraphs.

**Chapter 3** contains the first goal of this thesis; develop a method which evaluates the vehicle's dynamic properties for the ISO3888 part-2 double lane change test. An optimization method has been developed where the steering is controlled in order to achieve the highest possible entry speed to the test in an effort to isolate the vehicle's dynamic potential from the influence of a human driver when conducting this test. The vehicle modelling complexity is gradually increased by adding more detail and realism in the model. The results of the steering input optimization process were physically tested on a test track, where the correlation of the model to the real vehicle was evaluated. This tool can be used to tune vehicle properties or Electronic Stability Control (ESC) characteristics in order to achieve the highest entry speed possible in a Double Lane Change manoeuvre. The work presented on chapter 3 is carry-over work of [1]- which resulted to the conference paper: S. Angelis, M. Tidlund, A. Leledakis, M. Lidberg, M. Nybacka, D. Katzourakis, "Optimal Steering for Double-Lane Change Entry Speed Maximization," *in the proc. on the 12th International Symposium on Advanced Vehicle Control 2014*, AVEC14, Tokyo, Japan, 2014.

**Chapter 4** contains the second goal of this thesis; predicting driver reactions so as to tune and evaluate new Active safety systems (such as Lane Keeping Aid and Traffic Jam Assist). To do this, physical tests have been conducted with more than 50 drivers in total, where different steering wheel torque interventions have been tested in different conditions (Vehicle's speed, road lane width). A driver dynamical model has been developed and fitted on those test data, this model could help reduce complexity in the development of safety features, moving towards a virtual evaluation.

All the references used can be found in **Chapter 5**.

**Chapter 6 (Appendices)** contains the description of the ISO 3888 Double Lane Change and detailed figures from the physical testing conducted on the test track.

# 2 LITERATURE STUDY

To facilitate the target described in section 1, this thesis revolved around Vehicle dynamics, tire models, optimal control, optimization, steering systems, electronic stability control, lane-keeping aid (LKA) and driver behaviour models.

## 2.1 Vehicle Overview

Modern vehicles consists of several subsystems-components [2] :

1. Chassis
2. Powertrain (Engine, transmission, differential(s), axle(s))
3. Suspension
4. Steering
5. Brakes
6. Instrumentation
7. Motion Control
8. Comfort-Entertainment

All those subsystems have to be tuned in order to work in the most sufficient way. Nowadays, most of those components are controlled from Electronic Control Units (ECUs), and are connected with the CAN-bus (the car's communication network) [3]. Despite the sophistication of those ECUs, an important factor in the Vehicle control loop is the human driver, as it is illustrated in Figure 1, this in conjunction with the unpredictable –in many cases- nature of human drivers, makes optimization not only trickier but also indispensable.

The following sections describe this thesis related and aforementioned subsystems.

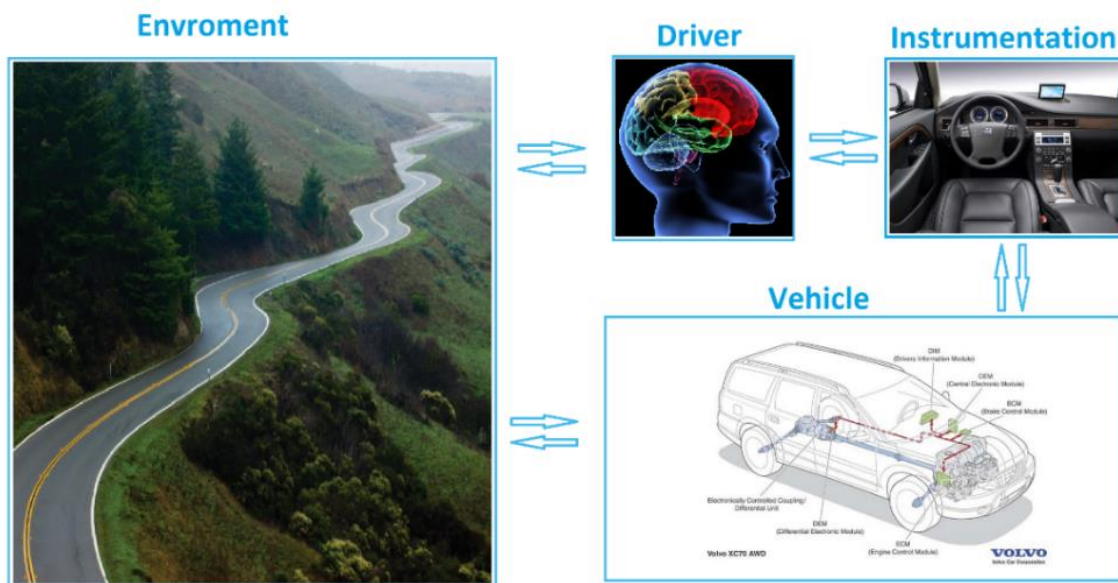


Figure 1 – Human interaction in the vehicle control loop.

# 2.2 Suspensions

Suspensions affect both the ride quality and the directional response of a vehicle. The main tasks of the suspensions are to [4] :

- Isolate the chassis from the roughness of the road surface and also keep the tires in contact with the road, (c.f. Figure 7)
- Maintain the “proper” steer (toe-in) and camber angles during all driving conditions
- Resist body-roll<sup>1</sup>, (c.f. Figure 5)

The main suspension design characteristics are:

- The springing medium (c.f. Figure 3), the material used to absorb the normal load disturbances.it can be: air, oil or coil springs
- The damper (c.f. Figure 3), which controls the oscillation (wheel’s travel speed). It usually consists of hydraulic valves and it aims to minimize the time that the suspension needs to settle in its normal state.
- Suspensions can be divided in 2 main groups according to their geometry (c.f. Figure 4, Figure 6). In the first group, called dependent, the wheels are usually connected with a beam or a live axle that holds the wheels parallel to each other. In the second group, called independent, wheels are allowed to move without affecting the opposite wheel. There is also a third group called semi-dependent where the wheels affect the movement of the opposite wheel but they are not “rigidly” attached to each other.

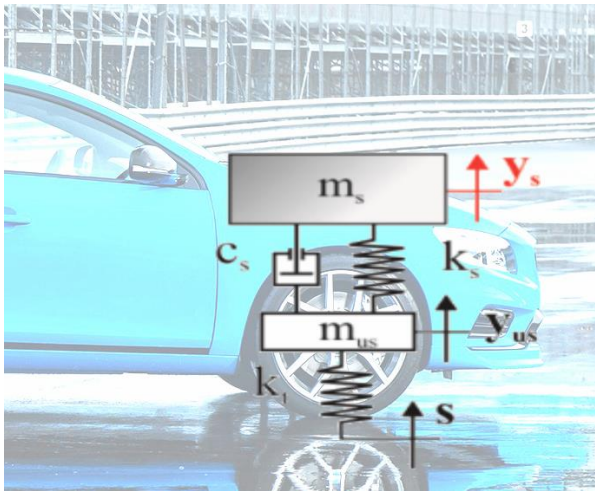


Figure 2 - Illustration of suspension system on a quarter car model [5].

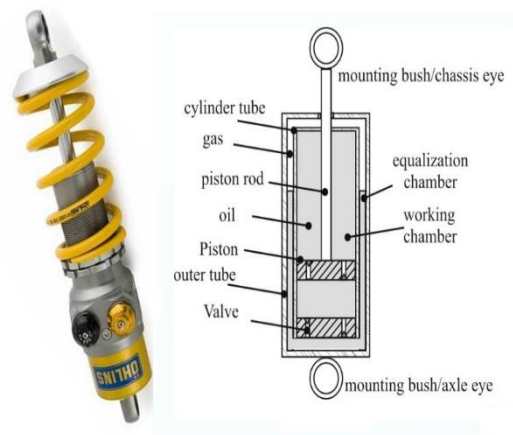


Figure 3 - Illustration of a coilover<sup>2</sup> suspension and damper’s structure [5].

The equations of motion of the quarter car model<sup>3</sup> (c.f. Figure 2) can be seen in (Eq. 1 - Eq. 2), [5], [6]:

$$m_s * \ddot{y}_s + c_s * \dot{y}_s - c_s * \dot{y}_{us} + k_s * y_s - k_s * y_{us} = 0 \tag{Eq. 1}$$

$$m_{us} * \ddot{y}_{us} - c_s * \dot{y}_s + c_s * \dot{y}_{us} - k_s * y_s + (k_s + k_t) * y_{us} = k_t * s \tag{Eq. 2}$$

where:

<sup>1</sup> Suspension movement occurs due to road surface unevenness, it is also introduced because of the vehicle’s acceleration; this effect is called load transfer.

<sup>2</sup> Coilover is short for “coil spring over shock». It consists of a shock absorber –damper- and a coil spring.

<sup>3</sup> Quarter car model is the most employed model, when suspension system is the main concern.

- $m_s$  is the sprung mass ,defined as the mass that is supported above the suspension
- $m_{us}$  is unsprung mass ,defined as the mass of the components suspended below the suspension (tire, rim, brakes, etc.),
- $c_s$  is the damping coefficient,
- $k_s$  is the spring rate<sup>4</sup>,
- $k_t$  is the tire stiffness,
- $y_s$  and  $y_{us}$  are the displacements of the sprung and unsprung mass respectively
- and  $s$  is the road input.

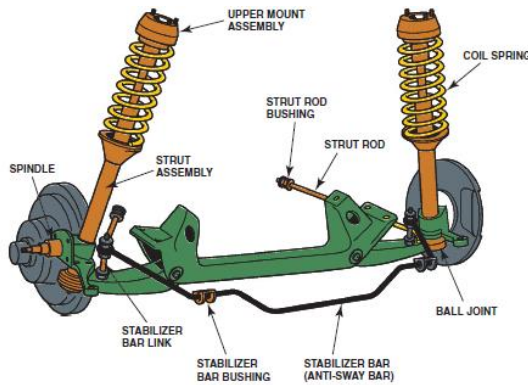


Figure 4 - MacPherson-strut, structure of the suspension is illustrated [7].

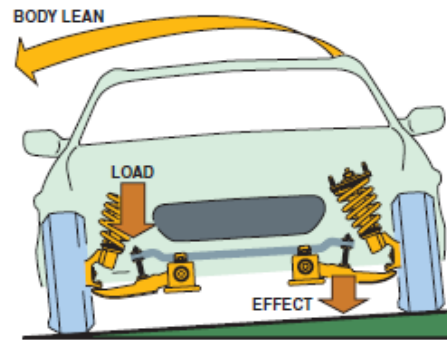


Figure 5 - As the body leans the stabilizer bar is twisted counteracting the body roll [7].

Modern front wheel drive cars (e.g. the Volvo S60) usually use MacPherson-strut suspensions for the front axle and Independent suspensions for the rear axle.

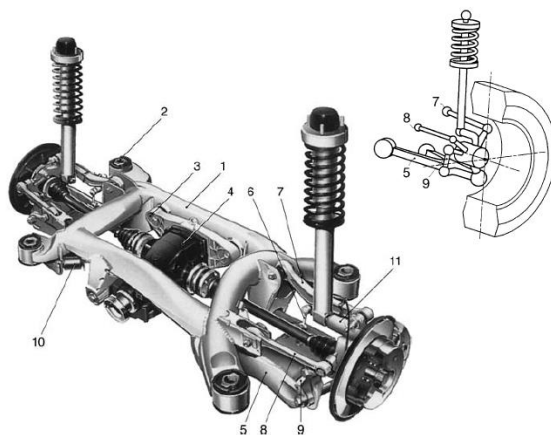


Figure 6 - Structure of a multilink independent rear suspensions is illustrated [8].

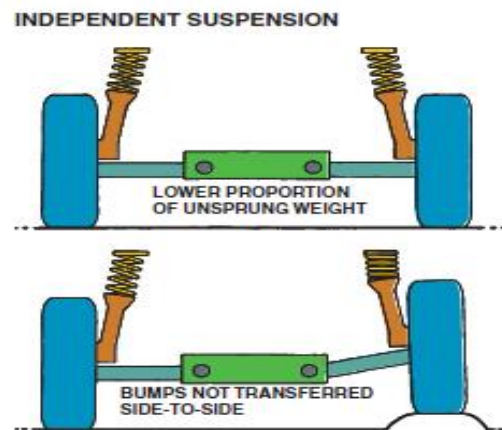


Figure 7 - Functionality of independent suspension illustration [7].

While a vehicle corners, the movement of suspension is focused on the intersection (instant centre) of the lines extended from the upper and lower suspension arms. The intersection between the line from where the wheel contacts the road to the instant centre and the vehicle body centreline is called “Roll centre” (c.f. Figure 8, Figure 9). Roll axis is the axis about which the body of a vehicle rolls. It is found by connecting the roll centre of the front and

<sup>4</sup> Spring rate is also called “suspension stiffness”.

rear suspensions of the vehicle [6]. The vertical distance between the CoG and the Roll axis determines the car's tendency to roll while cornering.

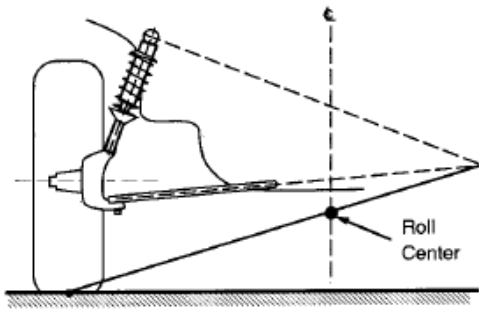


Figure 8 - MacPherson roll centre [4].

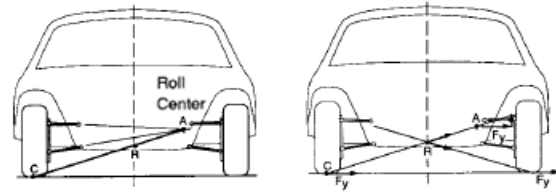


Figure 9 - Independent suspension roll centre [4].

Suspension geometry movement can be accurately analysed either with the use of special computer software, or with the use of a Kinematics and Compliance (K&C) rig [9].

## 2.3 Steering System

The main purpose of the steering system is to allow the driver to follow a desired path. The steering arrangement that has prevailed is to turn a hand-operated steering wheel positioned in front of the driver, which is connected with the front wheels via a steering column and several mechanical linkages (c.f. Figure 10, Figure 11); rods, arms, links, universal joints, vibration isolators, etc. [7]. The steering system could also transmit road feel to the driver as-well absorb<sup>5</sup> any excess vibrations caused from road surface.

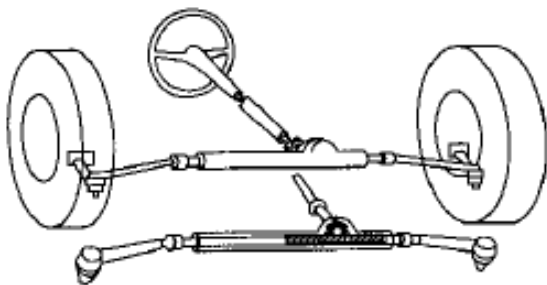


Figure 10 - Illustration of a commonly used Rack and pinion linkage [10].

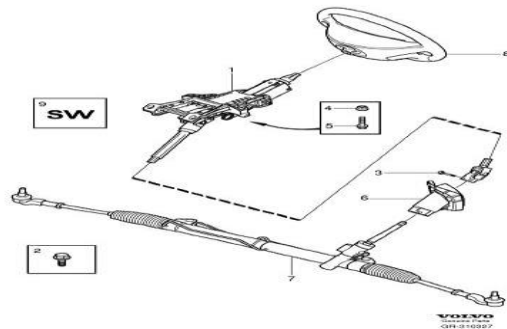


Figure 11 - Steering system of a Volvo S60.

The design of the steering system has an important influence both on the directional response of the vehicle [10] as well as on today's active safety systems; such as lane keeping aid.

In typical steering systems, the steering action is achieved by translational displacement of the relay linkage [10]. The arbitrary suspension motions that arise because of the steering actions are known as steering geometry errors. Steering geometry errors include:

<sup>5</sup> Absorbing vibrations caused by the road surface and transmitting road information to the driver are usually two conflicting targets.

- Toe change (c.f. Figure 12)
- Roll steer; also known as “bump steer”, which is the tendency of the wheel to steer when the suspension is moving (c.f. Figure 13).

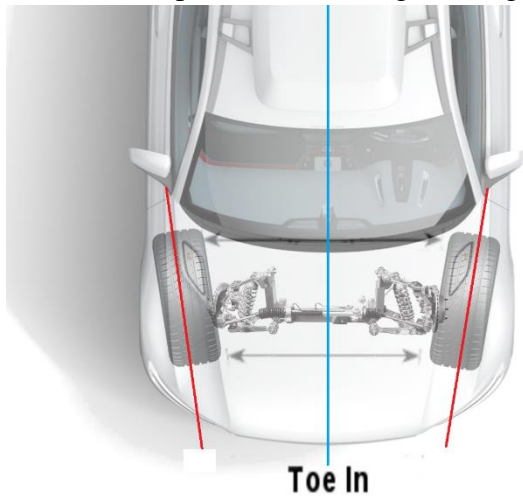


Figure 12 - Illustration of toe angle. When the front of the wheel points towards the centreline of the vehicle, toe angle is considered positive (called toe-in in that case).



Figure 13 – Illustration of Roll steer. Usually on modern vehicles, when the suspension is compressed the tire tends to steer towards the centreline of the vehicle.

The kinematic geometry of linkages is usually a trapezoid (c.f. Figure 15), which is a close approximate<sup>6</sup> of the Ackerman geometry (c.f. Figure 14) and requires that [10]:

$$\delta_o = \tan^{-1} \frac{L}{R+t/2} \approx \frac{L}{R+t/2} \quad \text{Eq. 3}$$

$$\delta_i = \tan^{-1} \frac{L}{R-t/2} \approx \frac{L}{R-t/2} \quad \text{Eq. 4}$$

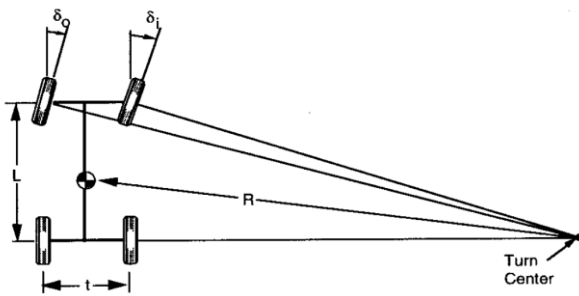


Figure 14 - Illustration of Ackerman turning geometry [10].

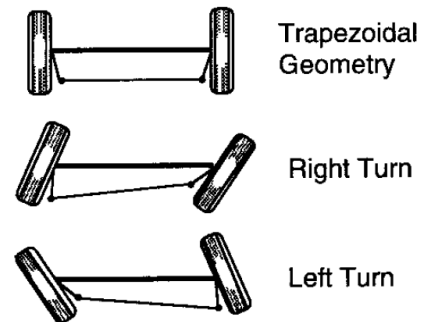


Figure 15 - Illustration of differential steer from a trapezoidal tie-rod arrangement [10].

All four wheels are in-practice steering (due to compliances; c.f. 2.4.2), knowing the precise turn centre can be difficult. The instantaneous turn centre (c.f. Figure 16) can be estimated when the whole vehicle is modelled. Most important factors that affect the instantaneous turn centre are: tires, suspension, chassis and of course the steering system.

<sup>6</sup> Perfect Ackerman geometry can be difficult to achieve, while satisfying all car designing constraints.

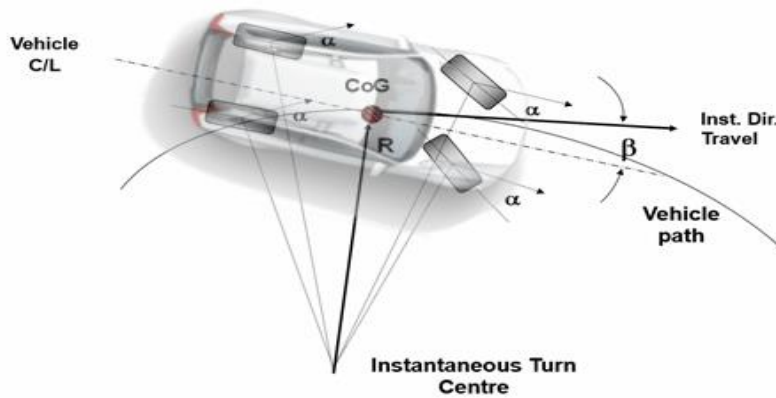


Figure 16 - Illustration of instantaneous turn centre.

## 2.3.1 Caster angle

The steering axis usually doesn't pass through the centre of the wheel. Caster is defined as the angle between the steering axis and the wheel centreline (c.f. Figure 17) extending perpendicular from the contact patch. Positive caster is defined as the steering axis tilting back from the wheel centreline in side view (perpendicular to the longitudinal-vertical axis).

The caster angle is considered to be one of the main parameters that affect the mechanical trail, defined as the distance between the intersection of the steering axis and the ground measured to the centre of the contact patch. Positive mechanical trail is defined as the steering axis intersecting the ground plane before the contact patch.

Mechanical trail in conjunction with pneumatic trail (2.4.2) produces a self-centring action<sup>7</sup> of steering, and gives a steering feedback for the driver [11].

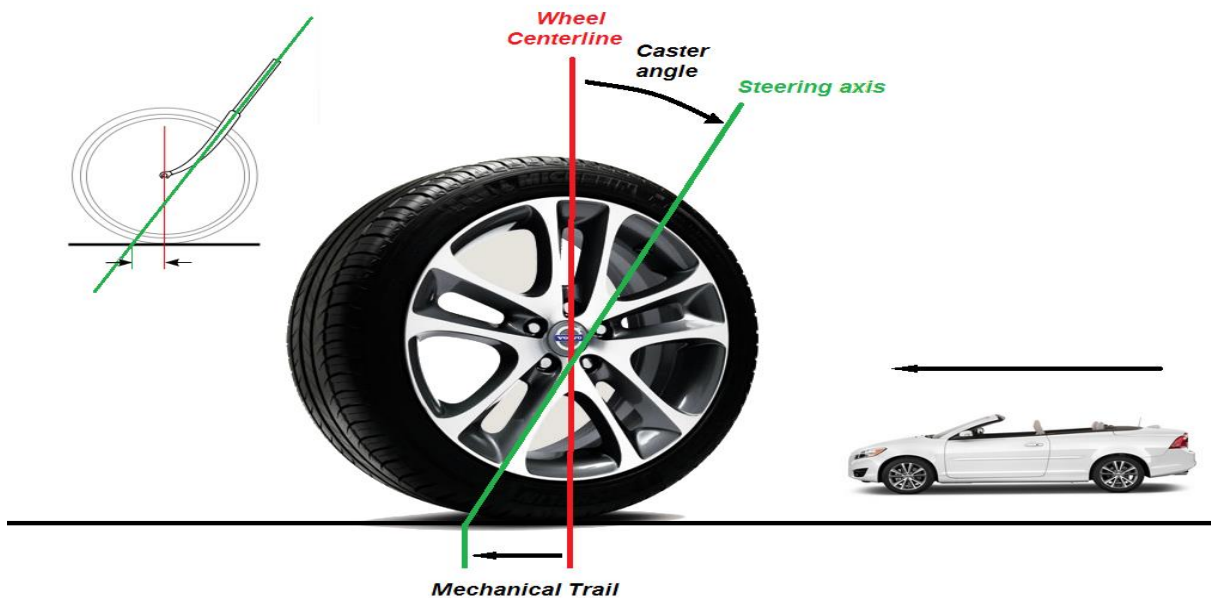


Figure 17 - Illustration of caster angle. Mechanical trail, defined as the perpendicular distance between the point of contact of the wheel and the ground, is also visible.

<sup>7</sup> *The mech. trail and pneumatic trail, multiplied with lateral force produce torque around the steering axis.*

## 2.3.2 Steering ratio

Steering ratio<sup>8</sup> is defined as the ratio of steering wheel rotation angle<sup>9</sup> to steer angle on road wheels. Increased steering ratio means that the steering wheel has to be turned more to achieve a certain amount of steer angle. In addition, increased steering ratio also means that the torque required to turn the steering wheel is decreased and therefore driver effort is also decreased. Variable steering ratio (c.f. Figure 18) can be made in order to improve steering operation characteristics [10].

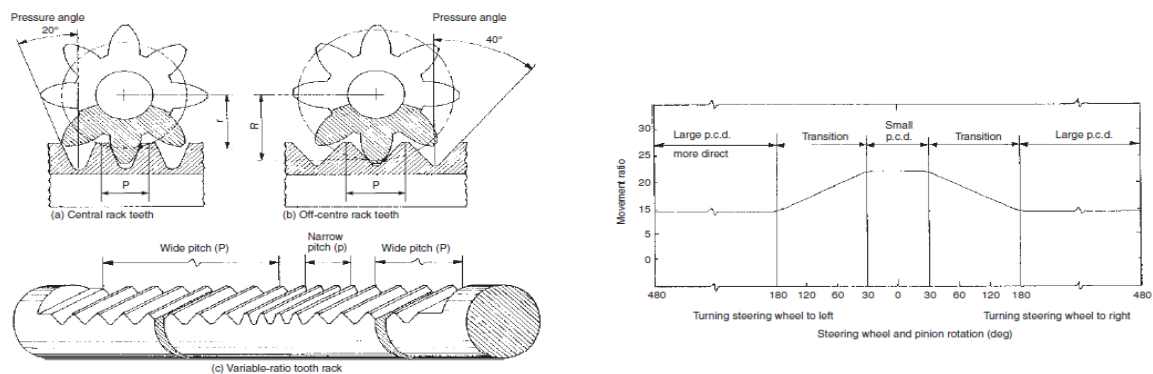


Figure 18 - Illustration of variable-ratio rack and pinion [12].

## 2.3.3 Power Assisted Steering

In an effort to reduce the driver's effort, power assisted steering<sup>10</sup> has been introduced in the early 1900; first on trucks and some year's later on cars.

The first power assisted steering systems were hydraulic power assisted steering (HYPAS), while Electric power assisted steering (EPAS) (c.f. Figure 19) is the system used by most modern vehicles. In EPAS, the power assist is generated from a DC electric motor, which also allows the integration of safety and driver support systems (e.g. Lane Keeping Aid and Park Assist Pilot) without the need of added hardware.

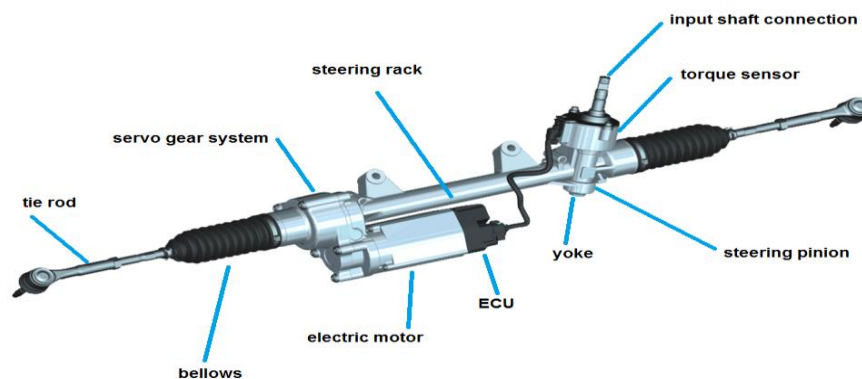


Figure 19 - Configuration of a ZF LS Servoelectric EPAS system with paraxial servo unit [13].

<sup>8</sup> Steering ratio for passenger vehicles usually is in the range [15, 20], [6].

<sup>9</sup> Actual steering wheel angle can vary significantly from the steering column angle on the steering rack because of compliances [6].

<sup>10</sup> Power assist is one of the most important factors that affects the vehicle's steering feel.

## 2.4 Tire Models

One of the most important factors of vehicle dynamics modelling is considered to be tire modelling (c.f. Figure 20). Fundamental principles of tire behaviour will be presented in this chapter.

### 2.4.1 Slip Angle

Slip angle is the angular difference between the direction of the wheel's plane and the direction the contact patch of the tyre is pointing. Slip angle (c.f. Figure 21) is the result of the sidewall's deformation under lateral load. This slip angle results in a force perpendicular to the wheel's direction of travel -the cornering force- which causes changes in the vehicle direction during the manoeuvre.

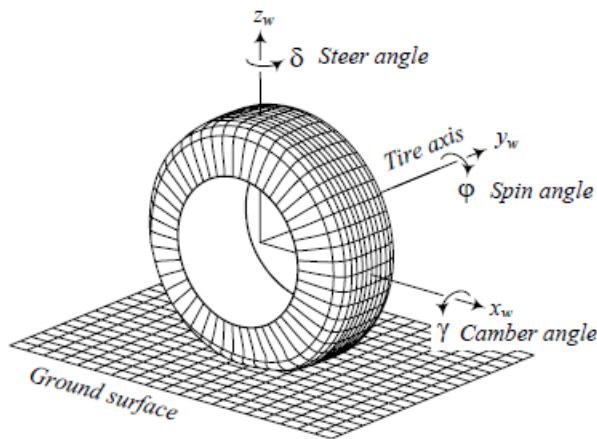


Figure 20 - Degrees of freedom of a wheel in respect to vehicle's body [6].

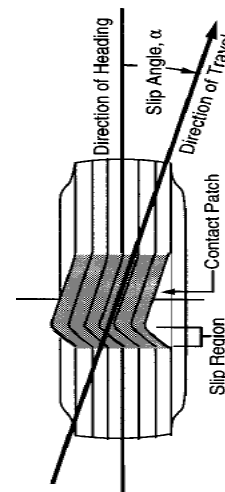


Figure 21 - Rolling tire deformation under lateral force [10].

A non-zero slip angle arises because of deformation in the tire. As the tire rotates, the friction between the contact patch and the road results in individual tread elements remaining stationary with respect to the road. This tire deflection gives rise to the slip angle and the cornering force [14].

### 2.4.2 Camber

Camber angle is the angle between the vertical axis of the wheel and the vertical plane or the vertical plane of the vehicle body. When the camber angle is measured in respect to the ground<sup>11</sup>, it is denoted as  $\gamma$  (c.f. Figure 23), it is considered positive when the wheel is tilted in the clockwise direction as seen from behind [15] [16] [10] [17] [14]. When it is measured in respect to the vehicle body, it is denoted as  $\varepsilon$  (c.f. Figure 22); if the top of the wheel is farther out than the bottom it is called positive camber<sup>12</sup>, else it is called negative camber.

<sup>11</sup> Camber angle measured in respect to the ground,  $\gamma$ , is also called inclination angle.

<sup>12</sup>It should be not noted that when both the left and right wheel have positive camber  $\varepsilon$  (in respect to vehicle body) they are tilted towards opposite directions

As a rule, the wheels on a vehicle have a pre-set camber angle in order to achieve the desired ride and handling characteristics (e.g. performance and safety) [14] [18]. This camber pre-set, which the wheels have when at rest, is called static camber [1].

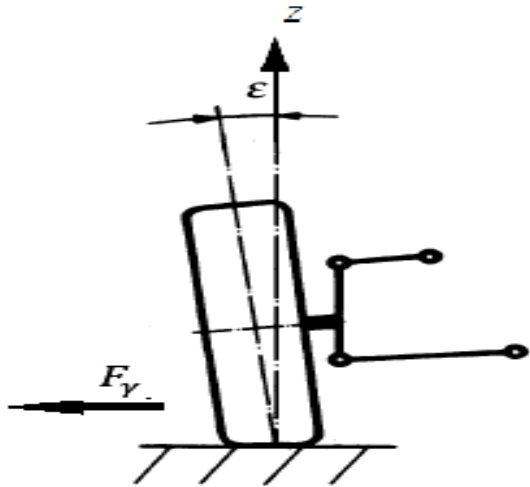


Figure 22 - Positive camber angle definitions with respect to the vehicle [6].

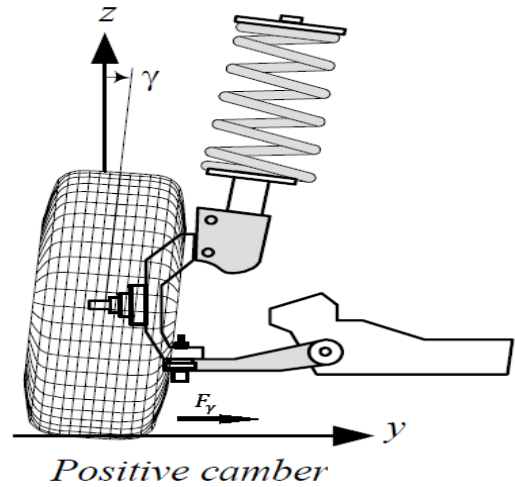


Figure 23 - Positive camber angle definitions with respect to the ground [10].

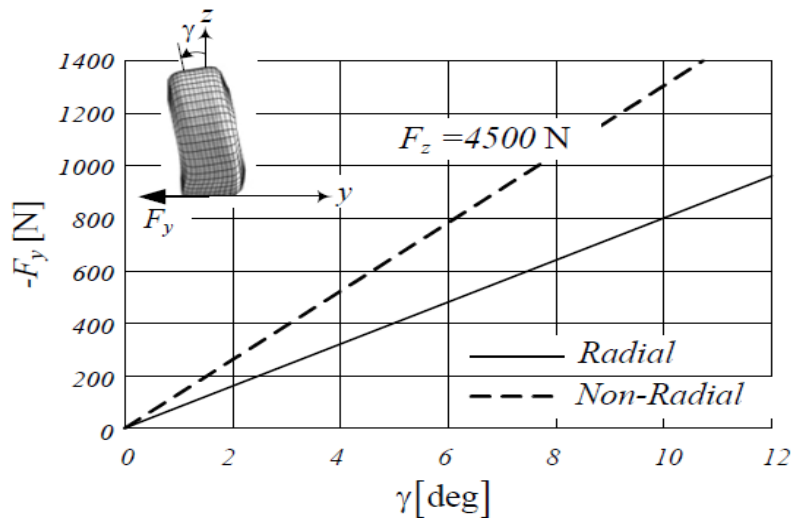


Figure 24 - Camber force as a function of camber angle for 2 different tire samples (Radial/Non-radial) and constant normal load [6].

The camber angle is affected by the suspension movements, which occurs when the vehicle is travelling (because of body roll, steer and road surface unevenness). This change to the camber angle depends on the suspension design and is called camber gain. The camber of the wheel generates a force towards the direction of the tilt when the wheel rolls, as shown also in Figure 24, termed as camber thrust [16]. The lateral force due to camber can be calculated as [17] [10]:

$$F_\gamma = -C_\gamma \gamma, \quad \text{Eq. 5}$$

where  $C_\gamma$  is called the camber stiffness and the minus sign is a convention such that  $C_\gamma$  is positive.

<sup>13</sup> For radial tires the camber stiffness is usually smaller because of the reduced lateral stiffness of the tire [10].

## 2.4.3 Lateral force load dependency

When the normal load of the wheel, denoted as  $F_z$ , the tire thread can stick to the road better [6]. As can be seen in Figure 25, for a constant slip angle ( $\alpha$ ) the lateral force increases when the normal load increase. It can also be noticed that the maximum lateral force is pushed to higher slip angles, when the normal load is increased.

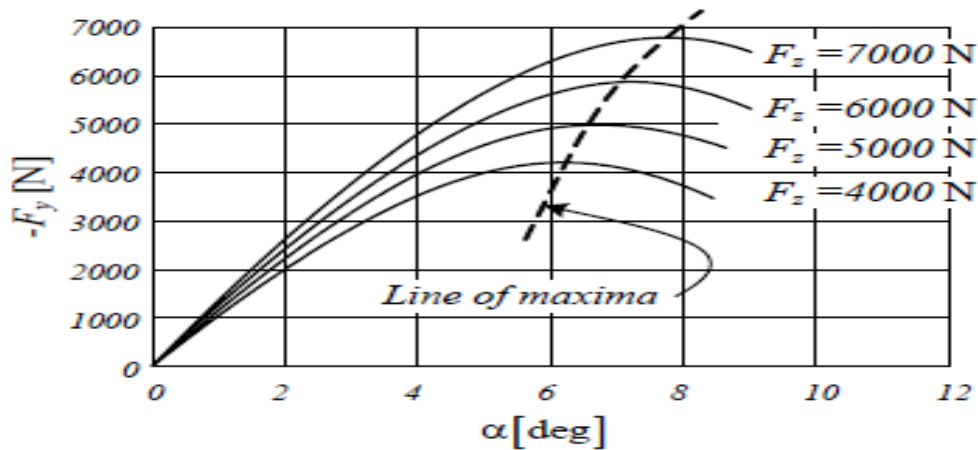


Figure 25 - Effect of normal load on lateral force as a function of slip angle [6].

By applying the equation of friction coefficient:

$$\mu = \frac{\text{Frictional force}}{\text{Normal Load}} = \frac{\sqrt{F_X^2 + F_Y^2}}{F_z} \text{ considering } F_X \approx 0 \rightarrow \frac{F_Y}{F_z}, \quad \text{Eq. 6}$$

the curve of lateral force vs slip angle can be normalized<sup>14</sup>.

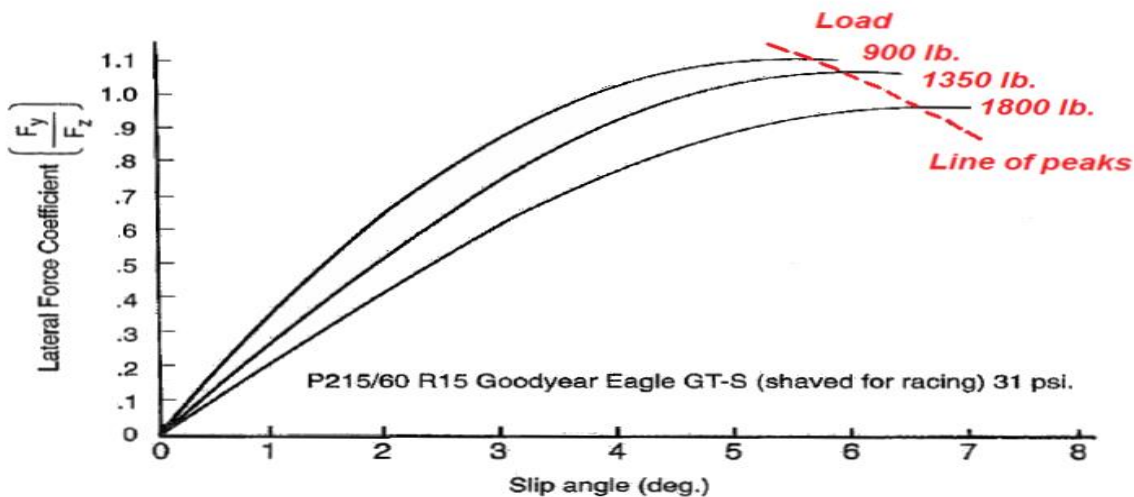


Figure 26 - Normalized lateral force as a function of slip angle [16].

From Figure 26, it can be noticed that the lateral force coefficient is usually higher for lighter loads. This effect is called load sensitivity, the variation of the lateral force coefficient with normal load is important in vehicle dynamics and racing [19].

<sup>14</sup> In this case the term  $\frac{F_Y}{F_z}$  is also called Lateral force coefficient [10].

## 2.4.1 Transient Tires

When a car is steering, the tires deform laterally (c.f. Figure 27) which causes a slip angle. The lateral force that will be generated because of the slip angle however will not appear instantly (c.f. Figure 28). The length that the tire will have to travel during this delay period (between time that the slip angle is introduced and when cornering force reaches its steady state value) is called Relaxation length ( $L_{relax}$ ) [20] [15] [10]. Relaxation length is a property of the pneumatic tire, which according to Pacejka is "approximately equal to half the contact length of the tyre". The relaxation length is related with the slip angle. More specifically, the higher the slip angle, the shorter<sup>15</sup> the relaxation length becomes [14].

A way to define this transient behaviour is through the first order differential equation

$$\tau \dot{f}_y(a, t) + f_y(a, t) = f_{yss}(a), \quad \text{Eq. 7}$$

where  $\tau$  is a time constant and  $f_{yss}$  is the steady state value of the lateral force for a given slip angle ( $a$ ). The time constant is related to the relaxation length as:

$$\tau = \frac{L_{relax}}{V_x} \quad \text{Eq. 8}$$

where  $V_x$  is the tire's longitudinal velocity.

In Eq. 8 the relaxation length is taken as a constant value in order to simplify the equation.

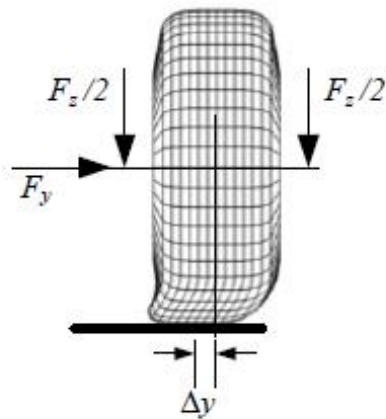


Figure 27 - Front view of a laterally deflected tire [6].

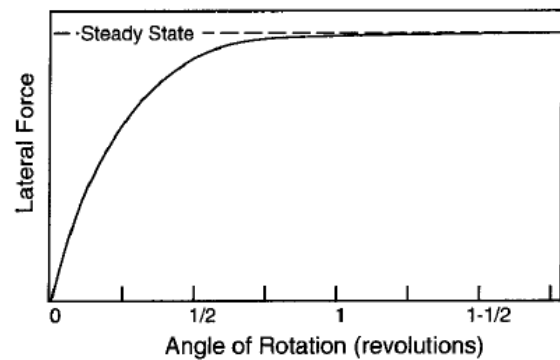


Figure 28 - Lateral force with respect to revolution of the tire [10].

## 2.4.2 Pneumatic Trail

The lateral force produced when the tire has developed a slip angle (2.4.1), can be considered as the sum of every tiny element's (c.f. Figure 29) area multiplied with the stress in that area :

$$F_y = \int \tau(x, a) dA \quad \text{Eq. 9}$$

<sup>15</sup> The delay time is also reduced

The asymmetric stress along the length of the contact patch, causes the resultant lateral force ( $F_y$ ) to be a force applied to some distance ( $a_{x\alpha}$ ) behind the centre of the contact patch<sup>16</sup> and makes a moment ( $M_z$ ), called aligning moment [6]. Aligning moment always tend to reduce the slip angle.

$$M_z = F_y * a_{x\alpha} \quad \text{Eq. 10}$$

The pneumatic trail for low slip angles in the linear tire region is almost constant<sup>17</sup>. For higher slip angles, the tire deformation becomes more symmetric, and thus the pneumatic trail becomes smaller reducing to almost zero, and in some cases it might even change sign [15] [16] [21] [14]. Pneumatic trail also increases with normal load (c.f. Figure 30).

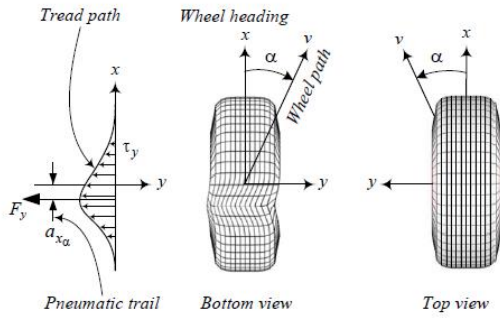


Figure 29 - Stress distribution  $\tau_y$ , resultant lateral force  $F_y$  and pneumatic trail  $a_{x\alpha}$  during cornering [6].

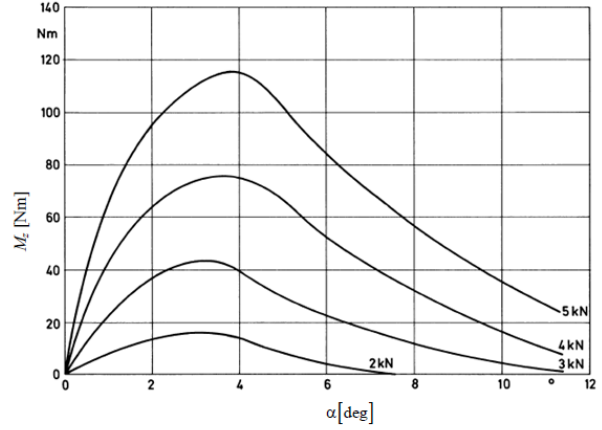


Figure 30 - Aligning moment as a function of slip angle for different normal loads [8].

## 2.4.3 Linear Tire Model

For small slip angles the lateral force increases approximately linearly for the first few degrees of slip, called the elastic region (c.f. Figure 31), and then increases non-linearly to a maximum before beginning to decrease. This linear relationship can be formulated as:

$$F_y = -C_a a, \quad \text{Eq. 11}$$

where  $C_a$  is called the cornering stiffness of the tire, defined as [15]:

$$C_a = -\left(\frac{\partial F_y}{\partial a}\right)_{a=0}. \quad \text{Eq. 12}$$

and  $\alpha$  (slip angle) can be calculated as [20]:

$$\alpha_f = \tan^{-1} \frac{v_y + f\dot{\psi}}{v_x} - \delta \approx \frac{v_y + f\dot{\psi}}{v_x} - \delta \quad \text{Eq. 13}$$

$$\alpha_r = \tan^{-1} \frac{v_y - b\dot{\psi}}{v_x} \approx \frac{v_y - b\dot{\psi}}{v_x}, \quad \text{Eq. 14}$$

with  $\delta$  being the steering wheel angle for this specific wheel.

<sup>16</sup> This phenomenon, of a force applied at a certain distance, gives rise to a moment. This moment tends to steer the wheel back to its straight position, and is therefore called aligning moment. The aligning moment is an important concept of the steering design [9] [10] [10].

<sup>17</sup> In this model, a typical value for the pneumatic trail at low lateral accelerations was used, equal to approximately 30mm [16].

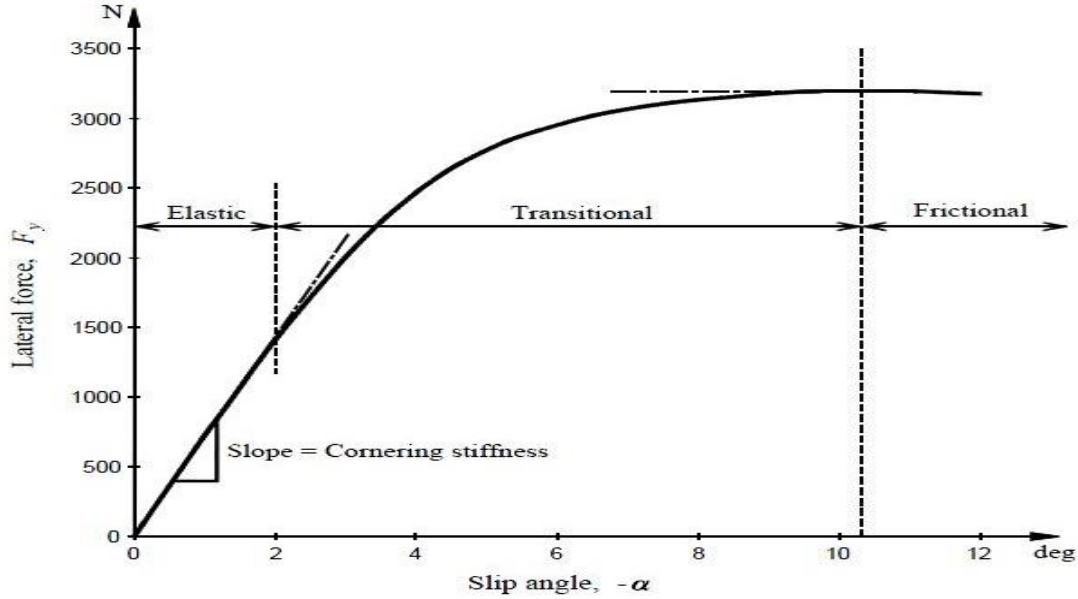


Figure 31 – Illustration of a typical Pneumatic tire behaviour. For small slip angles (while the tire is in the elastic region), the lateral force can be considered as linearly proportional to the slip angle [15]. The numbers and regions noted above depend on factors like tire size, tire pressure and normal load.

## 2.4.4 Pacejka's Magic Formula

Magic Formula, developed by Egbert Bakker, Lars Lidner and Hans B. Pacejka [22] has been widely used in industry and academic environments to calculate tire force and moment characteristics. The Magic Formula is a semi-empirical<sup>18</sup> tire model, which utilizes a combination of trigonometric functions to fit the tire model to experimental data.

The Magic Formula model can give satisfactory results even for large slip angles, where the tire is not considered to be in its linear region<sup>19</sup>.

Since its first appearance in 1987, various modifications have been made to improve the accuracy and to extend the capabilities of the model, and include factors like the camber angle, the tire inflation pressure, the rolling resistance and the overturning moment, and depending on the vehicle type or the phenomena that one wishes to study, each version may better apply to some certain situations [20] [21].

The most used version of the formula is:

$$\begin{aligned}
 f(u) &= D \sin \left( C \tan^{-1} \left( B u - E (B u - \tan^{-1}(B u)) \right) \right), \\
 F(U) &= f(u) + S_v, \\
 u &= U + S_h,
 \end{aligned}
 \tag{Eq. 15}$$

where  $F(U)$  represents the output, that is the lateral or longitudinal force, or the self-aligning torque and  $U$  denotes the input, that is usually the slip angle ( $\alpha$ ) or the longitudinal slip ( $\kappa$ ), calculated as [26] :

$$\kappa = \frac{V_{wheel} - V_{vehicle}}{V_{vehicle}}
 \tag{Eq. 16}$$

<sup>18</sup> The formulas aren't derived from a physical background that models the tire's structure and properties, they are mathematical approximations of curves that were obtained from measurements.

<sup>19</sup> The linear region is usually considered for up to 0.4g [10] [21].

An early version of Eq. 15, gives a relation between the friction coefficient( $\mu$ ) and the resultant tire slip ( $s$ ) at a given tire. The expression holds as follows:

$$\mu(s) = D \sin(C \tan^{-1}(Bs)), \quad \text{Eq. 17}$$

where  $D$ ,  $C$  and  $B$  are the peak value factor, shape factor and stiffness factor respectively.

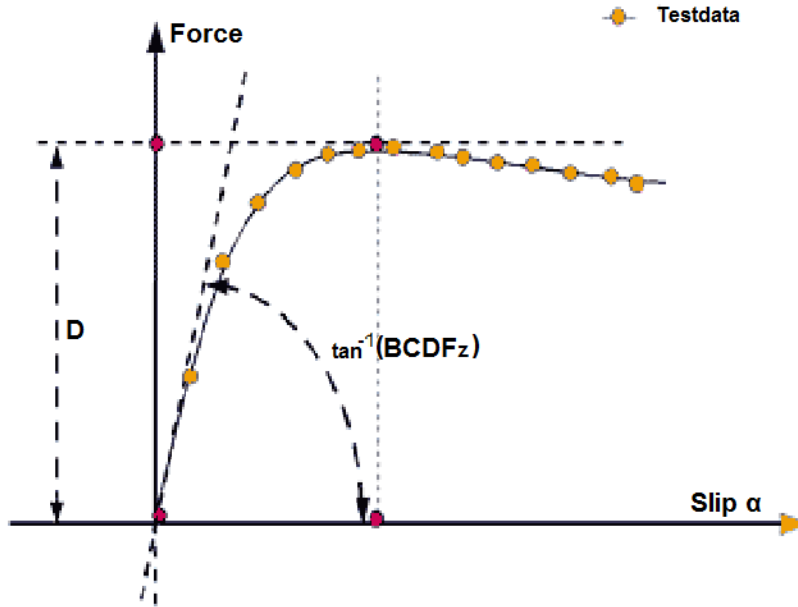


Figure 32 – Illustration of the magic formula tire .The example curve shown has been fitted on test data [23].

The product  $B \cdot C \cdot D \cdot F_z$  (c.f. Figure 32), where  $F_z$  is the normal load on the tire, represents the cornering stiffness ( $C_{ij}$ ), of the tire with index  $i, j$  [24] [25].

The resultant slip ( $s$ ) is given by:

$$s = \sqrt{s_x^2 + s_y^2}, \quad \text{Eq. 18}$$

where the indices  $x$  and  $y$  denote the longitudinal and lateral slip respectively [24] [20] [15].

From the friction coefficient ( $\mu$ ), assuming linear dependence of the tire friction forces on the tire vertical force, the resultant friction force on the plane of the road surface can be calculated as:

$$f = \sqrt{f_x^2 + f_y^2} = \mu f_z, \quad \text{Eq. 19}$$

where the friction coefficient is related to its longitudinal and lateral component according to:

$$\mu = \sqrt{\mu_x^2 + \mu_y^2} \quad \text{Eq. 20}$$

and the lateral and longitudinal forces are then obtained from Eq. 21 [24] [20] [15] :

$$\begin{aligned} f_x &= \mu_x f_z = -\frac{s_x}{s} \mu f_z = -\frac{s_x}{s} f \\ f_y &= \mu_y f_z = -\frac{s_y}{s} \mu f_z = -\frac{s_y}{s} f \end{aligned} \quad \text{Eq. 21}$$

Assuming the above behaviour, the tire's force potentials move inside a so called “friction circle”, or in general a “friction ellipse” (c.f. Figure 33), as indicated by Eq. 20.

The total horizontal fractional force cannot exceed the maximum value, which is dictated by the current friction coefficient and normal load.

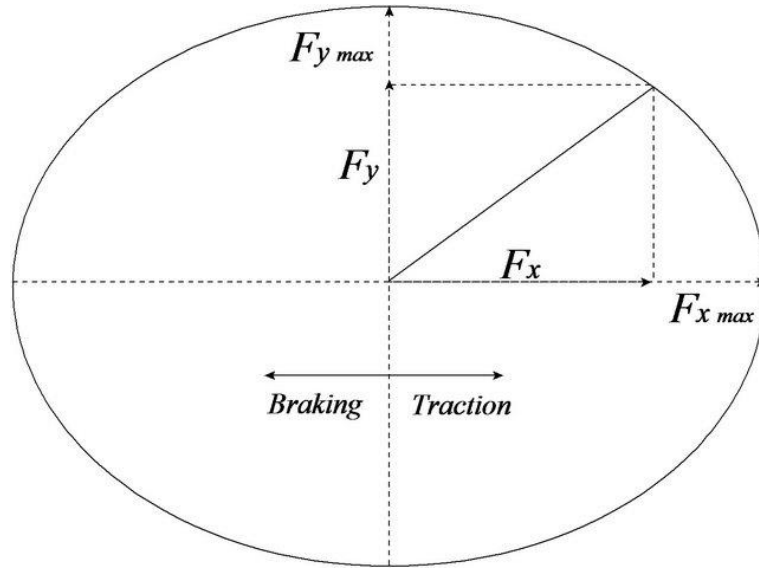


Figure 33 - Illustration of the friction ellipse, the total force can never exceed a certain limit [26].

### 2.4.4.1 Tire Parameters Estimation

The procedure of performing a parameter estimation of the tire properties can be performed in three steps, which are described in this chapter and are all based on the paper “An enhanced generic single track vehicle model and its parameter identification for 15 different passenger cars” [27].

#### 2.4.4.1.1 Circular driving test – Effective cornering stiffness estimation

Using the single track model to simplify the calculations, the vehicle’s effective cornering stiffness<sup>20</sup> for the front and rear axle, can be estimated from the results of circular driving tests. The necessary data for calculating the effective cornering stiffness are the vehicle’s lateral acceleration, forward velocity, lateral velocity, yaw rate and steering wheel angle

Initially the slip angles of the front and rear wheel are calculated using equation (Eq. 13) and (Eq. 14). The semi steady-state test assumes  $\ddot{\psi} = 0$ , since the turning radius is approximately the same. Then, from Eq.34 and Eq.35, the lateral forces on the front and rear axle are calculated as:

$$F_f = \frac{b}{L} m \alpha_y \quad \text{Eq. 22}$$

$$F_r = \frac{f}{L} m \alpha_y \quad \text{Eq. 23}$$

Next, the lateral forces at the front and rear are plotted against the respective slip angles, resulting in a graph similar to Figure 31. The gradient of the curve for zero slip angle is the axle’s effective cornering stiffness [15] [16], which is defined as:

$$C_a = \left( \frac{\partial F_y}{\partial \alpha} \right)_{\alpha=0}, \quad \text{Eq. 24}$$

as also mentioned in Eq. 12.

<sup>20</sup> “Effective” cornering stiffness describes the contribution of additional phenomena to the axle’s cornering stiffness. An axle’s cornering stiffness does not depend only on the tires but also on phenomena like camber forces, tire load sensitivity, steering elasticity and compliance steer, all of which contribute to the reduction of the cornering stiffness imposed by the tires alone [6] [11].

### 2.4.4.1.2 Pseudorandom steering test – Yaw inertia calculation

The yaw inertia of the vehicle can be calculated using the results of a pseudorandom steering test. Using this test the transfer functions from the measured steering angle to measured lateral acceleration and yaw rate can be obtained by calculating the fraction of the fast Fourier transform (FFT) of the output signal (lateral acceleration or yaw rate) over the FFT of the input signal (steering angle). From the bicycle model the expressions in Eq. 25 and Eq. 26, for analytically calculating these transfer functions, are obtained [17]:

$$\frac{\dot{\psi}}{\Delta} = \frac{fC_fms + \frac{L}{v_x}C_fC_r}{mI_zs^2 + \frac{(f^2C_f + b^2C_r)m + I_z(C_f + C_r)}{v_x}s + \frac{L^2C_fC_r}{v_x^2} + m(bC_r - fC_f)} \quad \text{Eq. 25}$$

$$\frac{A_y}{\Delta} = \frac{v_x^2}{L + K_{us}v_x^2} \left( \frac{1 + \frac{b}{v_x}s + \frac{I_z}{LC_r}s^2}{1 + v_x \frac{(f^2C_f + b^2C_r)m + I_z(C_f + C_r)}{LC_fC_r(K_{us}v_x^2 + L)}s + \frac{mI_zv_x^2}{LC_fC_r(K_{us}v_x^2 + L)}s^2} \right) \quad \text{Eq. 26}$$

with the understeer gradient:

$$K_{us} = \frac{m(bC_r - fC_f)}{LC_fC_r} \quad \text{Eq. 27}$$

The yaw inertia,  $I_z$ , value is then calculated by an optimization, where the error between the transfer functions calculated from the measurements and the transfer functions calculated analytically from the bicycle model is minimized by varying the  $I_z$  value accordingly.

### 2.4.4.1.3 Magic formula coefficients

Next, the D value of the magic formula model for the tires can be calculated from a severe lane change manoeuvre test, like the double lane change. A number of lane change manoeuvres are conducted and recorded. For the coefficients calculation, the manoeuvre with the highest achieved lateral acceleration is selected. From that manoeuvre, the peak lateral force of the tires is obtained and therefore the D value of the magic formula is found (since D defines the peak value of the magic formula curve).

The C value can be assumed to be 1<sup>21</sup>, which means that the curve of the magic formula does not fall for large slip angles (i.e. the peak value force is not decreasing for large slip angles), which then leads to the calculation of the B value as:

$$B = \frac{C_{Fa}}{CD}, \quad \text{Eq. 28}$$

where  $C_{Fa}$  is the tire cornering stiffness.

<sup>21</sup> The  $C = 1$  assumption facilitates an approximation of the magic formula curve for the tire. In general, C can be determined by the use of regression procedures [72].

## 2.5 Vehicle Dynamic Models

With the purpose of describing the motion of a vehicle in space, many different Vehicle dynamics models can be used. This chapter will focus on VDMs that have been used for this thesis. The coordinate system used in all cases is the German DIN system (c.f. Figure 34) (also known as ISO 8855) [28].

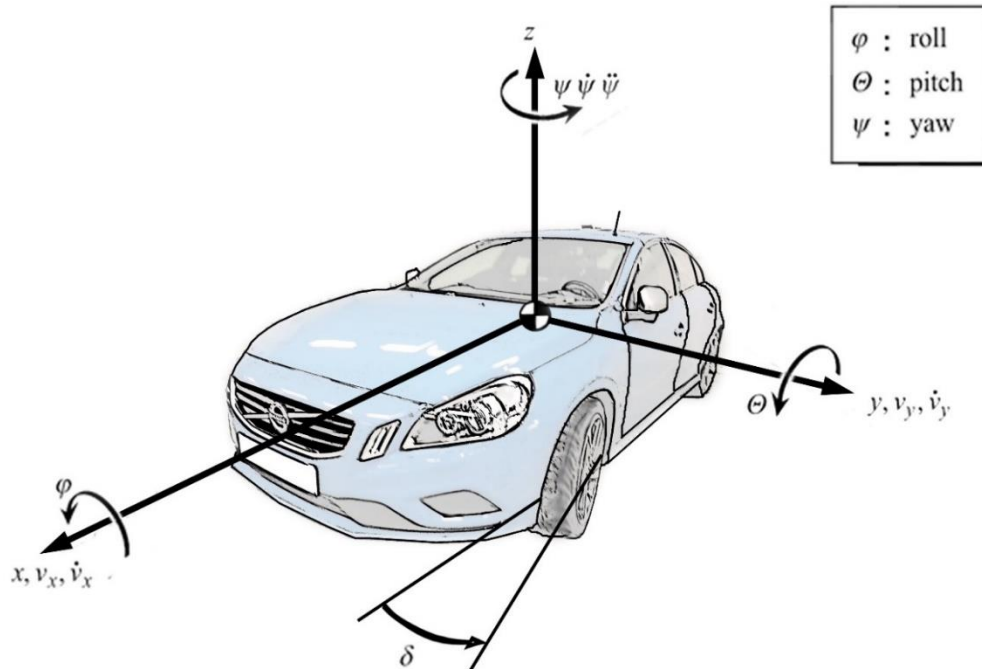


Figure 34 - DIN coordinate system illustration [1].

The forward movement of the vehicle is described by the x-axis, the lateral movement is described by the y-axis and the vertical movement is described in the z-axis. The steering angle, denoted as  $\delta$ , is positive when turning towards the left.

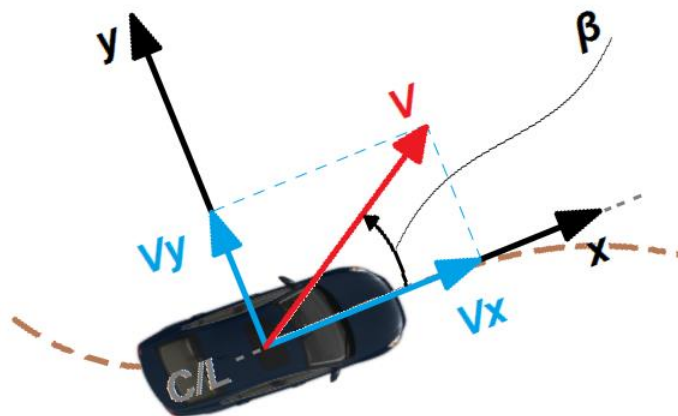


Figure 35 - Vehicle sideslip angle illustration.

Vehicle's slip angle (c.f. Figure 35) (sideslip angle), is the angle between the longitudinal axis (C/L) of the vehicle and the velocity vector acting on its centre of gravity, or:

$$\beta = \tan^{-1}(v_y/v_x), \quad \text{Eq. 29}$$

where  $v_y$  and  $v_x$  are the vehicle's lateral and longitudinal velocity respectively [20] [29].

## 2.5.1 Point Mass Model

The Point mass model is the simplest VDM that can be used. It considers the car as a point mass, located in the centre of gravity of the car. This VDM is an approximation of what an ordinary driver unknowingly assumes, when he tries to follow a path with his vehicle [20]. Lateral and longitudinal forces define the trajectory of the vehicle, assuming that the heading angle of the car is always tangent to the trajectory it follows. In order to be usable as a VDM, forces should be constrained since it has no physical “grip limits”.

The equations of motion for the point-mass model, with respect to the vehicle coordinate system are:

$$m * a_y = F_y \quad \text{Eq. 30}$$

$$m * a_x = F_x \quad \text{Eq. 31}$$

$$\psi = \text{atan}\left(\frac{dY}{dX}\right) \quad \text{Eq. 32}$$

## 2.5.2 Single Track Model

Single Track Model (STM) (c.f. Figure 36) also known as “bicycle model” is the simplest model that captures the basic dynamic behaviour (lateral and the yaw motion) of a vehicle [30]. Its simplest form is a two-degree of freedom model while the most widely used is the three-degree of freedom bicycle model, which includes the longitudinal motion in order describe the vehicle’s motion in the X-Y plane.

Using the presumption that the two wheels are symmetrical, this model can reduce both axles (front and rear) into a single wheel. Also, the vehicle’s centre of gravity (CoG) is considered to be on the road level, which means that load transfer effects (pitch or roll movement are ignored) are neglected. The bicycle model is considered to give satisfactory results for lateral accelerations less than 4[m/s<sup>2</sup>], where the tires are considered to be in the linear region.

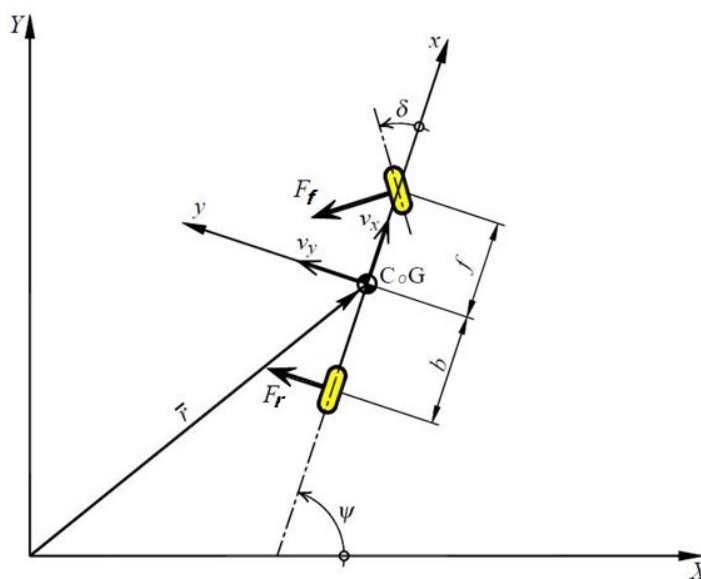


Figure 36 - 3 DOF (longitudinal, lateral and yaw motion) bicycle model. [17]

The equations of motion for the bicycle model, with respect to the vehicle coordinate system, can be derived using small angle approximation as [20]:

$$m(\dot{v}_x - \dot{\psi}v_y) = -F_f \sin(\delta) \approx -F_f \delta, \quad \text{Eq. 33}$$

$$m(\dot{v}_y + \dot{\psi}v_x) = F_r + F_f \cos(\delta) \approx F_r + F_f \quad \text{Eq. 34}$$

$$I_z \ddot{\psi} = fF_f \cos(\delta) - bF_r \approx fF_f \delta - bF_r \quad \text{Eq. 35}$$

$$\dot{X} = v_x \cos(\psi) - v_y \sin(\psi) \quad \text{Eq. 36}$$

$$\dot{Y} = v_x \sin(\psi) + v_y \cos(\psi), \quad \text{Eq. 37}$$

where  $m$  and  $I_z$  are the vehicle's mass and yaw inertia respectively and on the right side of the approximated equal sign small angle approximations,  $\delta \ll 1$ , have been applied. The rear axle distance from the CoG is termed as  $b$  while the front axle distance is termed as  $f$ . The vehicle's CoG velocities in the global coordinates  $X$  and  $Y$ .

Due to the fact that left and right wheels are considered to be symmetrical, lateral forces of the tires act exactly in the centre of their contact patch with the road, i.e. no pneumatic trail. The axles' kinematics and elasto-kinematics are modelled in the tires.

## 2.5.3 Two Track Model

The two-track model<sup>22</sup> extends the single track model in the following basic ways:

- Left and right wheels are not considered symmetrical
- The centre of gravity can be modelled and positioned at a certain lateral position with respect to the vehicle's longitudinal symmetry axis.
- The vehicle's centre of gravity lies at a certain height above the ground.

The extensions mentioned above allow:

- different steering angles between the left and right wheel (required by the Ackermann geometry)
- different static load between the left and right wheels
- different wheel loads during a manoeuvre (load transfer)
- pitch and roll motions

The normal load on each wheel can then be calculated by [17] [16]

$$F_{zfl} = \frac{mgb \frac{t_{wf}}{2}}{Lt_{wf}} - \frac{mh \frac{t_{wf}}{2}}{Lt_{wf}} \mathbf{a}_x - \frac{m}{t_{wf}} \left( \frac{h_e K_f}{K_f + K_r - mgh_e} + \frac{b}{L} \mathbf{e}_f \right) \mathbf{a}_y, \quad \text{Eq. 38}$$

$$F_{zfr} = \frac{mgb \frac{t_{wf}}{2}}{Lt_{wf}} - \frac{mh \frac{t_{wf}}{2}}{Lt_{wf}} \mathbf{a}_x + \frac{m}{t_{wf}} \left( \frac{h_e K_f}{K_f + K_r - mgh_e} + \frac{b}{L} \mathbf{e}_f \right) \mathbf{a}_y, \quad \text{Eq. 39}$$

$$F_{zrl} = \frac{mgf \frac{t_{wr}}{2}}{Lt_{wr}} + \frac{mh \frac{t_{wr}}{2}}{Lt_{wr}} \mathbf{a}_x - \frac{m}{t_{wr}} \left( \frac{h_e K_r}{K_f + K_r - mgh_e} + \frac{f}{L} \mathbf{e}_r \right) \mathbf{a}_y, \quad \text{Eq. 40}$$

$$F_{zrr} = \frac{mgf \frac{t_{wr}}{2}}{Lt_{wr}} + \frac{mh \frac{t_{wr}}{2}}{Lt_{wr}} \mathbf{a}_x + \frac{m}{t_{wr}} \left( \frac{h_e K_r}{K_f + K_r - mgh_e} + \frac{f}{L} \mathbf{e}_r \right) \mathbf{a}_y, \quad \text{Eq. 41}$$

<sup>22</sup> Two track model is based on "Dynamik der Kraftfahrzeuge" [30].

where  $K_f$  and  $K_r$  are the roll stiffness<sup>23</sup> at the front and rear respectively,  $e_f$  and  $e_r$  are the heights of the roll centre at the front and rear respectively.  $h_e$  is the distance of the centre of gravity from the roll axis, given by:

$$h_e = h - \frac{fe_b + be_f}{L} \quad \text{Eq. 42}$$

In (Eq. 38) up to (Eq. 41), the distance from CoG to the side was estimated to half the track width of the vehicle:

$$W_f = W_r = \frac{t_w}{2} \quad \text{Eq. 43}$$

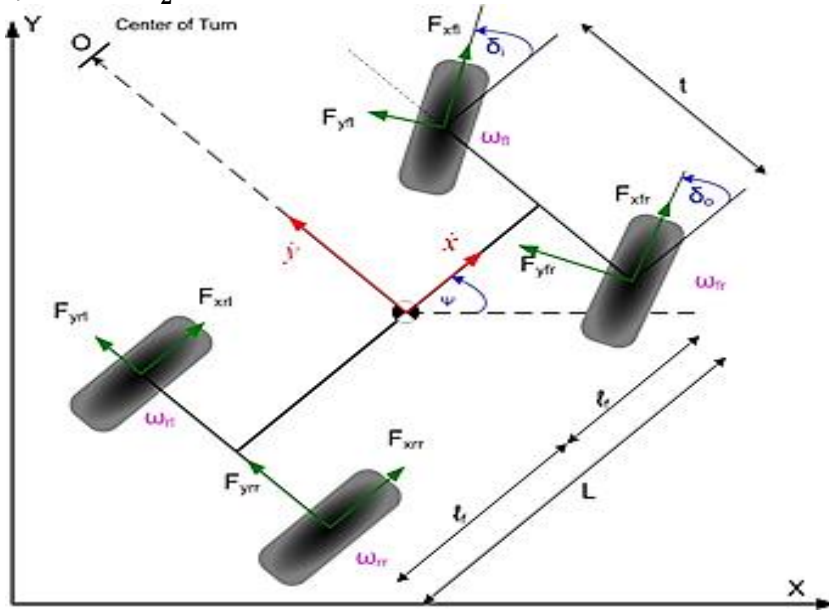


Figure 37 - Two track model with notations [31]; index  $i$  is front or rear and index  $j$  is left or right when referring to one of the vehicle's wheels or corners.

The equations of motion in the case of the two-track vehicle, (c.f. Figure 37), are given by:

$$m(\dot{v}_x - \dot{\psi}v_y) = F_{xfl} \cos \delta_i + F_{xfr} \cos \delta_o + F_{xrl} + F_{xrr} - F_{yfl} \sin \delta_i - F_{yfr} \sin \delta_o, \quad \text{Eq. 44}$$

$$m(\dot{v}_y + \dot{\psi}v_x) = F_{yrl} + F_{yrr} + F_{xfl} \sin \delta_i + F_{xfr} \sin \delta_o + F_{yfl} \cos \delta_i + F_{yfr} \cos \delta_o, \quad \text{Eq. 45}$$

$$I_z \ddot{\psi} = f(F_{yfl} \cos \delta_i + F_{yfr} \cos \delta_o + F_{xfl} \sin \delta_i + F_{xfr} \sin \delta_o) - b(F_{yrl} + F_{yrr}) + W_l(F_{yfl} \sin \delta_i + F_{yrl} - F_{xfl} \cos \delta_i - F_{xrl}) + W_r(F_{xfr} \cos \delta_o + F_{xrr} - F_{yfr} \sin \delta_o), \quad \text{Eq. 46}$$

and the wheel rotation dynamics by:

$$I_w \dot{\omega}_{ij} = T_{ij} - F_{xij}r. \quad \text{Eq. 47}$$

Translation between the local and global coordinate systems can still be performed with Eq.36 and Eq.37.

<sup>23</sup> The term "roll stiffness" includes not only the stiffness imposed by antiroll bars, but also from the suspension geometry, springs, frame, and all the factors that contribute to the axle's total roll stiffness in general.

## 2.6 Safety Systems

### 2.6.1 Electronic Stability Control (ESC)

Electronic stability control<sup>24</sup> (ESC) is a system used to prevent deviation from the desired path [20]. In order to develop ESC systems, the closed loop control requires the vehicle to be equipped with a yaw rate sensor, a lateral acceleration sensor, wheel speed sensors and a steering wheel angle sensor.

Yaw rate is determined by the steering wheel angle and travelling speed, while it is affected by surface-tire friction coefficient, slip angle, etc. [20]. The vehicle's yaw rate is controlled by the steering wheel angle, and could pose difficulty for the driver to utilize the maximum available physical adhesion between the tires and the road [32] [33]. At the same time the need for driving stability motivates the ESC principle [20].

Three main categories of ESC systems have been developed [20]:

1. Differential braking, where yaw moment is controlled by braking individual wheels.
2. Steer-by-wire, where a correction steering angle is added to driver's input
3. Active Torque Distribution, where active differentials control the drive torque independently on each wheel

For our research we will focus on differential braking systems (c.f. Figure 38).

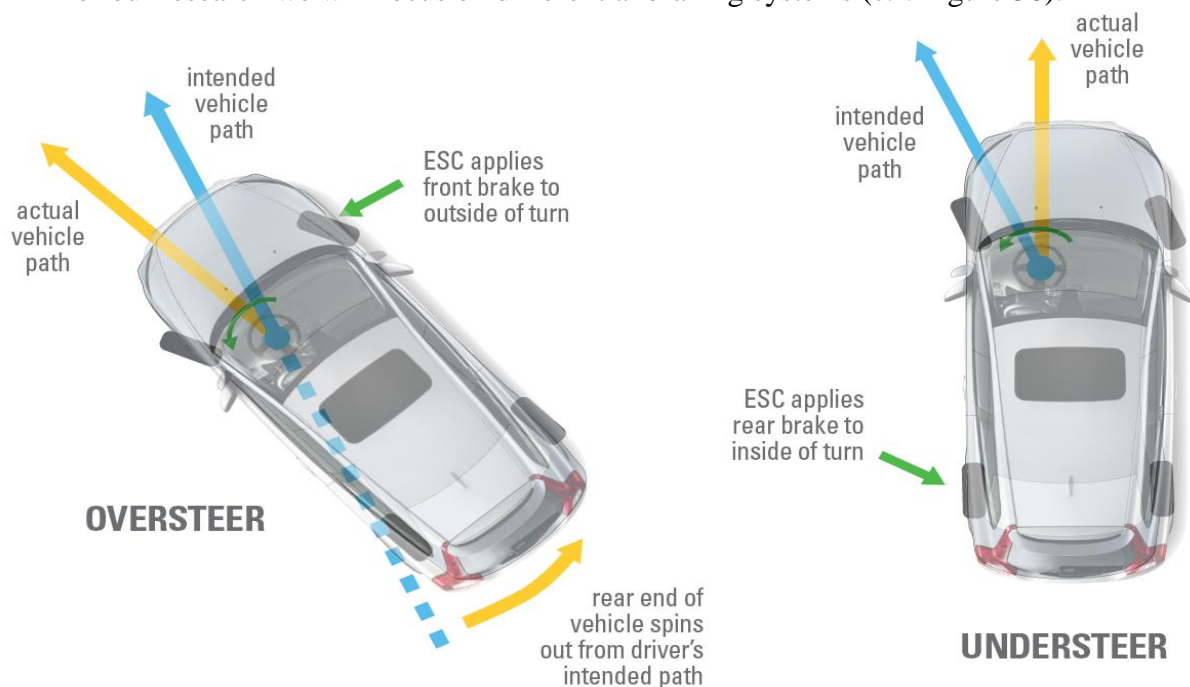


Figure 38 - Example of an Oversteer and Understeer situation, where a simplified ESC applies differential braking.

Assuming that certain vehicle and environment properties are known (friction coefficient, tire cornering stiffness, etc.), the sensors make it possible to calculate the desired slip angle as described by Eq. 48 [20]:

<sup>24</sup> ESC may also be referred as yaw stability control systems; automotive manufacturers use numerous other branded names (DSTC, ESP, DSC, VDC, etc.)

$$\beta_d = \frac{b - \frac{f m V^2}{2 C_{ar}(f + b)}}{(f + b) + \frac{m V^2 (f C_{af} - b C_{ar})}{2 C_{af} C_{ar}(f + b)}} \delta_{ss} \quad \text{Eq. 48}$$

The steady state relation between the steering angle and the radius of the vehicle trajectory can be calculated according to:

$$\frac{1}{R} = \frac{\delta_{ss}}{(f + b) + \frac{m V^2 (f C_{af} - b C_{ar})}{2 C_{af} C_{ar}(f + b)}}, \quad \text{Eq. 49}$$

which implies that the desired yaw rate is given by Eq. 50 [20]:

$$\psi_d = \frac{\dot{x}}{R} = \frac{\dot{x} \delta_{ss}}{(f + b) + \frac{m \dot{x}^2 (f C_{af} - b C_{ar})}{2 C_{af} C_{ar}(f + b)}} \quad \text{Eq. 50}$$

and the yaw acceleration is given by Eq. 46.

The friction coefficient of the road, influences the yaw rate that the vehicle can develop. An upper limit for the yaw rate that the controller can achieve is given by [20]:

$$\dot{x} \dot{\Psi} - \tan(\beta) \ddot{x} + \frac{\dot{x} \dot{\beta}}{\sqrt{1 + \tan^2(\beta)}} \leq \mu g \quad \text{Eq. 51}$$

The desired yaw torque to track the target yaw rate and slip angle is the calculated [20]. The objective of tracking yaw rate and slip angle can be done with sliding mode control design, where the sliding surface is chosen so either the yaw rate, the slip angle or a combination of them is tracked [34] [35] [36] [37]. Rajamani [20] suggests the use of the formula given in Eq. 52, and also suggests the reader who wants an introduction to the subject to look further in the text by Slotine and Li [38].

$$s = \dot{\Psi} - \dot{\Psi}_d + \xi(\beta - \beta_d) \quad \text{Eq. 52}$$

In Eq. 52,  $\xi$  is a weighting factor for the slip angle contribution,  $\beta$  is the sideslip angle,  $\beta_d$  is the desired sideslip angle and  $s$  can be seen as a surface. If one can ensure that the vehicle response converges to  $s = 0$  the desired yaw rate and slip angle are obtained. The differentiation of Eq. 52 is then given by Eq. 53 [20]:

$$\dot{s} = \ddot{\Psi} - \ddot{\Psi}_d + \xi(\dot{\beta} - \dot{\beta}_d) \quad \text{Eq. 53}$$

By assuming a small steering angle, a fixed brake ratio ( $\rho$ ) between the front and rear wheel on each side of the car, the yaw torque generated by the brakes is defined by Eq. 54:

$$M_{\psi b} = \frac{l_w}{2} (F_{xfr} - F_{xfl}) \quad \text{Eq. 54}$$

and the yaw acceleration is given by Eq. 55 :

$$\ddot{\Psi} = \frac{1}{I_z} [f(F_{yfl} + F_{yfr}) \cos(\delta) - b(F_{yrl} + F_{yrr}) + (\cos(\delta) + \rho) M_{\psi b}] \quad \text{Eq. 55}$$

Setting  $\dot{s} = -\eta s$  when substituting for  $\ddot{\Psi}$  it yields the control law in Eq. 56 [20]:

$$M_{\psi b} = \frac{\frac{b(F_{yrl} + F_{yrr})}{I_z} - \frac{f(F_{yfl} + F_{yfr})}{I_z} - \eta s + \ddot{\Psi}_d - \xi(\dot{\beta} - \dot{\beta}_d)}{\rho + \cos(\delta)} \quad \text{Eq. 56}$$

Estimations for the sideslip angle, sideslip angle derivative and each of the lateral tire forces are needed, and for the interested reader some literature [39] [33] [40] [41] is suggested. After the desired torque ( $M_{\psi b}$ ) produced by the differential braking has been calculated, the

brake pressure can be calculated as the torque produced by differential braking is directly coupled to the dynamics of the wheels. If only the front wheels are used for braking the resulting equations for left ( $P_{bfl}$ ) and right ( $P_{bfr}$ ) brake pressure can be seen in Eq. 57 and Eq. 58 respectively [20].

$$P_{bfl} = P_0 - \alpha_{const} \frac{\left(\frac{2M_{\psi b}}{l_w}\right) r_{eff}}{A_w \mu_b R_b} \quad \text{Eq. 57}$$

$$P_{bfr} = P_0 + (1 - \alpha_{const}) \frac{\left(\frac{2M_{\psi b}}{l_w}\right) r_{eff}}{A_w \mu_b R_b} \quad \text{Eq. 58}$$

Where  $P_0$  the brake pressure at the wheel at the ESC is initiated and  $\alpha_{const}$  is a constant that should be chosen in the range  $0 \leq \alpha_{const} \leq 1$ .

If small steering angles cannot be assumed, the yaw torque that should be generated by the brakes needs to be calculated from each force for each wheel in Eq. 46.

## 2.6.2 Lane Keeping Aid (LKA)

Lane Keeping Aid is an active safety feature that uses sensors (c.f. Figure 39) in order to identify if a vehicle begins to move out of its lane and then uses actuators and corrects the steering wheel keeping the vehicle inside the lane.

This system is the evolution of systems like Lane Departure Warning (LDW), which means that it has the added functionality of not only warning the driver that the vehicle is about to depart from its lane but can also actively prevent that.

The actuator used could be an external electric motor on the steering column, or in case the vehicle is using Electric power assisted steering, the power assist motor could be used without any need of added hardware.



Figure 39 - Illustration of a LKA system. The vehicle identifies the road lane markers using optical sensors (camera) and acts on the steering to correct the path if the vehicle is about to move out of its lane.

## 2.7 Driver Behaviour Models

Modelling of human driver involves many difficulties because of the -sometimes-unpredictable nature of the driver. Driver’s reactions are not only based upon the demands of the driving situation but also upon the physical and psychological condition of the driver as well as driver’s understanding and acquired experience of the vehicle.

Many different models of human drivers have been developed using many different tools such as [42]:

- PID controller<sup>25</sup>
- Fuzzy theory control

One example of a PID controller, which is consisted of 2 subsystems for longitudinal and lateral dynamics can be seen in the following figures.

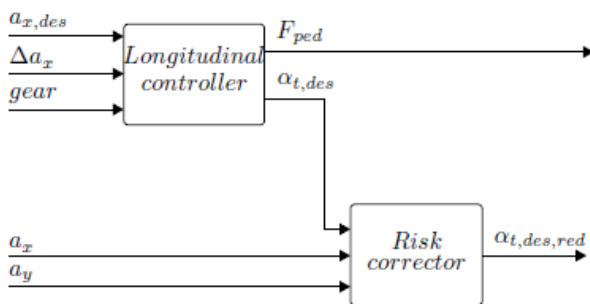


Figure 40 - Longitudinal PID C. structure. [42]

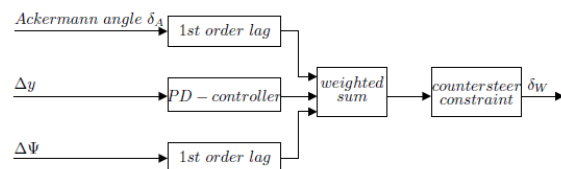


Figure 41 - Lateral PID C. structure [42].

The SDM (c.f. Figure 42) [43] consists of 2 main subsystems; the driver and the “vehicle and environment”. This driver behaviour model simulates the drivers neuromuscular (NMS) as well as Central-nervous-System (CNS).The signal “desired path” represents the driver’s command and can be changed according to the task he is performing. The predicted path is calculated from the vehicle dynamics model, which includes the steering system model as well and gives all the required states to the NMS and CNS subsystems.

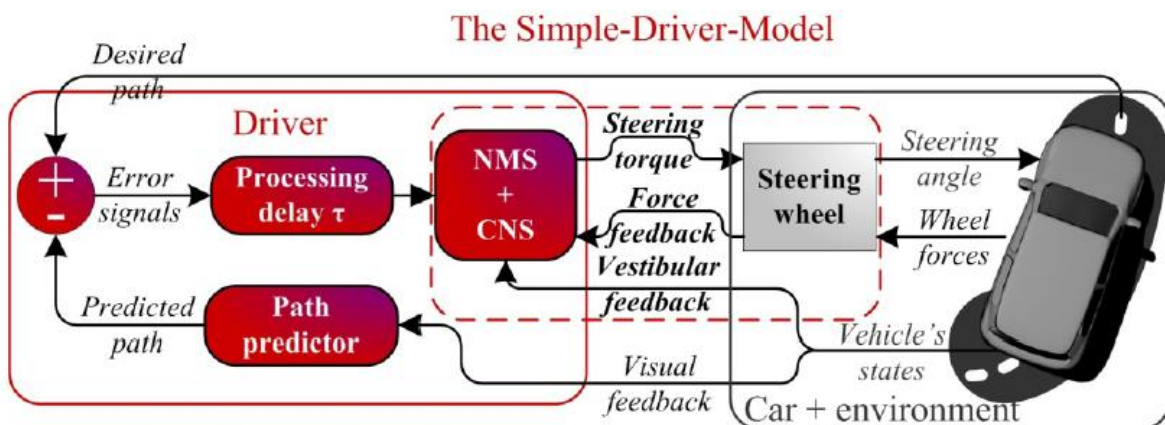


Figure 42 - The SDM structure [43].

<sup>25</sup> The PID controller reduces the errors very well but doesn't behave like a human driver.

A more realistic hybrid driver behaviour model, which describes the complete cognitive process can be seen in Figure 43. This models includes [42]:

1. Strategic tasks (e.g. choice of route)
2. Navigational tasks
3. Tasks related to the road (e.g. lane keeping)
4. Traffic related tasks (e.g. interaction with other road users, collision avoidance)
5. Adherence to rules (e.g. traffic signs, signals, etc.)

As it can be seen from the following figure, this system represents the complete Vehicle, including vehicle dynamics, driver and an accurately defined environment.

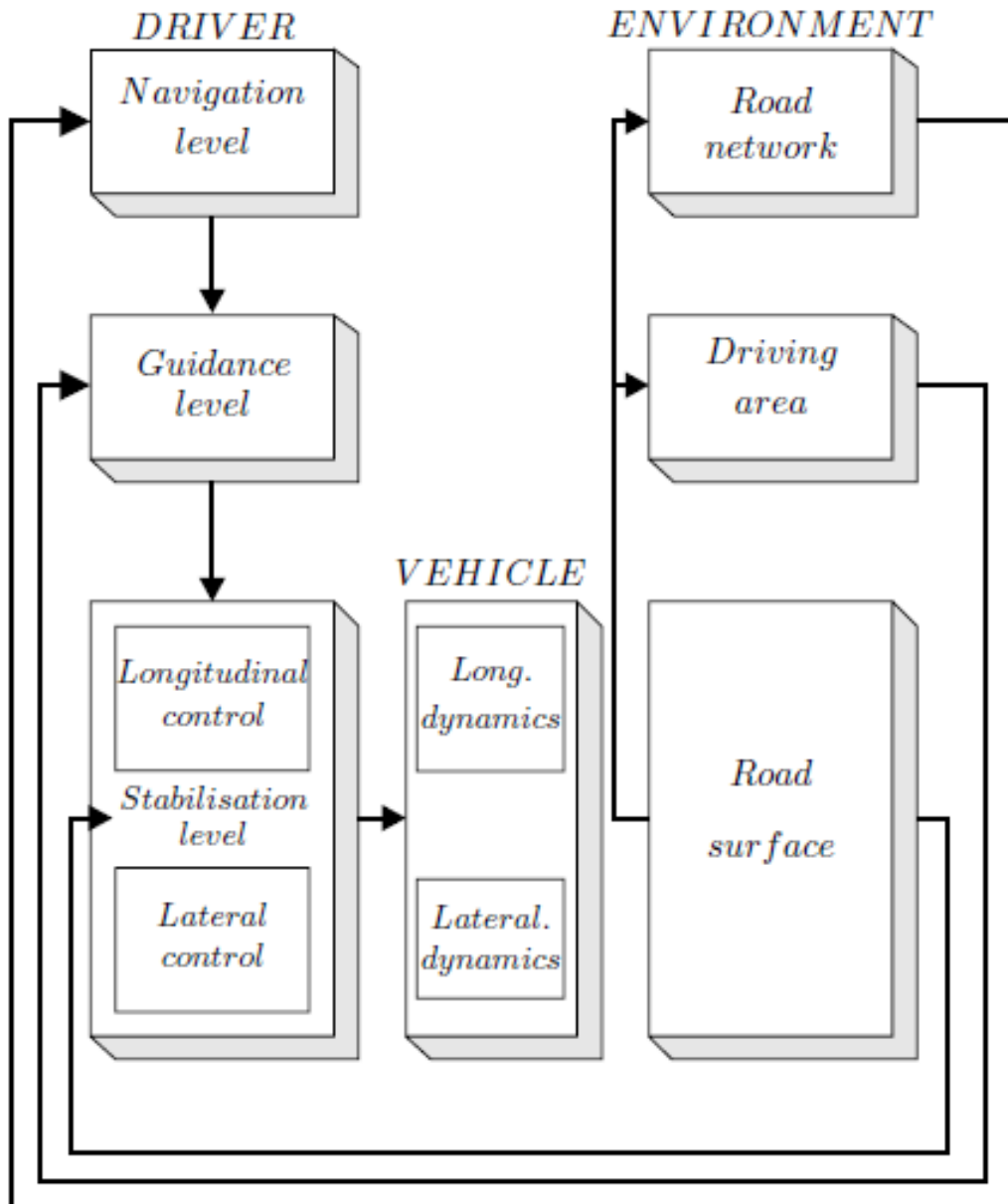


Figure 43 - Structure of the Hybrid driver behaviour model [42].

# 3 DOUBLE LANE CHANGE OPTIMIZATION

This study introduces a method for estimating the vehicle's maximum entry speed for an ISO3888 part-2 double-lane change (DLC) test in simulation. Pseudospectral collocation in TOMLAB/ PROPT calculates the optimal steering angle that maximizes the entry speed. The rationale is to estimate the vehicle's performance in the design phase and adapt the tuning to improve DLC ratings. A two-track vehicle dynamics model (VDM) employing non-linear tires, suspension properties and a simplified Dynamic Stability and Traction Control (DSTC) system was parameterized as a 2011 T5 FWD Volvo S60 using in-field tests and its corresponding kinematics and compliance (K&C) measurements. A sensitivity analysis on the parameters revealed certain trends that influence the entry speed, which can be varied from 69.4 up to 73.3 km/h when adapting certain vehicle features. To evaluate the method, the generated optimal steering control inputs for the simulated S60 were applied on the actual car motivating the further development of the method.

## 3.1 Introduction-Problem Definition

Tuning a vehicle, and more specifically the DSTC, involves physical vehicle testing; a time consuming and costly procedure. It is normally performed in an early phase in the development process, where only prototype vehicles are available. The corresponding vehicle's performance from the tuning is rated by independent organizations, such as the EuroNCAP, using tests such as the ISO 3888 part-2 DLC (c.f. Figure 44). EuroNCAP assesses the DSTC by performing a series of tests, where the steering and yaw behaviour can be simultaneously evaluated [44]. The DSTC and the vehicle's handling are also rated subjectively [45] [46].



Figure 44 - ISO 3888 part-2 double-lane change; instance from testing.

Although the aforementioned methods are often used for handling rating, they are sometimes characterized unsuitable for objective assessment of the vehicle's performance,

because the driver is involved in the control loop [47]. Objectivity can be ensured by examining solely the vehicle's behaviour. Substituting test drivers by a controller, which would generate the optimal steering inputs for achieving maximum entry speed, would enable the definition of an objective performance metric [48] and a tool to assess the vehicle's handling, early in the development process.

It is envisioned that in an effort to improve development efficiency, promote safety and reduce prototype vehicles, the DSTC tuning in future vehicles will be achieved using computer-aided-engineering (CAE) tools. This is expected to reduce cost and lead-time, facilitate objective assessment of the car's safety and offer numerically optimized tuning sets; better and safer cars for the road.

## 3.2 Optimal Steering Input Generation

The optimal steering input generation can be formulated as an optimal control problem, with the objective to maximize the vehicle's entry speed while satisfying the vehicle dynamics and DLC path constraints. The augmented objective function of this problem can be given as:

$$J = -V_x|_{X=0} + W_\delta \int_{t=0}^{t=t_{final}} \delta^2 dt + W_\psi \int_{t=0}^{t=t_{final}} \dot{\psi}^2 dt + W_{t_f} t_f, \quad Eq. 59$$

where  $V_x$  denotes the vehicle's longitudinal speed,  $t_f$  the time needed to complete the manoeuvre,  $\delta$  the steering rate,  $\dot{\psi}$  the yaw rate and  $W_\delta$ ,  $W_{t_f}$ ,  $W_\psi$  are weighting factors. The objective function aims to minimize the negative entry speed  $-V_x|_{X=0}$  (corresponding to maximization of the entry speed) and is augmented with 3 energy related terms ( $\delta^2$ ,  $\dot{\psi}^2$ ,  $t_f$ ) so as to regulate the optimal steering input. This approach is motivated by the numerical difficulties that arise when solving a boundary value problem associated with the original "bang-bang" optimal control problem. It can be noticed that the obtained auxiliary optimal control with the augmented objective function approaches the original optimal control problem as  $W_\delta$ ,  $W_\psi$  and  $W_{t_f}$  approach zero. The solution of the initial optimal control problem is then reduced to the solution of a sequence of auxiliary optimal control problems.

### 3.2.1 Optimization Method

The infinite dimensional optimal control problem defined above is converted into a finite dimensional optimization problem using a direct transcription method and the resulting optimization problem is solved using TOMLAB/PROPT [49] in Matlab. PROPT uses a Gauss pseudospectral collocation method for solving the optimal control problem, meaning that the solution takes the form of a polynomial, and this polynomial satisfies the differential algebraic equations (DAE) and the path constraints at the collocation points.

## 3.2.2 Path constraints

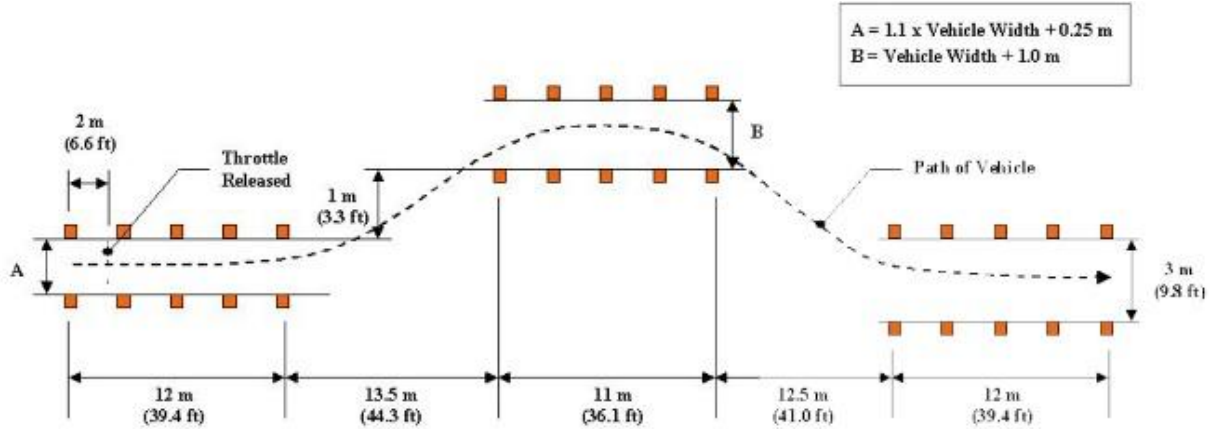


Figure 45 - ISO 3888 course, part-2 obstacle avoidance manoeuvre (DLC).

The DLC track is shown in Figure 45. The track boundaries are described with mathematically smooth functions, since discontinuities are not recommended in optimization problems [49]. Eq. 60 describes the lateral position boundary; the terms  $A_{tr}$ ,  $B_{tr}$  and  $C_{tr}$  correspond to the notation used in Figure 45 while  $a_{tr}$  defines the smoothness of each corner. The body dimensions (four sides of the car) were discretised into body-points subject to the track constraints.

$$\left[ \begin{array}{l} \frac{1 + A_{tr}}{2} \left( 1 + \tanh\left(\frac{X - 25.2}{a_{tr}}\right) \right) - \frac{A_{tr}}{2} \\ + \frac{1 + C_{tr}}{2} \left( 1 - \tanh\left(\frac{X - 36.8}{a_{tr}}\right) \right) - 1 + C_{tr} \end{array} \right] \leq Y \quad \text{Eq. 60}$$

$$\leq \left[ \begin{array}{l} \frac{1 + B_{tr}}{2} \left( 1 + \tanh\left(\frac{X - 12.3}{a_{tr}}\right) \right) \\ + \frac{A_{tr}}{2} + \frac{1 + B_{tr}}{2} \left( 1 - \tanh\left(\frac{X - 48.7}{a_{tr}}\right) \right) - 1 - B_{tr} \end{array} \right]$$

## 3.2.3 Complexity built-up hierarchy

The optimization method involved an iterative process starting with a centreline guess of a point mass, with the results used as the guess to the next more sophisticated VDM.

### 3.2.3.1 Initial guess

The first optimization problem started from a guess of the manoeuvre completion time  $t_g = 3.05$  s and 15% percentage drop of the entry speed  $v_d$ . The states of the vehicle were then estimated according to Eq. 61 to Eq. 65.

$$X_g = \frac{61}{t_g} t \quad \text{Eq. 61}$$

$$Y_g = \frac{A + B + 2}{4} \left( 1 + \tanh\left(\frac{X_g - 20}{a_g}\right) \right) - \frac{B + C + 2}{4} \left( 1 + \tanh\left(\frac{X_g - 43}{a_g}\right) \right) \quad \text{Eq. 62}$$

$$v_{x_g} = \frac{61}{t_g} \left( 1 + \frac{v_d}{100} \left( 1 - \frac{t}{t_g} \right) \right) \quad \text{Eq. 63}$$

$$v_{y_g} = \dot{Y}_g/3 \quad \text{Eq. 64}$$

$$\psi_g = \tan^{-1} \left( \frac{\dot{Y}_g}{\dot{X}_g} \right), \delta_g = \frac{\psi_g}{2} \quad \text{Eq. 65}$$

### 3.2.3.2 Point mass model

The VDM used for the 1st optimization step is a point mass model with acceleration and body-dimension constraints. The kinematics equations used are given from Eq. 66 to Eq. 74.

$$\mathbf{V}_X = \dot{\mathbf{X}} \quad \text{Eq. 66}$$

$$\mathbf{V}_y = \dot{Y} \quad \text{Eq. 67}$$

$$\mathbf{a}_X = \dot{\mathbf{V}}_X \quad \text{Eq. 68}$$

$$\mathbf{a}_y = \dot{\mathbf{V}}_y \quad \text{Eq. 69}$$

$$\psi = \text{atan} \left( \frac{dY}{dX} \right) \quad \text{Eq. 70}$$

$$V_x = V \cdot \cos(\psi) \quad \text{Eq. 71}$$

$$V_y = V \cdot \sin(\psi) \quad \text{Eq. 72}$$

$$a = \sqrt{a_x^2 + a_y^2} \quad \text{Eq. 73}$$

$$\dot{\mathbf{V}} = \mathbf{0} \quad \text{Eq. 74}$$

The point mass model assumes that the vehicle's longitudinal velocity  $V_X$  will always be tangent to the trajectory (Eq. 70), ( $0^\circ$  slip angle) and that the resultant velocity will be constant throughout the manoeuvre (Eq. 74). The acceleration constraints derive from the vehicle's technical specifications: time from 0 to 100 km/h ( $t_{0to100}$ ) in 6.6 s and brake distance from 100 to 0 km/h in 37 m ( $d_{100to0}$ ).

$$-\frac{(100/3.6)^2}{2 \cdot d_{100to0}} \leq a_x \leq \frac{100/3.6}{t_{0to100}} \text{ m/s}^2 \quad \text{Eq. 75}$$

$$|a_y| \leq 10.3 \text{ m/s}^2 \quad \text{Eq. 76}$$

$$|a| \leq \mu g, g = 9.81 \text{ m/s}^2 \quad \text{Eq. 77}$$

The optimal solution search was performed sequentially with  $n = 20, 40, 60$  and  $90$  collocation points [50] with the weight factors  $W_\delta = 0.05$ ,  $W_{t_f} = 0.4$  and  $W_\psi = 0.1$  for (Eq. 59).

### 3.2.3.3 Single-track model (STM) with linear tires

A 3 degree-of-freedom (DOF) (translational and yaw motion) STM [51] was used as the next VDM. The STM assumes small angles, lateral tire forces which are linearly dependent on their slip angles and longitudinal aerodynamic drag force; the equations of motion can be found in the literature [52, pp. 29, 97]. The steering angle  $\delta$  constitutes the sole control variable for the optimization. The solution search was performed with  $n = 30, 50, 60$  and  $80$  collocation points sequentially with cost function of (Eq. 59) and the same weight factors with the point mass model. Furthermore, the corresponding variable constraints are given in Table 1.

Table 1. Constraints for the linear STM.

Variable constraints	Description
$V_x \geq 10$	Longitudinal speed (m/s)
$-20 \leq V_y \leq 20$ $V_y(t = 0) = 0$	Lateral speed (m/s)
$-\pi/2 \leq \psi \leq \pi/2, \psi(t = 0) = 0$	Yaw angle (rad)
$-4 \leq \dot{\psi} \leq 4$ $\dot{\psi}(t = 0) = 0$	Yaw rate (rad/s)
$-0.541 \leq \delta \leq 0.541$	Steering angle (rad)
$-4\pi \leq \dot{\delta}_{sw} \leq 4\pi$	Steering wheel rate (rad/s)
$X(t = 0) = 0$ $X(t = t_{final}) = 61$	Vehicle's centre-of-gravity (CoG) longitudinal position (m)
$width/2 - A/2 \leq Y(t = 0) \leq A/2 - width/2$ $width/2 + A/2 - C \leq Y(t = t_{final})$ $\leq A/2 - width/2$	Vehicle's CoG lateral position (m)
$C_f = \frac{BCD}{2} F_{zf} / C_r = \frac{BCD}{2} F_{zr}$	Front/rear axle cornering stiffness (N/rad) <sup>26</sup>

### 3.2.3.4 Single-track model (STM) with non-linear tires

The results from the STM with linear tires constitute the initial guess for a STM with non-linear tires. The tire model used here is a simplified Magic Formula [53] (c.f. Eq. 78) where  $D$ ,  $C$  and  $B$  are the peak value factor, shape factor and stiffness factor respectively.  $F_{zi}$  is the normal load on the axle; the indices  $i, j$  in the rest of the paper stand for  $i$ :  $f$  (front)  $r$  (rear),  $j$ :  $l$  (left)  $r$  (right). The product  $BCD \cdot F_{zi}$  represents the cornering stiffness  $C_i$  on the axle.

$$\mu(s) = D \sin(C \tan^{-1}(Bs)) \quad \text{Eq. 78}$$

The resultant tire slip  $s_i$  for each tire was defined as in eq. Eq. 79.  $V_{ix}$  and  $V_{iy}$  are the  $x$  and  $y$  velocity components on the tire frame,  $s_{ix}$  and  $s_{iy}$  Eq. 80 the corresponding tire slips and  $r$  the wheel radius.

$$s_i = \sqrt{s_{ix}^2 + s_{iy}^2} \quad \text{Eq. 79}$$

$$s_{ix} = \frac{V_{ix} - \omega_i r_i}{\omega_i r_i}, s_{iy} = \frac{V_{iy}}{\omega_i r_i} \quad \text{Eq. 80}$$

$$\mu_{ix} = -\frac{s_{ix}}{s_i} \mu_i, \mu_{iy} = -\frac{s_{iy}}{s_i} \mu_i \quad \text{Eq. 81}$$

Eq. 81 calculates the tire's  $x$  and  $y$  friction coefficients. The front  $F_{zf}$  and rear  $F_{zr}$  normal forces at the tires are calculated with Eq. 82, with  $\frac{mh}{L} a_x$  being the longitudinal acceleration induced load transfer, due to the height  $h$  of the CoG. The tire forces at each tire frame are given in eq. Eq. 83.

$$F_{zf} = \frac{mgb}{L} - \frac{mh}{L} a_x, F_{zr} = \frac{mgf}{L} + \frac{mh}{L} a_x \quad \text{Eq. 82}$$

$$F_{xi} = \mu_{ix} F_{zi}, F_{yi} = \mu_{iy} F_{zi} \quad \text{Eq. 83}$$

The dynamical equations for the model are given through (Eq. 84) to (Eq. 90), where,  $m$  is the vehicle's mass,  $I_z$  its moment of inertia around the vertical axis (yaw inertia),  $I_w$  the moment of inertia of each wheel and front  $T_f$  and rear  $T_r$  the applied torque [52] [54]. The objective function (Eq. 59) was the same as in the linear tires' case in the STM using once again an iterative solution strategy with increasing number of collocation points;  $n = 50, 60$  and  $80$ .

<sup>26</sup> Half (in magnitude) of the product  $BCD$  (estimated in 3.2.4) was used.

The constraints changed and/or added to the linear STM constraints (c.f. Table 1) appear in Table 2.

$$m(\dot{v}_x - \dot{\psi}v_y) = F_{xf} \cos \delta - F_{yf} \sin \delta + F_{xr} - \frac{1}{2} \rho A C_d V_x^2 \quad \text{Eq. 84}$$

$$m(\dot{v}_y + \dot{\psi}v_x) = F_{yr} + F_{xf} \sin \delta + F_{yf} \cos \delta \quad \text{Eq. 85}$$

$$I_z \dot{\psi} = f(F_{yf} \cos \delta + F_{xf} \sin \delta) - bF_{yr} \quad \text{Eq. 86}$$

$$I_w \dot{\omega}_f = T_f - F_{xf} r \quad \text{Eq. 87}$$

$$I_w \dot{\omega}_r = T_r - F_{xr} r \quad \text{Eq. 88}$$

$$\dot{X} = v_x \cos(\psi) - v_y \sin(\psi) \quad \text{Eq. 89}$$

$$\dot{Y} = v_x \sin(\psi) + v_y \cos(\psi) \quad \text{Eq. 90}$$

Table 2. Constraints for the non-linear STM model.

Variable constraints	Description
$10/r \leq \omega_i \leq 180/r$	The <i>i</i> (front/rear) wheel's rotational speed (rad/s)
$\omega_i r \leq 1.2V_x$	Indirect limitation on <i>i</i> (front/rear) wheel slip

### 3.2.3.5 Two-track Model

The final VDM comprised of a 7-DOF VDM (longitudinal, lateral and yaw movement and the 4 wheels' rotational dynamics) including roll (static load transfer), non-linear tires ('87 Magic formula [55] with transient effects (tire-relaxation [56]) and suspension properties (lateral force compliance, camber change, roll steer and roll stiffness [56]) as-well-as a simplified DSTC implementation. A DSTC was modelled as a yaw rate error controller utilizing trigonometric functions for approximating its discontinuous behaviour; discontinuities are not recommended in optimization problems [49].

The current optimization step was initialized using the non-linear STM result as a start guess and the same weight factors and objective function as with the non-linear tires STM. The adapted constraints appear in Table 3.

Table 3. Constraints for the full vehicle model.

Variable constraints	Description
$10/r \leq \omega_{ij} \leq 80/r$	<i>i, j</i> wheel's rotational speed rad/s
$\omega_{ij} r \leq 1.2V_x$	Indirect limitation for <i>i, j</i> wheel slip

#### 3.2.3.5.1 Wheel kinematics; roll kinematics, roll steer and lateral force compliance

The vehicle's centre-of-gravity (CoG) lies at a certain height above the ground changing the wheels' normal load and roll angle. (Eq. 91) to (Eq. 94) calculate the induced load transfer [19, p. 683] and static roll angle  $\varphi$  (Eq. 94);  $K_f/K_r$  are the front/rear roll stiffness<sup>27</sup>,  $e_f/e_r$  is the height of the roll centre at the front/rear and  $h_e$  is the distance of the CoG from the roll axis.

<sup>27</sup> The term roll stiffness includes not only the stiffness imposed by antiroll bars, but also from the suspension geometry, springs, frame, and all the factors that contribute to the axle's total roll stiffness in general.

$$F_{zfl} = \frac{mgb \frac{t_W}{2}}{Lt_W} - \frac{mh \frac{t_W}{2}}{Lt_W} a_x - \frac{m}{t_W} G_{front} a_y$$

$$F_{zfr} = \frac{mgb \frac{t_W}{2}}{Lt_W} - \frac{mh \frac{t_W}{2}}{Lt_W} a_x + \frac{m}{t_W} G_{front} a_y \quad \text{Eq. 91}$$

$$\text{with } G_{front} = \left( \frac{h_e K_f}{K_f + K_r - mgh_e} + \frac{b}{L} e_f \right)$$

$$F_{zrl} = \frac{mgf \frac{t_W}{2}}{Lt_W} + \frac{mh \frac{t_W}{2}}{Lt_W} a_x - \frac{m}{t_W} G_{rear} a_y$$

$$F_{zrr} = \frac{mgf \frac{t_W}{2}}{Lt_W} + \frac{mh \frac{t_W}{2}}{Lt_W} a_x + \frac{m}{t_W} G_{rear} a_y \quad \text{Eq. 92}$$

$$\text{with } G_{rear} = \left( \frac{h_e K_r}{K_f + K_r - mgh_e} + \frac{f}{L} e_r \right)$$

$$h_e = h - \frac{f e_b + b e_f}{L} \quad \text{Eq. 93}$$

$$\varphi = \frac{mh_e}{K_f + K_r - mgh_e} a_y \quad \text{Eq. 94}$$

During cornering, the front wheel angle can change a) due to roll steer induced from body roll motion<sup>28</sup> and b) due to lateral force compliance steer induced by the suspension's compliance to lateral forces applied at the tire-road contact [19] [4] [57].

Table 4. Roll steer coefficients  $\frac{\partial \delta_i}{\partial \varphi}$  [deg/deg] for the Volvo S60.

	Left wheel	Right wheel	Mean	
Front axle	-0.135	-0.111	-0.123	$\frac{\partial \delta_f}{\partial \varphi}$
Rear axle	-0.00	-0.01	0	$\frac{\partial \delta_r}{\partial \varphi}$

The ratio of the induced wheel angle over the corresponding roll angle is the roll steer coefficient  $\frac{\partial \delta_i}{\partial \varphi}$  (steering angle  $\delta$  function of the roll angle  $\varphi$ ). The roll angle is positive when the vehicle leans to the right as seen from the rear. The roll steer coefficient can be measured using kinematics and compliance (K&C) tests; the values used for the Volvo S60 are shown in Table 4 (the mean value of the right and left wheel's roll steer was used for the front and rear axles). The values depict that during cornering the front wheels steer outwards with respect to the curve; the rear wheels have negligible roll steer. For the front axle, a negative roll steer coefficient results in an understeer effect and the opposite applies for the rear axle [4]. The change in the steering angle due to roll steer is calculated with (Eq. 95).

$$\delta_{rsf} = \frac{\partial \delta_f}{\partial \varphi} \varphi, \delta_{rsr} = \frac{\partial \delta_r}{\partial \varphi} \varphi \quad \text{Eq. 95}$$

The lateral force compliance steer can be regarded as the wheel steering angle change when a lateral force is applied at a) the tire-ground contact patch at the wheel centre ( $X = 0$ ) and b) at a distance of  $X = 30$  mm behind<sup>29</sup> the centre of the tire-ground contact patch. The distance  $X = 30$  mm is an approximate value for a typical tire's pneumatic trail at small slip angles [56]. For small slip angles/linear tire region the pneumatic trail is almost constant. For

<sup>28</sup> Even though this is undesirable, it is a very common characteristic of most of the suspension and steering systems, which depends on their geometry [43, 15].

<sup>29</sup> The word behind here indicates the direction that is opposite to the tire's longitudinal travelling direction at the tire frame's coordinate system.

larger slip angles/non-linear tire region the pneumatic trail reduces [19] [56] [53]. The wheel steering angle change will therefore depend on the distance from the contact patch centre where the lateral force will be applied. The lateral force compliance steer coefficient  $LF_{cij}$  is a function of the pneumatic trail and in principle interpolates linearly the lateral force compliance steer [deg/kN] between its value for  $X = 0$  mm and  $X = 30$  mm. The resultant formula is given in Table 5.

Table 5. Lateral force compliance steer coefficient  $LF_{cij}$ .

	<i>Left wheel</i>	<i>Right wheel</i>
<i>Front axle</i>	$LF_{cfl} = -2.633t_{pfl} - 0.029$	$LF_{cfr} = -3.233t_{pfr} - 0.046$
<i>Rear axle</i>	$LF_{crl} = -1.8t_{prl} + 0.07$	$LF_{crr} = -1.5667t_{prl} + 0.065$

The front and rear axle lateral force compliance steer is given in (Eq. 96) and is the mean of the left and right wheel of the corresponding axle (Eq. 97). The tire's pneumatic trail is calculated as in [58].

$$\delta_{cij} = LF_{cij}F_{yij} \quad \text{Eq. 96}$$

$$\delta_{cf} = \frac{\delta_{cfl} + \delta_{cfr}}{2}, \delta_{cr} = \frac{\delta_{crl} + \delta_{crr}}{2} \quad \text{Eq. 97}$$

### 3.2.3.5.2 Tire lateral dynamics and camber thrust

A tire will typically require half to one rotation to build its steady state lateral force [52]; this distance can be referred as the relaxation length  $L_{relax}$ . This transient behaviour can be modelled through the first order differential equation (Eq. 98) [52, p. 429] where  $\tau$  is a time constant and  $f_{yss}$  is the steady state value of the lateral force for a given slip angle  $a$ . The time constant is related to the relaxation length as in (Eq. 99) where  $V_x$  is the tire's longitudinal velocity. According to [53], the higher the slip angle, the shorter the relaxation length becomes.

$$\tau \dot{f}_y(a, t) + f_y(a, t) = f_{yss}(a) \quad \text{Eq. 98}$$

$$\tau = \frac{L_{relax}}{V_x} \quad \text{Eq. 99}$$

During cornering the camber angle  $\varepsilon$  of the wheel with respect to the body changes; the camber angle gain  $\partial\varepsilon_{ij}/\partial\varphi$  with respect to body roll for the S60 is given in Table 6.

Table 6. Camber gain per roll angle  $\partial\varepsilon_{ij}/\partial\varphi$  [deg/deg].

	<i>Left wheel</i>	<i>Right wheel</i>
<i>Front axle</i>	<b>+0.243</b>	<b>-0.264</b>
<i>Rear axle</i>	<b>+0.452</b>	<b>+0.434</b>

The camber thrust, the lateral force due to tire camber angle, derives from the wheel's camber-inclination angle  $\gamma$  relative to the ground; the left and right angle  $\gamma_{ij}$  is calculated with (Eq. 101).

$$\varepsilon_{ij} = \frac{\partial\varepsilon_{ij}}{\partial\varphi} \varphi \quad \text{Eq. 100}$$

$$\gamma_{il} = \gamma_{i0} + \varphi - \varepsilon_{il} \quad \text{Eq. 101}$$

$$\gamma_{ir} = \gamma_{i0} + \varphi + \varepsilon_{ir} \quad \text{Eq. 102}$$

$$F_{\gamma ij} = -C_{\gamma} \gamma_{ij}$$

The factor  $\gamma_{i0}$  in (Eq. 101) is the static camber of the wheels (S60; front wheels  $\gamma_{f0} = -0.7^\circ$  and rear wheels  $\gamma_{r0} = -1.3^\circ$ ). The camber thrust for each tire is calculated with (Eq. 102) using as camber stiffness  $C_\gamma = 2000$  [N/rad]. The camber thrust is added (Eq. 105) to the steady state lateral force (Eq. 84).

$$\begin{aligned}\delta_f &= \delta + \delta_{rsf} + \delta_{cf} & \text{Eq.} \\ \delta_r &= \delta_{rsr} + \delta_{cr} & \text{103}\end{aligned}$$

$$\dot{F}_{yij}(\mathbf{a}, \mathbf{t}) = \left( (F_{yijss}(\mathbf{a}) - F_{yij}) - F_{yij}(\mathbf{a}, \mathbf{t}) \right) \frac{V_{xij}}{L_{relax}} \quad \text{Eq. 104}$$

$$\begin{aligned}m(\dot{v}_x - \dot{\psi}v_y) = & \\ (F_{xfl} + F_{xfr}) \cos \delta_f + (F_{xrl} + F_{xrr}) \cos \delta_r - (F_{yfl} + F_{yfr}) \sin \delta_f - (F_{yrl} & \\ + F_{yrr}) \sin \delta_r - \frac{1}{2} \rho A C_d V_x^2 & \text{Eq.} \\ m(\dot{v}_y + \dot{\psi}v_x) = & \text{105}\end{aligned}$$

$$\begin{aligned}(F_{yrl} + F_{yrr}) \cos \delta_r + (F_{xrl} + F_{xrr}) \sin \delta_r + (F_{xfl} + F_{xfr}) \sin \delta_f + (F_{yfl} & \\ + F_{yfr}) \cos \delta_f & \text{Eq.} \\ & \text{106}\end{aligned}$$

$$\begin{aligned}I_z \ddot{\psi} = & \\ f[(F_{yfl} + F_{yfr}) \cos \delta_f + (F_{xfl} + F_{xfr}) \sin \delta_f] - b[(F_{yrl} + F_{yrr}) \cos \delta_r & \\ + (F_{xrl} + F_{xrr}) \sin \delta_r] + W_l(F_{yfl} \sin \delta_f & \text{Eq.} \\ + F_{yrl} \sin \delta_r - F_{xfl} \cos \delta_f - F_{xrl} \cos \delta_r) & \text{107} \\ + W_r(F_{xfr} \cos \delta_f + F_{xrr} \cos \delta_r - F_{yfr} \sin \delta_f - F_{yrr} \sin \delta_r) & \end{aligned}$$

$$I_w \dot{\omega}_{ij} = T_{ij} - F_{xij}r \quad \text{Eq. 108}$$

The dynamical equations for the two-track model are given through (Eq. 103) to (Eq. 108) with  $m$  the vehicle's mass,  $I_w$  the moment of inertia of each wheel,  $F_{yijss}(a)$  the steady state lateral force (Eq. 84) of the  $i, j$  wheel for a given slip angle  $a$ ,  $W_r/W_l$  the distance of the right/left wheel from the axle's centreline and  $T_{ij}$  the drive/brake torque on the  $i, j$  wheel respectively.

### 3.2.3.5.3 Dynamic stability and traction control; DSTC

The DSTC has been modelled as a simple yaw rate error  $\dot{\psi}_e$  controller (Eq. 108) with the desired yaw rate  $\dot{\psi}_d$  estimated as eq. (Eq. 109) [52, p. 231].

$$\dot{\psi}_e = \dot{\psi} - \dot{\psi}_d \quad \text{Eq. 109}$$

$$\dot{\psi}_d = \frac{\dot{x}}{R} = \frac{\dot{x}\delta_{ss}}{(f+b) + \frac{m\dot{x}^2(fC_{\alpha f} - bC_{\alpha r})}{2C_{\alpha f}C_{\alpha r}(f+b)}} \quad \text{Eq. 110}$$

The DSTC braking logic is summarized below:

Understeer, thus brake:

- 1) Rear left  $ESC_{rl}$ :  $\dot{\psi}_d > 0$  and  $\dot{\psi}_e < 0$ .
- 2) Rear right  $ESC_{rr}$ :  $\dot{\psi}_d < 0$  and  $\dot{\psi}_e > 0$ .

Oversteer, thus brake:

- 3) Front left  $ESC_{fl}$ :  $\dot{\psi}_d < 0$  and  $\dot{\psi}_e < 0$ .
- 4) Front right  $ESC_{fr}$ :  $\dot{\psi}_d > 0$  and  $\dot{\psi}_e > 0$ .

The DSTC logic has been implemented using continuous functions as in (Eq. 111) to (Eq. 114).

$$ESC_{rl} = \frac{1}{4} \left( 1 + \tanh \left( \frac{-\dot{\psi}_e}{a_{DSTC}} \right) \right) \left( 1 + \tanh \left( \frac{\dot{\psi}_d}{a_{DSTC}} \right) \right) \quad Eq. 111$$

$$ESC_{rr} = \frac{1}{4} \left( 1 + \tanh \left( \frac{\dot{\psi}_e}{a_{DSTC}} \right) \right) \left( 1 + \tanh \left( \frac{-\dot{\psi}_d}{a_{DSTC}} \right) \right) \quad Eq. 112$$

$$ESC_{fl} = \frac{1}{4} \left( 1 + \tanh \left( \frac{-\dot{\psi}_e}{a_{DSTC}} \right) \right) \left( 1 + \tanh \left( \frac{-\dot{\psi}_d}{a_{DSTC}} \right) \right) \quad Eq. 113$$

$$ESC_{fr} = \frac{1}{4} \left( 1 + \tanh \left( \frac{\dot{\psi}_e}{a_{DSTC}} \right) \right) \left( 1 + \tanh \left( \frac{\dot{\psi}_d}{a_{DSTC}} \right) \right) \quad Eq. 114$$

$$T_{ij} = ESC_{ij} \begin{pmatrix} -\frac{T_{init}}{2} \left( 1 + \tanh \left( \frac{\dot{\psi}_e - \dot{\psi}_t}{a_{DSTC}} \right) \right) (1 + T_{if}(\dot{\psi}_e - \dot{\psi}_t)) \\ -\frac{T_{init}}{2} \left( 1 + \tanh \left( \frac{\dot{\psi}_e + \dot{\psi}_t}{a_{DSTC}} \right) \right) (1 - T_{if}(\dot{\psi}_e + \dot{\psi}_t)) \end{pmatrix} \quad Eq. 115$$

The applied braking torque at individual wheel is given by (Eq. 115); it is a function of the  $\dot{\psi}_e$  (when the error is greater than the threshold  $\dot{\psi}_t$ ),  $T_{init}$  is a linear increase gain,  $T_{if}$  the increase factor and  $a$  the smoothness factor (c.f. Figure 46).

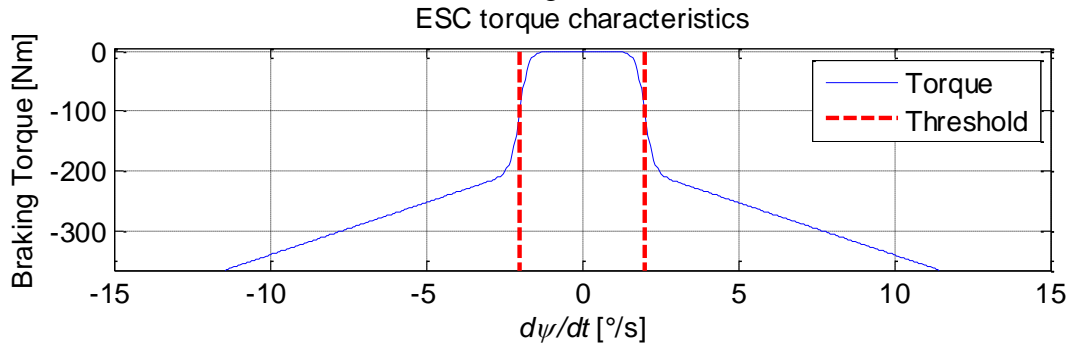


Figure 46 - DSTC torque characteristics;  $\dot{\psi}_e = 2^\circ$ ,  $T_{init} = 200 \text{ Nm}$ ,  $T_{if} = 5$  and  $a_{DSTC} = 0.005$ .

### 3.2.3.5.4 Two-track model optimization process

The optimal solution search is performed in 6 steps:

1) Set the start and finish point at the middle ( $Y$  position) of the 2 lines that define the lateral constraints of the track. The solution search was performed sequentially with  $n = 40, 60$  and  $80$  collocation points.

2) Solve the problem again using as a starting point the solution of the previous problem, without constraining the start ( $Y$  position) to the middle:  $n = 30, 50$  and  $80$ .

3) Add suspension-wheel kinematics and camber thrust (c.f. 3.2.3.5.1 and 3.2.3.5.2);  $n = 40, 60$  and  $80$ .

4) Add DTSC (c.f. 3.2.3.5.3);  $n = 20, 25, 40, 60$  and  $80$ .

5) Add tire lateral transient behaviour-dynamics (c.f. 3.2.3.5.2);  $n = 30$  and  $50$ .  $W_{t_f}$  (Eq. 59) is set to  $0.6$ .

6) Finally the solution is sought again incorporating all the above features but with increased number of body-points (c.f. 3.2.2);  $n = 30, 50, 60, 70$  and  $90$ .

## 3.2.4 Parameterization

The vehicle's nominal parameterization (c.f. Table 7) derives from Volvo's corresponding K&C measurements and design data. The vehicle's yaw inertia was estimated with the empirical formula  $I_z \approx 0.46mLw$  yielding a value of  $I_z = 3500 \text{ kgm}^2$ .

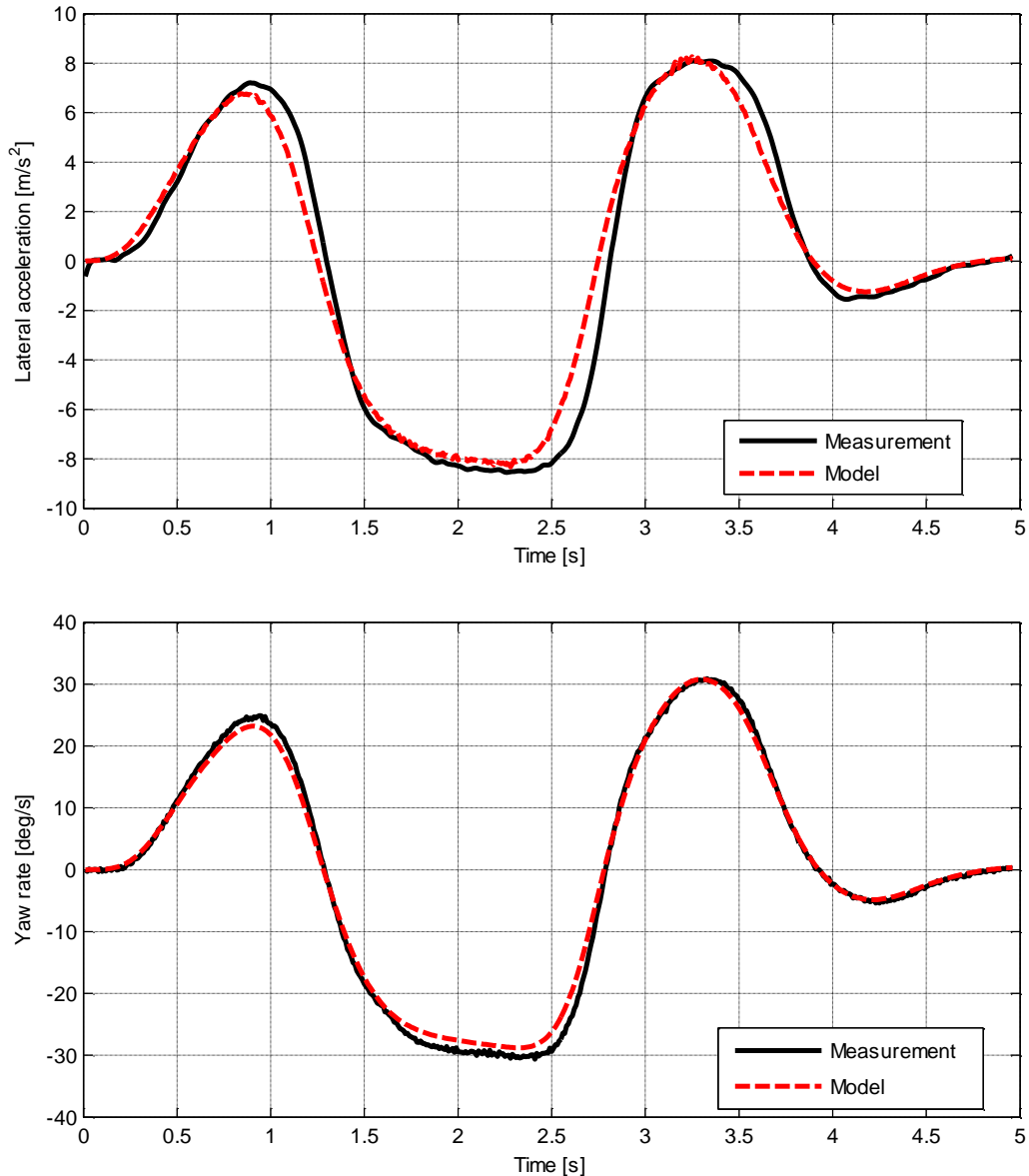


Figure 47 - Measured and simulated (STM) lateral acceleration (top) and yaw rate (bottom).

The Magic formula coefficients  $B$ ,  $C$ ,  $D$  [55] were estimated with DLC tests of the real S60 using a STM with non-linear tires; the recorded longitudinal velocity  $V_x$  and steering angle  $\delta$  were fed into the STM. The values were estimated by means of curve fitting using the *fmincon* function of Matlab (find minimum of constrained non-linear multivariable function). Physical DLC tests were performed with an actual Volvo S60 using a SR60 standard robot by Anthony Best Dynamics; the logged steering wheel angle and longitudinal speed were fed to the STM as inputs.

The minimization objective was the RMS error of lateral acceleration and yaw rate between the model and the real vehicle. The error derived from 9 DLC tests averaged together to avoid over fitting. The optimization process was run multiple times from different starting values, i.e. guesses, such that the case of local optima around a global one would be considered. Figure 47 illustrates the model measured and simulated results using the STM after the optimization process.

Table 7. VDM nominal data.

Parameter description	Value
Model name	Volvo S60, T5 automatic, 2011
Mass (driver + equipment) (m)	1823 kg
Yaw moment of inertia ( $I_z$ )	3500 kgm <sup>2</sup>
Body: length/width ( $v_{length}/v_{width}$ )	4.635/1.865 m
Wheelbase/ track width ( $L/t_W$ )	2.776/1.588 m
Distance of CoG from front/rear axle ( $f/b$ )	1.104 /1.666 m
Height CoG/ roll centre front/rear ( $h/e_f/e_r$ )	0.5/0.12/0.24 m
Roll stiffness: front/rear ( $K_f/K_r$ )	45/37.5 kNm/rad
Steering: maximum angle/rate ( $\delta_{max}/\dot{\delta}_{max}$ )	31°/720 °/s
Roll steer: front/rear ( $\frac{\partial \delta_f}{\partial \varphi} / \frac{\partial \delta_r}{\partial \varphi}$ )	0.123/0.007
Tires: pneumatic trail at linear range/ relaxation ( $t_{pij}/L_{relax}$ )	0.033/0.3 m
Tires-wheels	225/40/R18
Wheel radius (r)	0.316 m
Magic formula: B/C/D	7.541/1.490/1.123

## 3.3 DLC Optimization RESULTS

### 3.3.1 Sensitivity analysis

Table 8 shows the maximum entry speed achieved for different tuning setups by changing the front  $K_f$  and rear  $K_r$  roll stiffness, the front  $\frac{\partial \varepsilon_f}{\partial \varphi}$  and rear  $\frac{\partial \varepsilon_r}{\partial \varphi}$  camber gain, camber stiffness  $C_\gamma$  and the front  $\frac{\partial \delta_f}{\partial \varphi}$  and rear  $\frac{\partial \delta_r}{\partial \varphi}$  roll steer coefficient.

Table 8. Maximum entry speed (km/h) with tire lateral dynamics disabled (Eq. 103) and DSTC enabled while changing (multiplied with a gain factor  $G$ ) one feature value and keeping ( $G = 1$ ) the rest at their nominal values.  $G$  ranges from 0.25 (25%) up to 3 (300%). The entry speed with the nominal values was 70.8 km/h, the greatest was 73.25 km/h and the smallest was 69.43 km/h.

	$G$	3.00	1.50	1.00	0.75	0.25
Features	$K_f$	73.25	72.23	70.80	70.75	70.10
	$K_r$	70.93	70.85	70.80	72.39	72.68
	$C_\gamma$	69.43	70.56	70.80	71.08	72.69
	$\frac{\partial \varepsilon_f}{\partial \varphi}$	71.01	70.92	70.80	71.24	70.86
	$\frac{\partial \varepsilon_r}{\partial \varphi}$	72.09	71.19	70.80	70.83	70.45
	$\frac{\partial \delta_f}{\partial \varphi}$	72.08	70.96	70.80	71.13	72.06
	$\frac{\partial \delta_r}{\partial \varphi}$	70.91	72.14	70.80	72.02	70.97

### 3.3.2 Four optimization cases

Enabling the tire lateral dynamics and disabling the DSTC and by selecting the feature value which gave the maximum (Max) and minimum (Min) entry speed per row in Table 8, as well-as the nominal (Nom) features yielded 69.78, 64.16 and 68.60 km/h of entry speed correspondingly. Those three are illustrated in conjunction with a fourth optimization through Figure 48 to Figure 52 which had the nominal feature values (Table 7) and both DSTC and tire dynamics enabled (Nom DSTC) which yielded 71.99 km/h. Figure 53 displays the trajectory and DSTC related results from the Nom DSTC case.

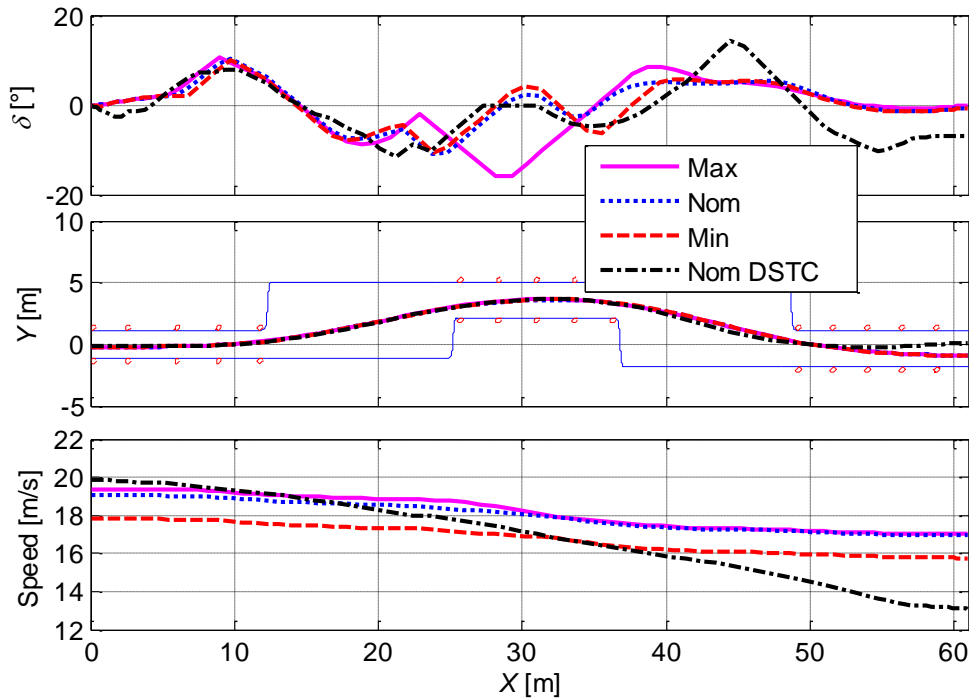


Figure 48 - Front wheels' steering angle  $\delta$  (top), lateral position  $Y$  (middle) and resultant speed (RMS of longitudinal and lateral speed) (bottom) for the optimization cases described in 3.3.2. The DSTC is disabled for the Max, Nom and Min cases and is enabled for the Nom DSTC case. Although all four cases had similar trajectories  $Y$ , the optimal steering angle  $\delta$  and velocity profile were considerably different; the Nom DSTC case has the highest entry speed (71.99 km/h).

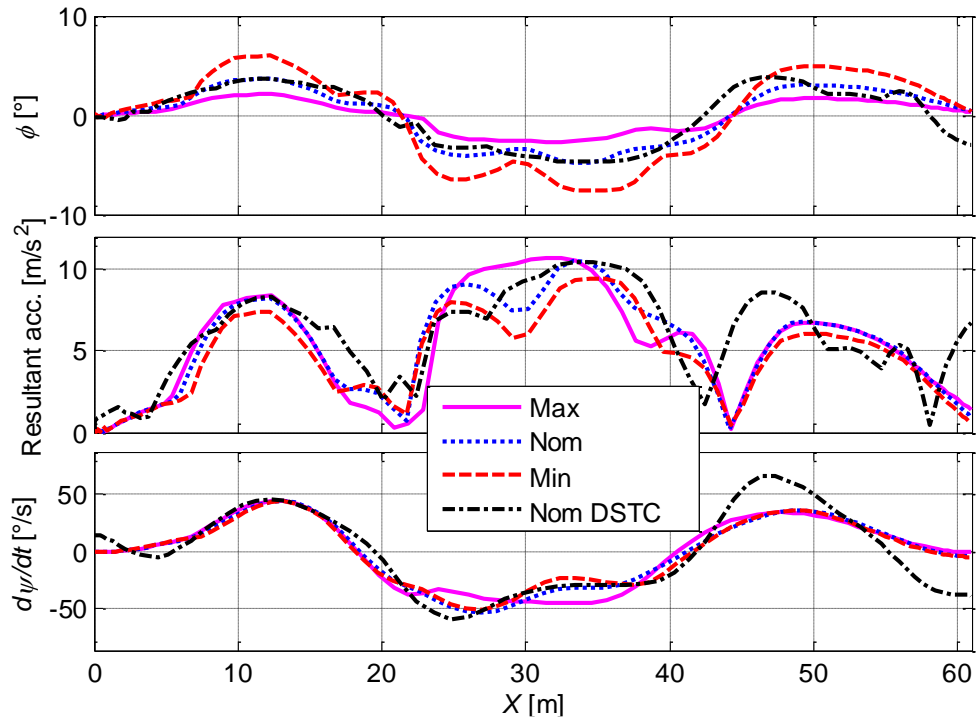


Figure 49 - Vehicle's roll angle  $\phi$  (top), resultant lateral acceleration (RMS of longitudinal and lateral acceleration) (middle) and yaw rate  $\dot{\psi}$  (bottom) for the optimization cases described in 3.3.2. The DSTC is disabled for the Max, Nom and Min and is enabled for Nom DSTC case. The Min yielded the greatest in magnitude roll angle due to the small roll stiffness value. The resultant acceleration and yaw rate start to considerably differ at approximately  $X = 20 \text{ m}$ .

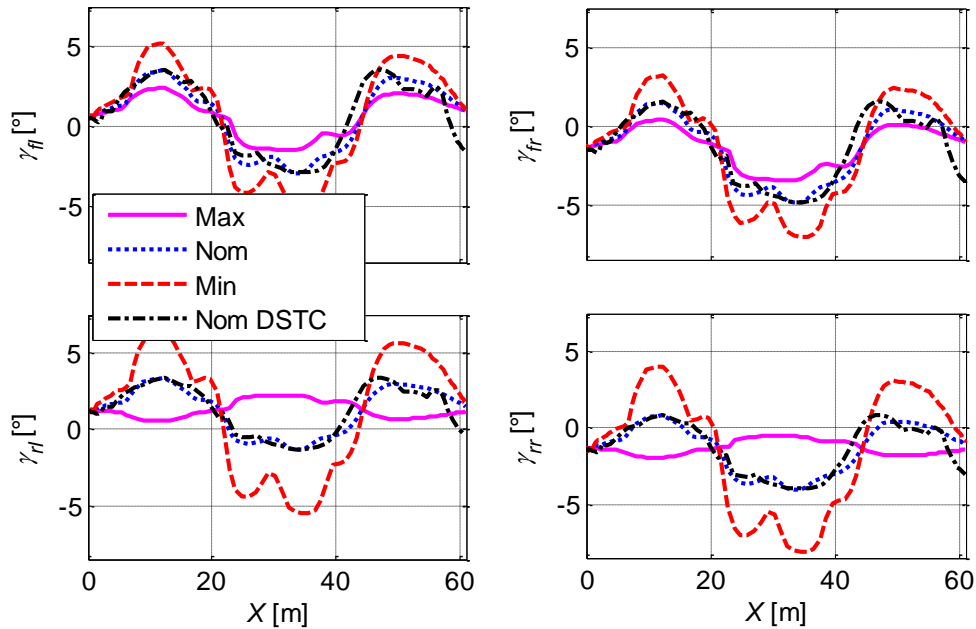


Figure 50 - Camber angles  $\gamma_{ij}$  (Eq. 101) for the optimization cases described in 3.3.2. The DSTC is disabled for the Max, Nom and Min and enabled for Nom DSTC case. The Min yielded the greater in magnitude camber values due to the small roll stiffness value and highest roll angles correspondingly (c.f. Figure 49).

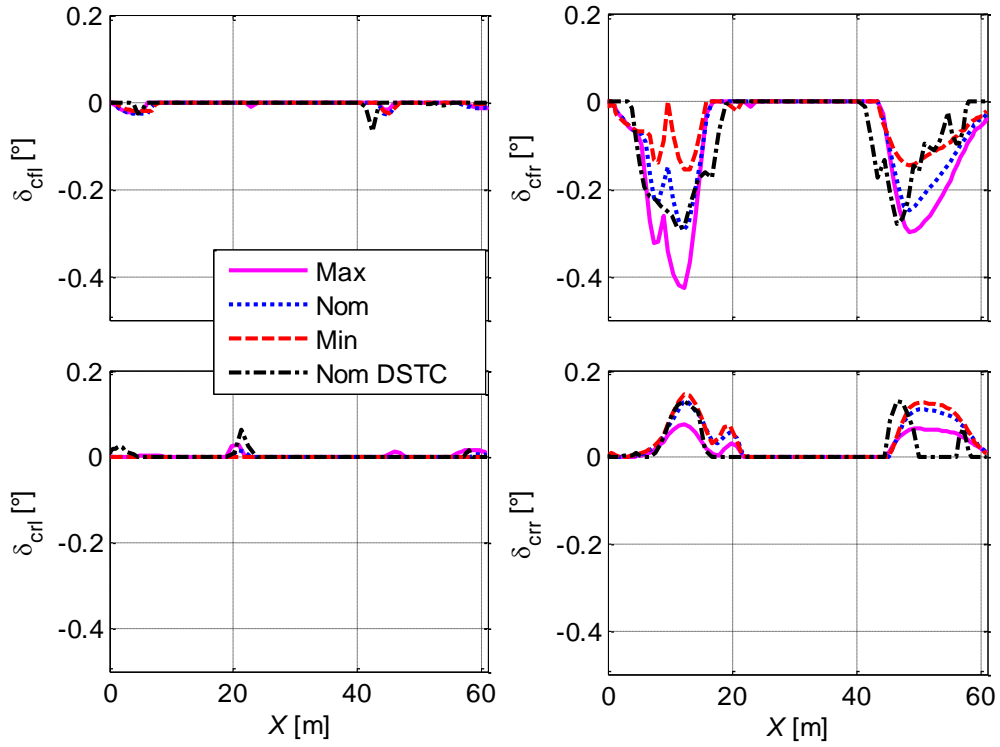


Figure 51 - Lateral force compliance steer  $\delta_{cij}$  (Eq. 96) for the optimization cases described in 3.3.2. The DSTC is disabled for the Max, Nom and Min and enabled for Nom DSTC case. On the 1st left turn the outer wheels (right) have considerable compliance steer while on the 2nd right turn the outer wheels (left) have almost negligible compliance steer due to the vanishing pneumatic trail (c.f. Table 5) modelled as in [58].

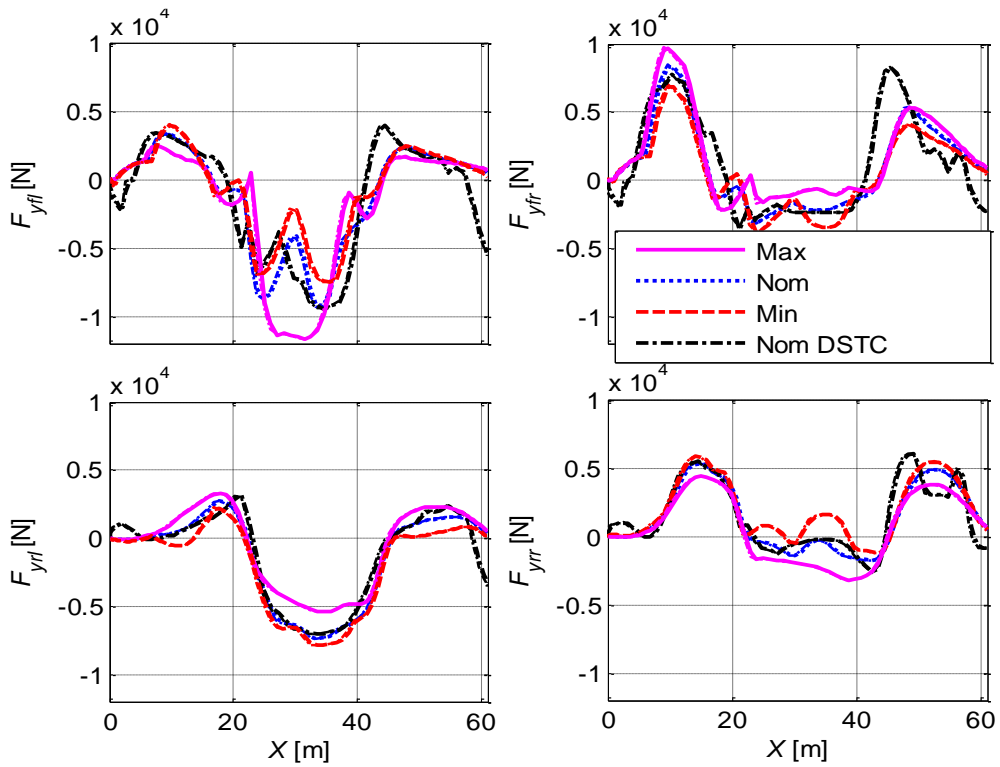


Figure 52 - Steady state  $F_{yij_{ss}}$  (thin lines) and transient  $F_{yij}$  (thick lines) lateral force (Eq. 104) for all four wheels for the optimization cases described in 3.3.2. The DSTC is disabled for the Max, Nom and Min and enabled for Nom DSTC case. The  $F_{yij}$  lags behind the  $F_{yij_{ss}}$  but the difference is minor and virtually invisible in the figure's print size.

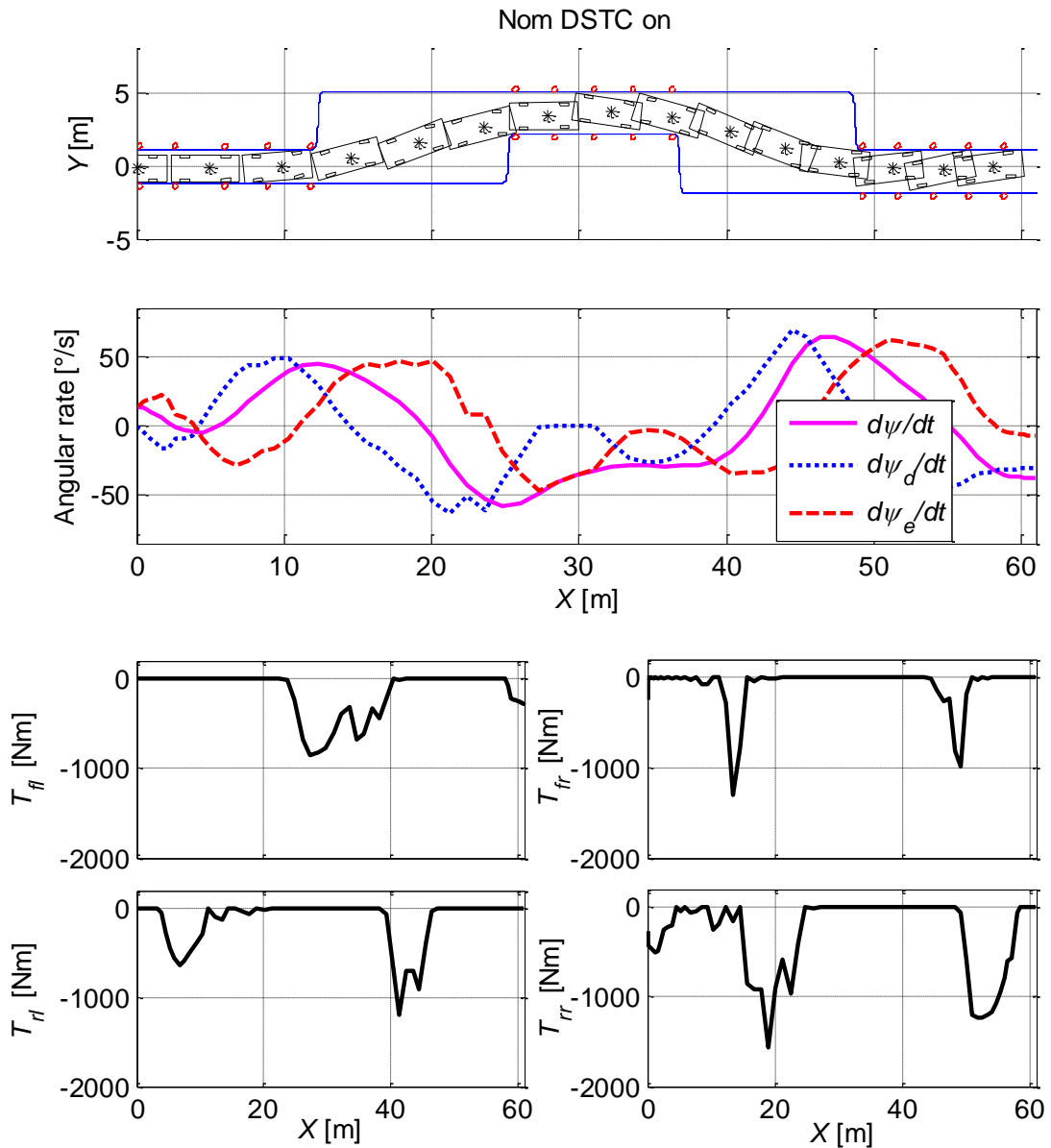


Figure 53 - DSTC Nom case results (c.f. 3.3.2); bird's eye view (body and the front wheels angles  $\delta$ ) of the vehicle (top), angular rates ( $\dot{\psi}$ ,  $\dot{\psi}_d$  and  $\dot{\psi}_e$ ) and braking torques  $T_{ij}$  from the DSTC. Individual vehicle frame in the trajectory subplot is 0.25 s apart from its neighbours; the vehicle develops high side-slip angle values especially at the end of the manoeuvre. The DSTC brakes the rear left wheel to compensate for small in magnitude  $\dot{\psi}$  in the 1st left turn, then the front right wheel to compensate for the increased in magnitude  $\dot{\psi}$  and so on according the logic described in 3.2.3.5.3.

## 3.4 Discussion

This paper proposed a method for generating the optimal steering control which maximizes a vehicle's entry speed for the ISO3888 part-2 double-lane change (DLC) manoeuvre (c.f. Figure 45). The proposed method involves an iterative process, starting from a centreline guess with the results being used as guess to the next more sophisticated vehicle dynamics model (VDM); the final VDM comprised of a 7-DOF VDM, non-linear tires with transient effects and suspension properties as-well-as a simplified dynamic stability and traction

control (DSTC). The optimal control problem is converted into a finite dimensional optimization problem using a direct transcription method and is solved using TOMLAB/PROPT [49] in Matlab.

### **3.4.1 Real vehicle testing and validation**

The same steering robot (SR60) and car used to estimate certain vehicle parameters (c.f. 3.2.4) were used to evaluate the method. The maximum entry speed achieved with the SR60, by manually tuning its control parameters for the DLC manoeuvre (a long iterative process necessitating multiple DLC runs without ensuring optimality), was 74.34 km/h and 65.88 km/h with and without DSTC respectively. It is hypothesized that a better tuning could have yielded higher entry speeds (the 1<sup>st</sup> author of the paper achieved more than 68 km/h in wet-driving with the DSTC disabled). The optimization results (c.f. 3.3.2) were 71.99 km/h and 70.80 km/h respectively. For comparison purposes, online reports for the DLC manoeuvre suggested maximum entry speed for the: Volvo S60 Polestar (STCC Racecar) 78 km/h, Audi A4 TDI 72 km/h, BMW 320d 74 km/h, BMW 335i AWD 75 km/h; the online sources are not verified and the authors do not take responsibility for the validity of the measurements.

To evaluate the feedforward-control potentials of the method, the generated optimal steering control input for the nominal simulated S60 was applied with the steering robot to the actual car. This method was expected to be fallible; any discrepancy between the model and the real vehicle (oversimplified DTSC etc.) and the testing surface would accumulate error. Multiple runs with the same steering angle and velocity profile yielded different trajectories suggesting that the current method has to be extended-improved.

Results from the steering robot testing session are located at the Appendix chapter 6.4.

### **3.4.2 Future work**

To improve realism, the VDM complexity as-well-as the modelled DSTC (c.f. 3.2.3.5.3) should become more sophisticated. Still though, despite the fact that the a sophisticated VDM can realistically model the tires, the vehicle's suspension characteristics as-well-as the DSTC functionalities, the final judgement of the vehicle is done with physical testing; this work will utilize the optimal steering input generated in a feed-forward manner and employ a feedback controller, which will compensate for the modelling errors and external disturbances during testing. Real vehicle tests will be used to verify its performance.

### **3.4.3 Rationale of this work and vision**

It is envisioned that manufactures in an effort to increase efficiency, promote safety and reduce prototype vehicles will tune and develop various dynamic related systems (DSTC, steering system, suspension etc.) using CAE tools. Besides the reduced cost and lead-time, CAE will facilitate objective assessment of the car's safety and numerically optimized tuning sets; safer and better cars for the road.

# 4 LANE KEEPING AID OPTIMIZATION

This research aims to optimize the torque profile that will be applied on the steering wheel in a Lane Keeping Aid (LKA) intervention (c.f. Figure 54) in order to maximize the vehicle's heading angle change. Influence of the driver's arms neuromuscular (NMS) characteristics was investigated during physical testing, and a driver dynamical model was built and optimized to best fit the results of physical tests. The rationale is to employ the knowledge of the driver's arm NMS admittance levels for tuning the driver-steering interface, e.g. EPAS properties, LKA torque intervention levels. The study has been performed in the Volvo Vehicle Dynamics & Active Safety department.

## 4.1 Problem statement

Vehicle and driver behaviour could be investigated and modelled to develop the overall system which can then be designed using CAE and mathematical optimization methods. Driver characteristics are affected from various factors; driver's experience, awareness level, gripping force [59]. During an evasive manoeuvre (such as the DLC) [60], driver's employs higher co-contraction in the his arms (making them stiffer), which actually means that he doesn't allow the steering wheel to move and tries to counteract to any external disturbance. This research aims in the development of a method that will allow us to develop better driver assist functions that will also include driver's reaction. In order to achieve this, tests were performed in a Volvo V60, modified to provide steering torque disturbances. During the physical testing phase, steering torque disturbances were applied and steering wheel angle was measured to assess the driver's arms' admittance.

A 2-stage optimization (two-stage optimization manner) was used with the purpose of 1<sup>st</sup> identifying the driver parameters (using data from the test-track experiments) and 2<sup>nd</sup> optimizing the steering torque profile (input of the system), with an objective function of maximizing vehicle's heading angle change.

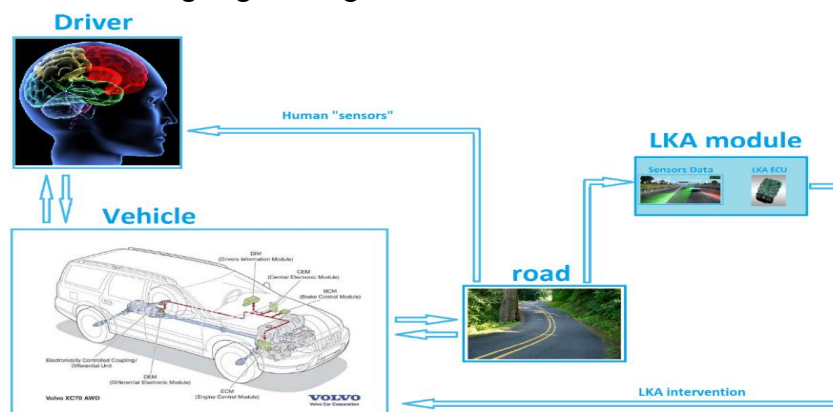


Figure 54 - LKA system layout.

# 4.2 Methodology

## 4.2.1 Car setup

The test vehicle was a Volvo V60 2013 (c.f. Figure 55), equipped with an Autobox control unit (c.f. Figure 58), controlling the stock EPAS motor (Controlled-EPAS). A MicroAutoBox control unit was used to execute Matlab/Simulink blocks in real time and request specific torque interventions in an automated order. All the Input/output data were logged in the host PC (c.f. Figure 56) via the dSPACE ControlDesk interface, which was also displaying all the vital information in the passenger cabin.

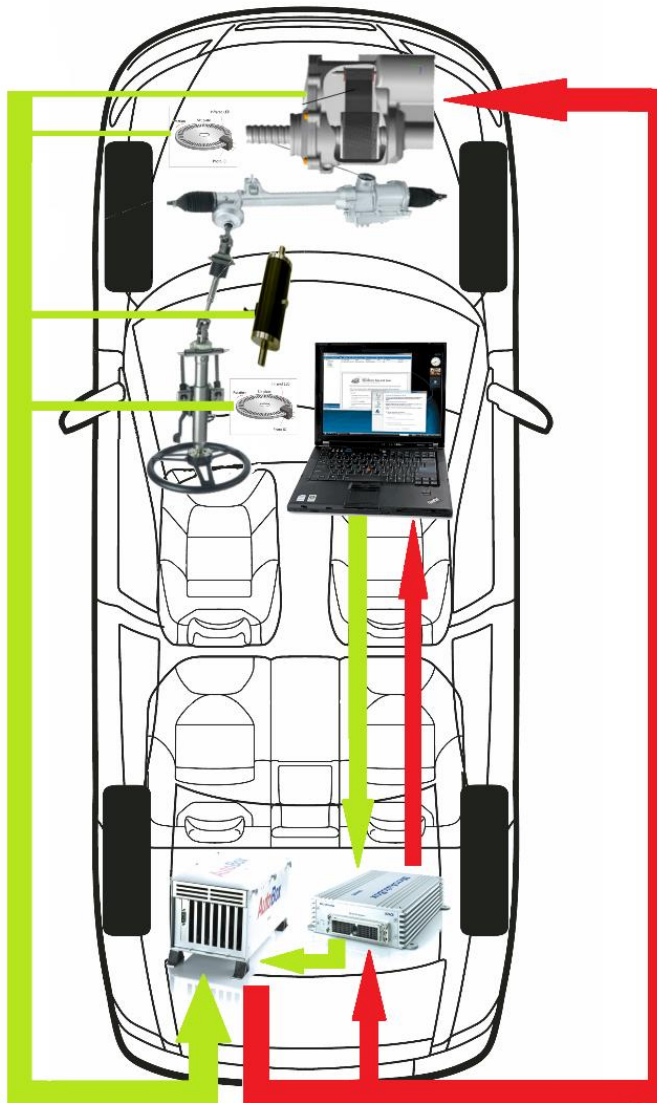


Figure 57 - Test vehicle's instrumentation architecture. Green arrows illustrate input connections.



Figure 55 - Test Vehicle.



Figure 56 - Computer mounted inside the vehicle.



Figure 58 - AutoBOX and Microautobox controllers.

The steering system of the vehicle used, which can be seen in detail in Figure 59, consists of:

- a variable ratio rack and pinion system, which was modelled in Simulink using a 1-dimensional lookup table (c.f. Figure 65 - Figure 66).
- a power assist unit, which was a standard EPAS with a special firmware in the ECU allowing external torque interventions to be requested directly (bypassing the stock LKA system).
- a torque sensor ,mounted on the torsion bar
- a angular position sensor mounted on the steering wheel.
- a supplementary angular position sensor mounted on the steering column from the yoke side.

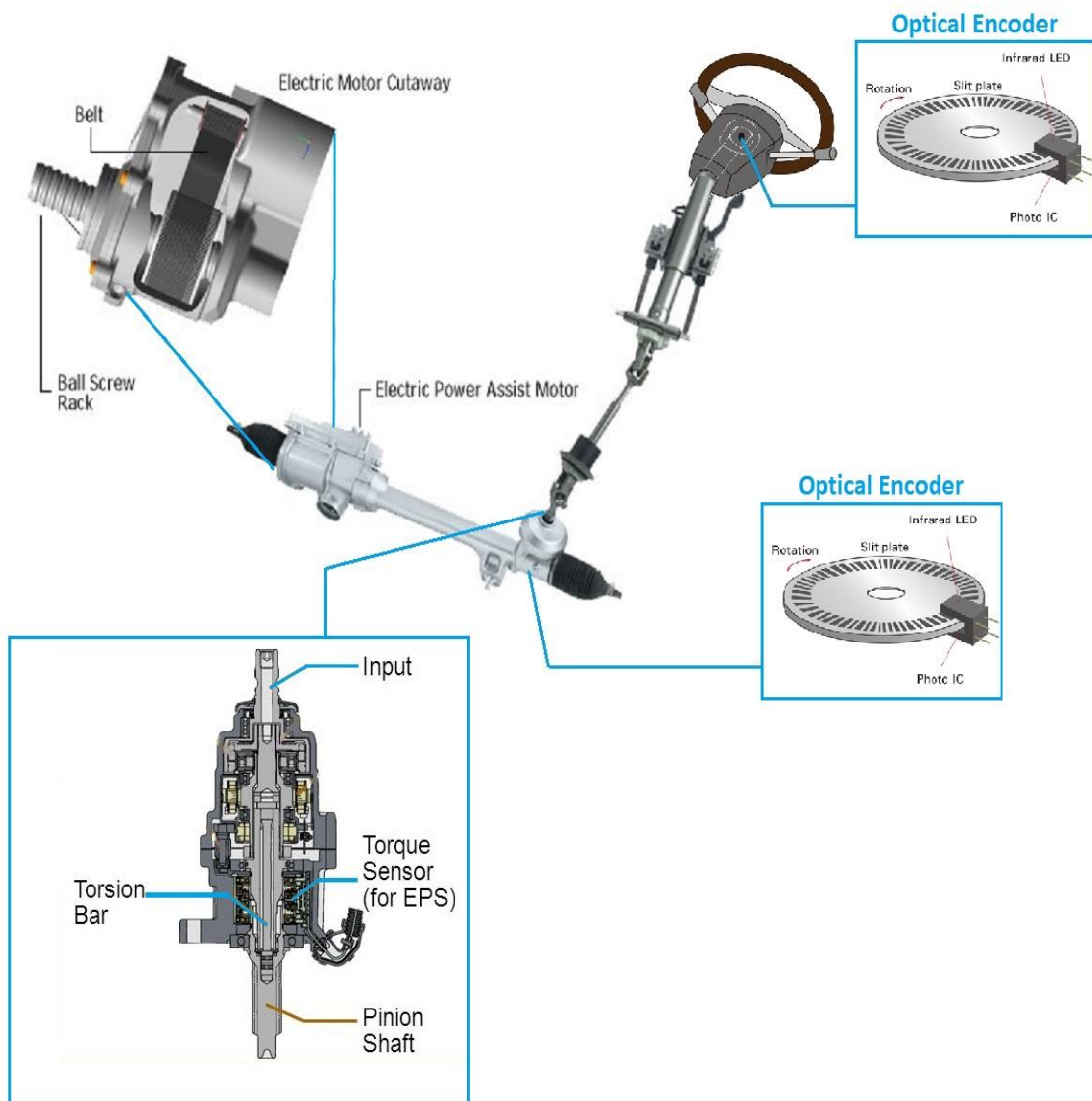


Figure 59 - Car steering system.

## 4.2.2 Preliminary Testing

In order to identify the main aspect of the driver's behaviour, some preliminary tests were conducted, which aimed to clarify how a driver responds when a steering wheel torque intervention is employed.

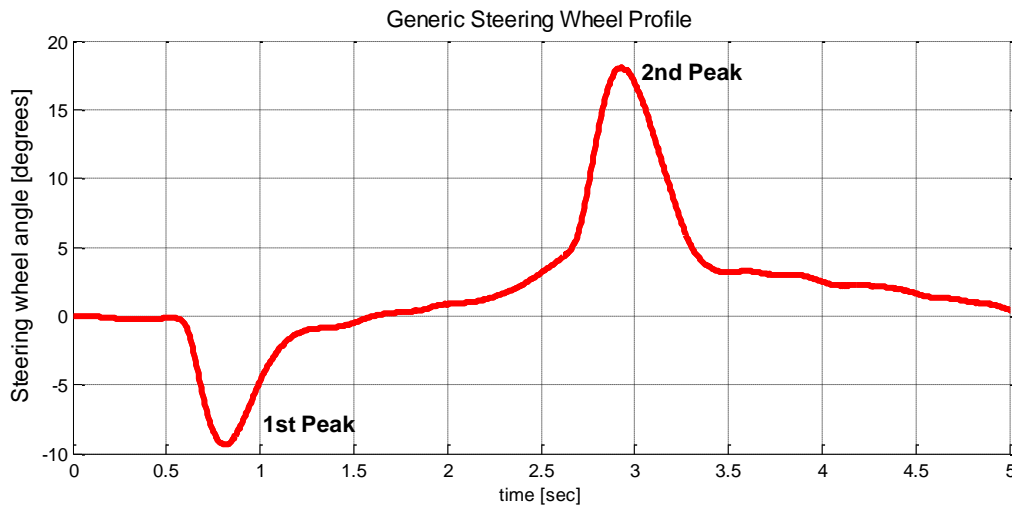


Figure 60 - A generic Steering wheel profile during the torque intervention.

The results from the preliminary physical testing indicate that there is a pattern (c.f. Figure 60), which seems to exist in most driver's reaction.

This generic pattern suggests that the steering wheel angle profile usually contains two overshoots. The 1<sup>st</sup> overshoot is due to the torque that is being applied at the beginning of the intervention, while the 2<sup>nd</sup> peak is at the instant that the torque stops being applied (end of the intervention). At that moment, the driver can't respond fast enough (stop counteracting) so the result is a torque to the opposite direction of the intervention, which steers the steering wheel.

Other useful observations from the preliminary test, suggest that when the driver is not actively steering (the steering wheel angle is close to 0° at the beginning of the intervention) are usually more consistent.

## 4.2.3 Physical Testing

After the preliminary testing session, the parameters, which could have a significant effect to driver's reaction were identified. Those parameters were considered to be:

- Torque Amplitude
- Existence of vibrations in the torque
- Road width
- Vehicle speed

The final experiments were designed and physical tests have been conducted in Volvo Proving Ground in Hällered and AstaZero active safety test area (c.f. Figure 61 - Figure 62), where drivers experienced a series of steering torque interventions. All vehicle states (e.g. velocity, lateral acceleration, yaw rate, etc.) have been logged (c.f. Figure 64) in the host PC and were later post-processed.

A total of 48 drivers were tested on 3 different test scenarios with 17 different torque profiles.

All the interventions started at random times towards a random direction without a predefined sequence in order to reduce driver adaptation. The test subjects didn't have complete knowledge about the purpose of the tests they were participating in. However, they still were aware that they were participating in an experiment, which consequently means that they were more observant than normal.

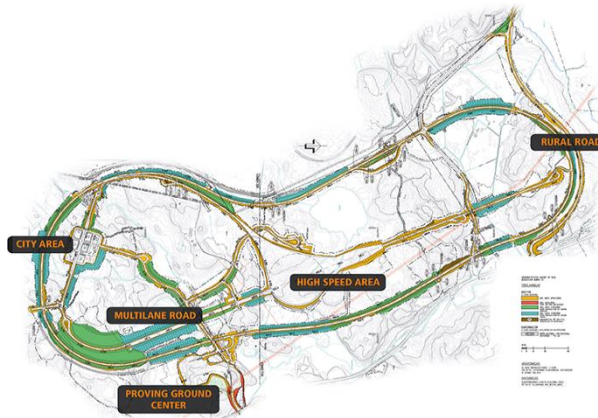


Figure 61 - AstaZero test environment.



Figure 62 - An instance of testing.

The test variables took values between the boundaries provided in the following table:

Table 9. Test variables boundaries.

Test Variable	Units	Lowest value	Highest value
Torque amplitude	Nm	1	4
Torque amplitude rate	$\frac{Nm}{s}$	5	20
Sinusoidal vibration amplitude	Nm	0	2
Road width	m	0.5	10+
Vehicle longitudinal velocity	$\frac{km}{h}$	30	100

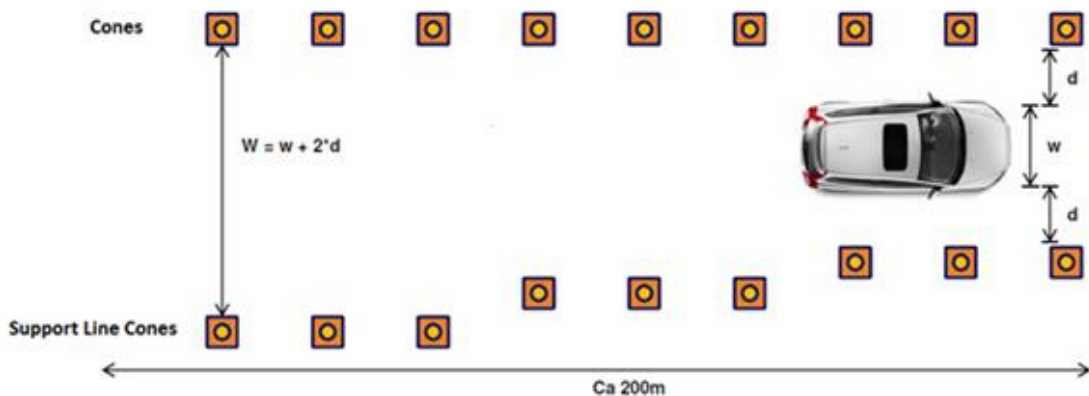


Figure 63 - Variable road width setup with cones; In the 3rd test the vehicle was limited to travel between 2 lines of cones, which were set at different distances.

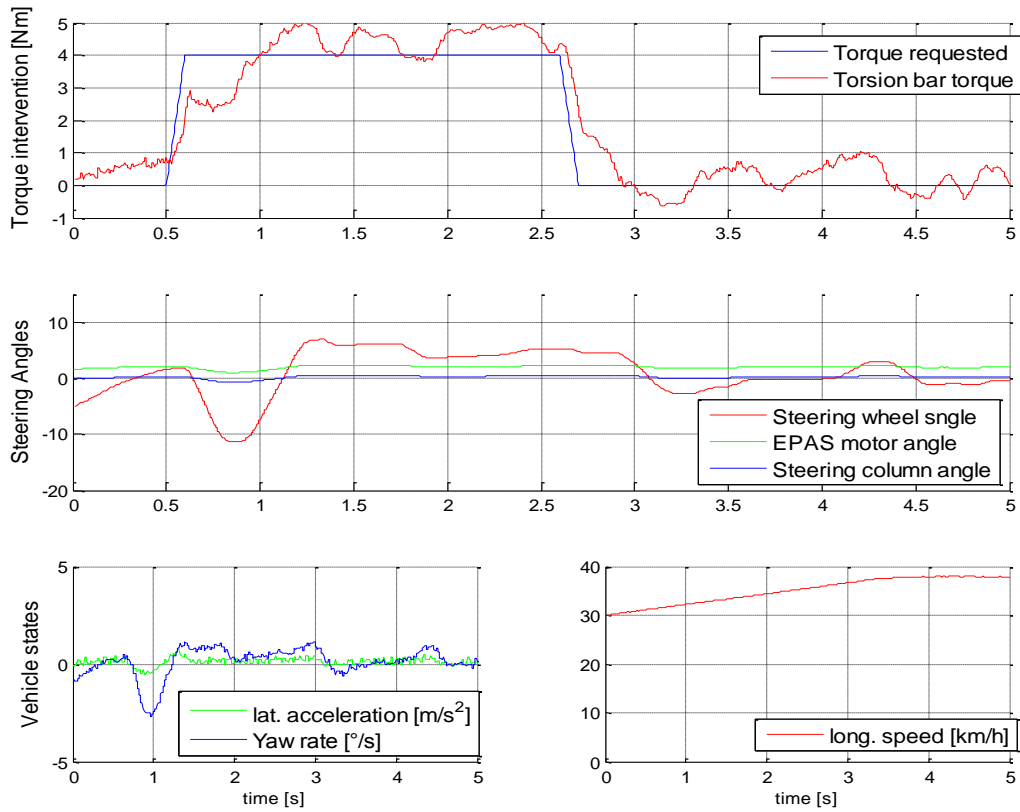


Figure 64 - Example of a test run. The vehicle and the steering states that have been logged are illustrated.

## 4.2.4 Test Data Post-processing

During data post-processing, the stock Steering wheel angle sensor data were found to be filtered. Since the interventions contained sinusoidal torque vibrations, which were transferred to the steering wheel, unfiltered data, that could as much frequency content as possible, were needed.

The following algorithm was used to calculate the steering wheel angle utilizing the steering column angle and the steering column torque data.

1. Steady state error ( $e_{ss}$ ) between the steering wheel and the steering column sensor was calculated at the point that the torsion bar torque was zero<sup>30</sup> (or as close to zero as possible).
2. The steering wheel angle was calculated as (Eq. 116) , (c.f. Figure 67):

$$\theta_{sw} = \theta_{clmn} - e_{ss} + \frac{T_d}{t_{stiff}(\theta_{clmn} - e_{ss})} , \quad \text{Eq. 116}$$

where  $T_d$  is the torsion bar torque measured.

Torsional stiffness was considered to be a function (c.f. Figure 68) of steering wheel angle (in order to properly model the steering column compliances) and was modelled in Simulink using a 1-dimensional Lookup Table. The variable-steering-ratio (c.f. Figure 65 - Figure 66) was also modelled in Simulink and was included in the steering wheel angle estimation.

<sup>30</sup>Zero torque on the torsion bar translates to a theoretical zero rotational deformation

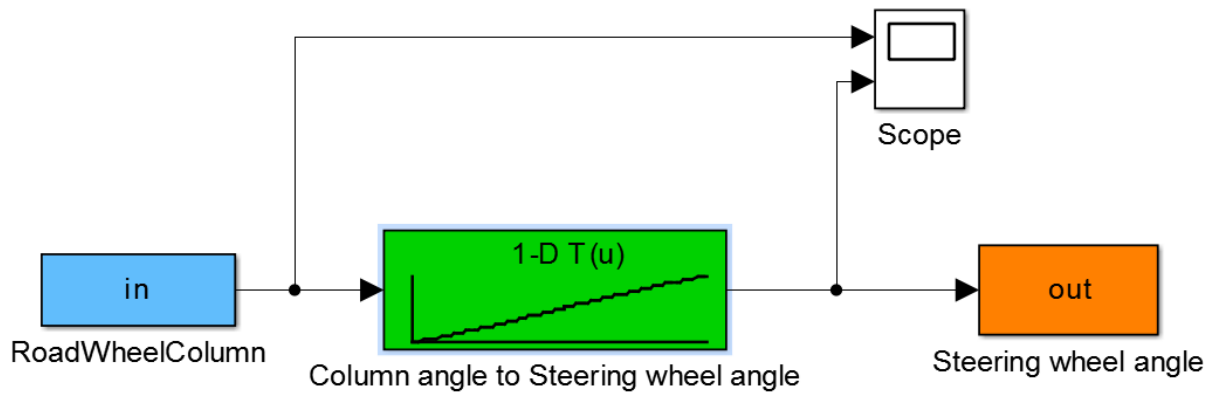


Figure 65 - Implementation of variable steering ratio.

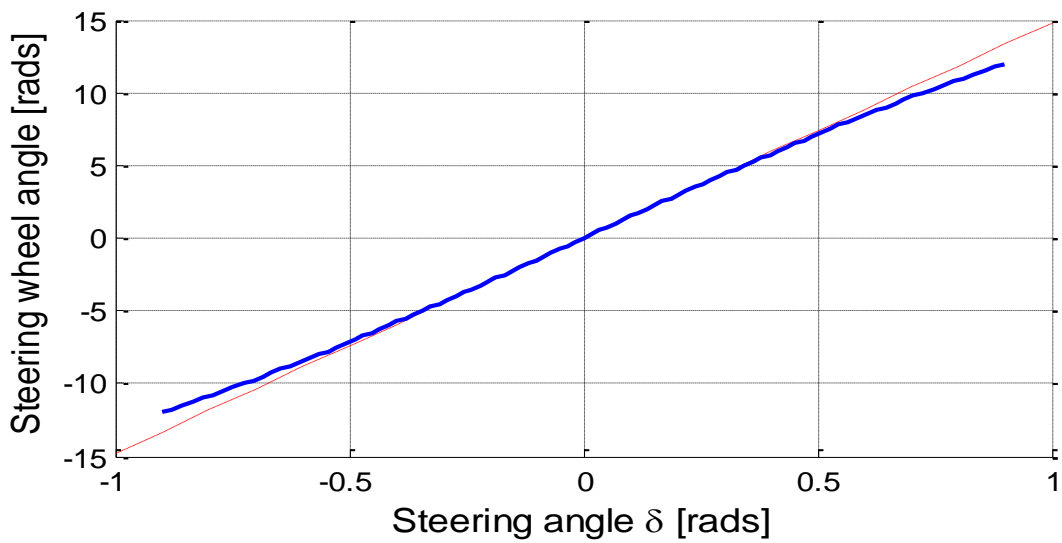


Figure 66 - Comparison with steering ratio 14.8.

The Simulink model that allowed us to convert the steering column angle to steering wheel angle can be seen in the next figure.

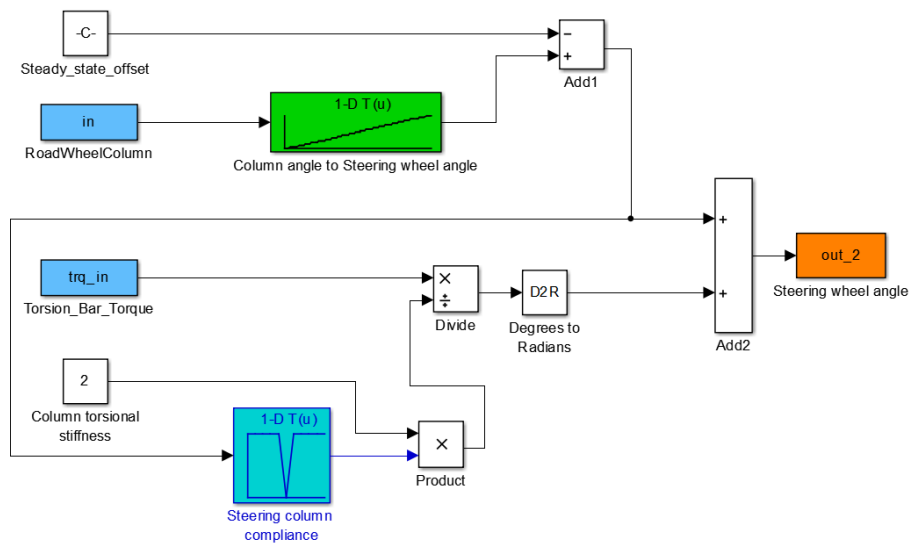


Figure 67 - Steering column sensor to steering wheel angle conversion.

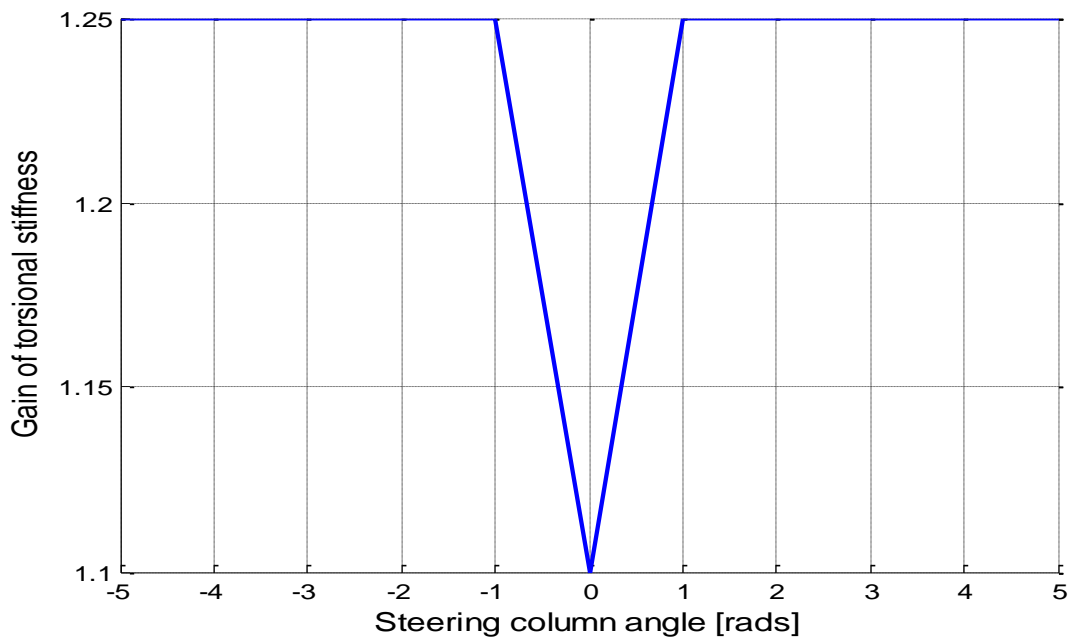


Figure 68 - Steering column compliance.

An example of the steering wheel angle estimation can be seen in the following figure.

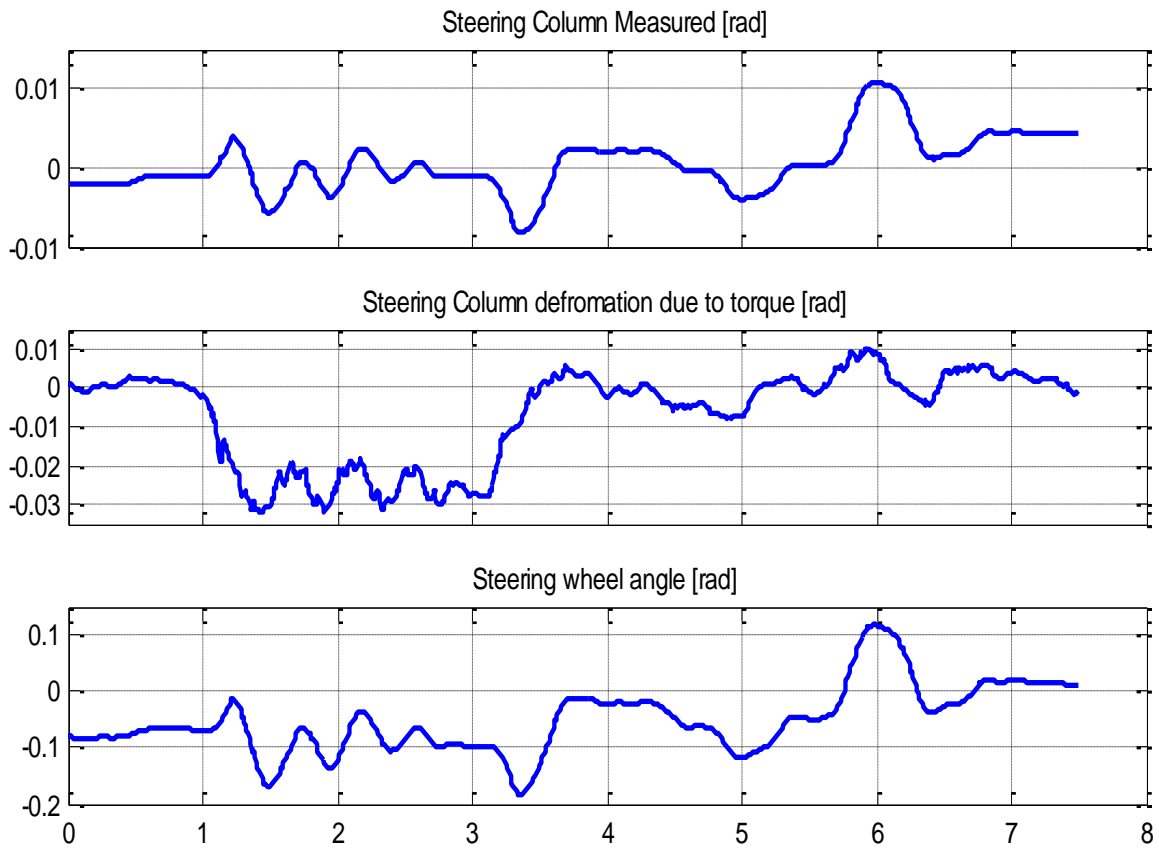


Figure 69 - Steering column angle measured and converted to steering wheel angle.

A statistical hypothesis test (student's t-test) has been performed (c.f. Figure 70), which determined that the variations between the tests data logged were generally significantly different for different test scenarios. The statistical-significant difference indicated as well that the selected test variables affected driver's behaviour.

More test data can be found in the Appendix chapter 6.4.

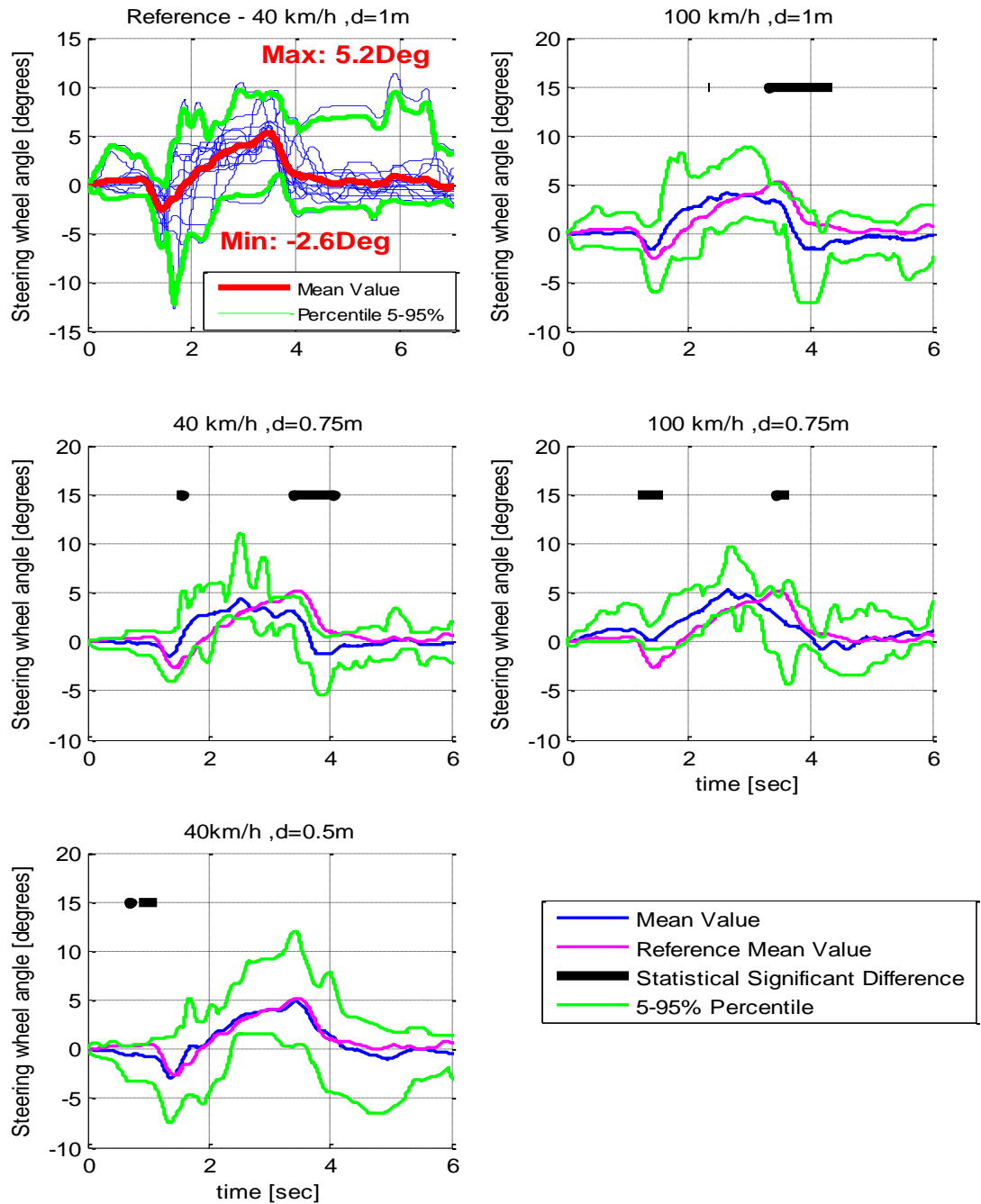


Figure 70 - t-test results; test runs were categorized according to vehicle speed and road width. When the driver is driving faster, his muscles are more co-contracted, which results in stiffer grip of the steering wheel, this concludes in smaller steering wheel angle overshoot. The effect of the road width is similar, when the driver drives on a wider road, he feels more relaxed and safe and therefore he is allowing a higher lateral deviation.

## 4.2.5 Driver Behaviour Model

Based on the post processing of the test data, the unaware driver<sup>31</sup> is believed to counteract on a steering torque intervention in an effort to maintain his desired path.

The developed driver behaviour model consists of two mass spring damper systems. The 1<sup>st</sup> system's input is torque, while the 2<sup>nd</sup> system's input is the derivative of torque.

The 1<sup>st</sup> system models the driver's attempt to keep the steering wheel angle close to zero, this leads to steering towards the opposite direction of the intervention.

The 2<sup>nd</sup> system models the inability of the driver to respond fast enough, when the rate of change of the torque is high. In that situation the driver tends to steer towards the same direction as the derivative of the torque. If the torque is increasing faster than driver's ability, then he will steer towards the side of the intervention. If the torque is decreasing faster than the driver can respond then he will steer towards the opposite direction of the intervention (because of the torque he is already applying to counteract it).

In both systems, the torque signal used was the torsion bar torque signal, which is considered to represent the torque that the driver is feeling through the steering wheel.

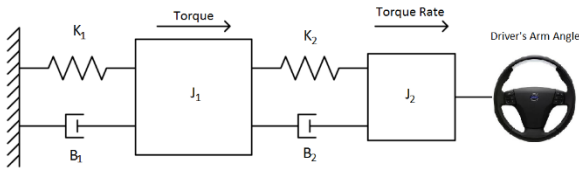


Figure 71 - Driver's dynamical model used.

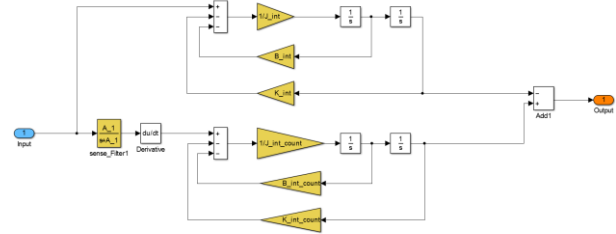


Figure 72 - Driver's dynamical model; Simulink implementation.

A filter was used to add a slight delay that models the driver's response time. The "filter" is modelled as a linear time-invariant (LTI) system, whose transfer function is (Eq. 117) and has the impulse response (Eq. 118)

$$H(s) = \frac{A_{-1}}{s + A_{-1}} \quad \text{Eq. 117}$$

$$h(t) = A_{-1} * e^{-A_{-1}*t} = A_{-1} * e^{-t/\tau}, \quad \text{Eq. 118}$$

where  $t \geq 0$  and  $\tau = \frac{1}{A_{-1}}$  is the time constant.

The system variables were identified (c.f. Figure 73) using an offline optimization process with Genetic algorithm, where the objective function (also known as fitness function in GA) was to minimize the error between the Model's response and the actual Test driver's response.

<sup>31</sup>As it has already been mentioned, the drivers were unaware of the intervention, however they knew that were participating in a test. This means that they were more focused than everyday driving. The observation that the driver is trying to counteract any steering intervention might not be correct if the drivers are distracted.

Table 10. Driver behaviour model control variables boundaries.

Control Variable	Description	Units	Lower bound	Upper bound	Optimized Value
$K_{int}$	1 <sup>st</sup> M-S-D system - stiffness	$\frac{Nm}{rad}$	10	100	96.377
$J_{int}$	1 <sup>st</sup> M-S-D system - moment of Inertia	$kg * m^2$	0.001	0.05	0.031
$B_{int}$	1 <sup>st</sup> M-S-D system - damping	$\frac{Nm}{rad/s}$	0.01	10	0.963
$A_{-1}$	2 <sup>nd</sup> M-S-D system - time constant	Hz	5	100	96.332
$K_{int\_c}$	2 <sup>nd</sup> M-S-D system - stiffness	$\frac{Nm}{rad}$	20	100	41.512
$J_{int\_c}$	2 <sup>nd</sup> M-S-D system -moment of Inertia	$kg * m^2$	0.5	2	0.643
$B_{int\_c}$	2 <sup>nd</sup> M-S-D system - damping	$\frac{Nm}{rad/s}$	1	15	9.368

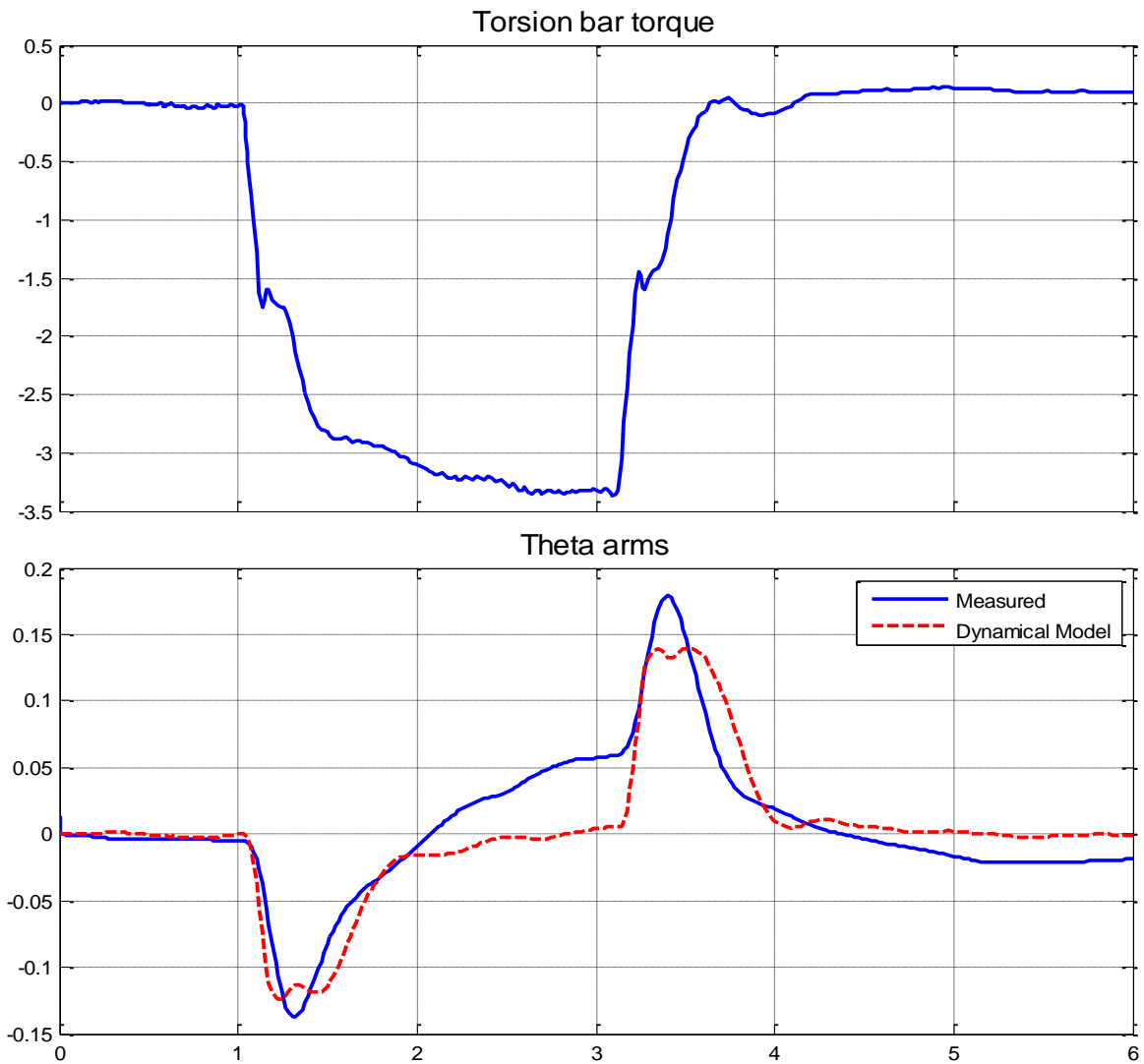


Figure 73 - Model's dynamical response in comparison to measured response. Theta arms represents the driver's arm angle, which is considered to be equal with the steering wheel angle.

## 4.3 Optimization Results

Optimization of the torque intervention profile was done with genetic algorithms. Each torque characteristic is represented using one gene. A chromosome is a set of parameters (genes) which define a proposed solution to the optimization problem. The solution domain (also called Phenotype space) is covered using an initial population of random possible solutions (chromosomes). Those chromosomes are being changed using genetic operators (such as Crossover and mutation) and the next generation is generated.

Table 11. GA design variables description and boundaries.

Chromosome	Intervention type	Description	Units	Lower bound	Upper bound	Optimized Value
1	<i>Sin. Frequency 1</i>	<i>Frequency</i>	<i>Hz</i>	<i>1</i>	<i>20</i>	<i>10.832</i>
2		<i>Amplitude</i>	<i>Nm</i>	<i>0</i>	<i>4</i>	<i>3.935</i>
3		<i>Starting time</i>	<i>s</i>	<i>0</i>	<i>4</i>	<i>2.968</i>
4		<i>Duration</i>	<i>s</i>	<i>0.2</i>	<i>2</i>	<i>1.201</i>
5		<i>Vibration Centre</i>	<i>Nm</i>	<i>-3</i>	<i>3</i>	<i>2.399</i>
6	<i>Sin. Frequency 2</i>	<i>Frequency</i>	<i>Hz</i>	<i>1</i>	<i>20</i>	<i>19.982</i>
7		<i>Amplitude</i>	<i>Nm</i>	<i>0</i>	<i>4</i>	<i>1.982</i>
8		<i>Starting time</i>	<i>s</i>	<i>0</i>	<i>4</i>	<i>0.136</i>
9		<i>Duration</i>	<i>s</i>	<i>0.2</i>	<i>2</i>	<i>1.836</i>
10		<i>Vibration Centre</i>	<i>Nm</i>	<i>-3</i>	<i>3</i>	<i>2.654</i>
11	<i>Constant Torque</i>	<i>Amplitude</i>	<i>Nm</i>	<i>-4</i>	<i>4</i>	<i>3.612</i>
12		<i>Starting time</i>	<i>s</i>	<i>1</i>	<i>3</i>	<i>1.803</i>
13		<i>Duration</i>	<i>s</i>	<i>1</i>	<i>2.1</i>	<i>1.485</i>
14	<i>Pulse</i>	<i>Amplitude</i>	<i>Nm</i>	<i>-4</i>	<i>4</i>	<i>0.068</i>
15		<i>Starting time</i>	<i>s</i>	<i>0.5</i>	<i>2</i>	<i>1.783</i>
16		<i>Duration</i>	<i>s</i>	<i>0.01</i>	<i>0.1</i>	<i>0.060</i>
17	<i>Linear increasing torque 1</i>	<i>Rate</i>	<i>Nm/s</i>	<i>-10</i>	<i>10</i>	<i>0.067</i>
18		<i>Starting time</i>	<i>s</i>	<i>0.1</i>	<i>2</i>	<i>1.704</i>
19		<i>Duration</i>	<i>s</i>	<i>0.05</i>	<i>1</i>	<i>0.939</i>
20	<i>Linear increasing torque 2</i>	<i>Rate</i>	<i>Nm/s</i>	<i>-10</i>	<i>10</i>	<i>0.409</i>
21		<i>Starting time</i>	<i>s</i>	<i>0.1</i>	<i>2</i>	<i>1.914</i>
22		<i>Duration</i>	<i>s</i>	<i>0.05</i>	<i>1</i>	<i>0.883</i>

The torque intervention created consists of 5 different interventions<sup>32</sup> (c.f. Figure 74), which are added to produce the final torque profile. Those chromosomes are described in (Table 11).

The best solution that was found using GA compared against an initial estimation, which can be seen in Figure 75 .

<sup>32</sup> In the GA those are considered to be the genes.

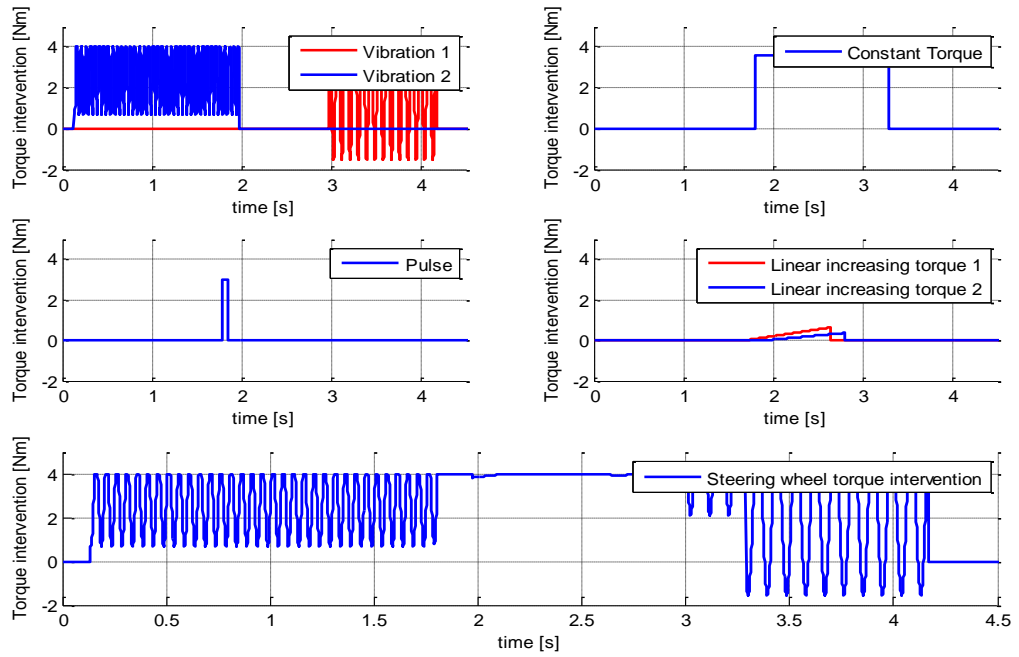


Figure 74 - Torque chromosomes.

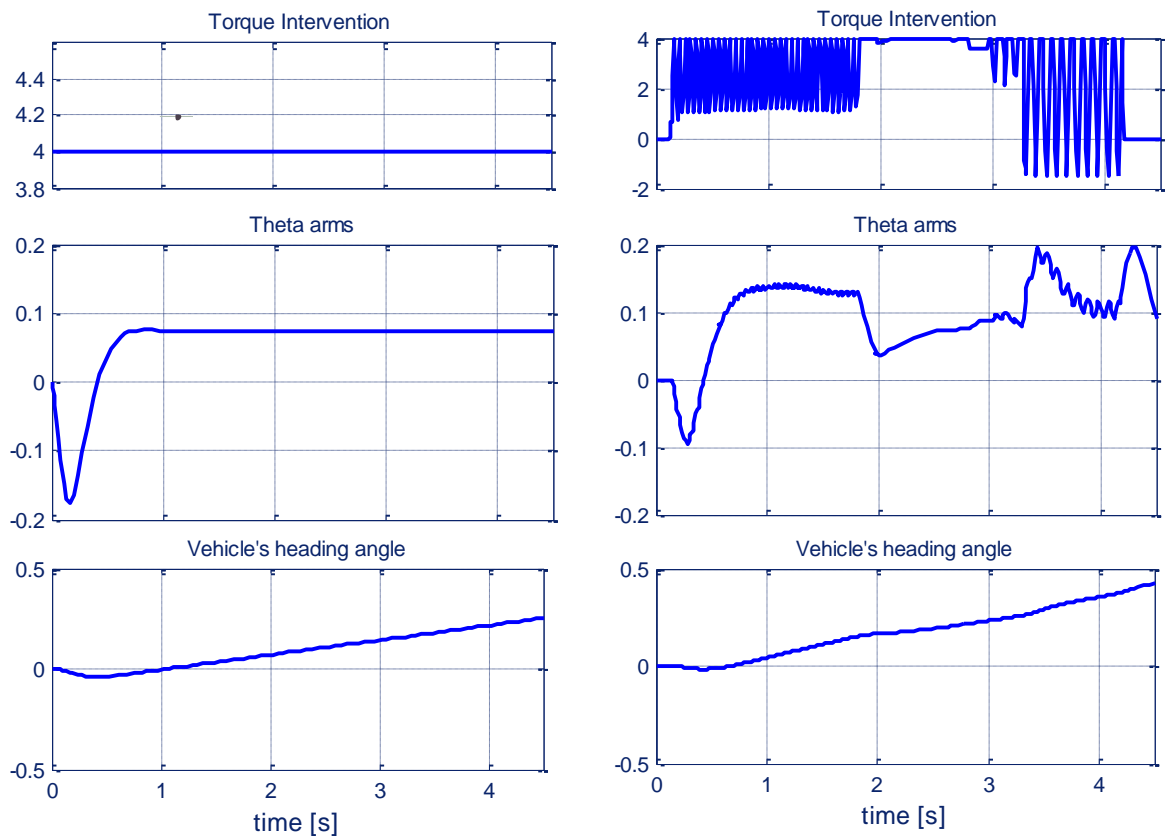


Figure 75 - Difference of torque profiles. The torque intervention on the left was an initial estimation, which supposed that with maximum torque, maximum vehicle's angle change would be achieved. In the figure in the right, best solution found using GA optimization can be seen. The difference between those 2 scenarios is noticeable.

## 4.4 Discussion

This research proposed a method for maximizing vehicle's heading angle change during a Lane Keeping Aid intervention. The objective could easily be adapted (e.g. maximize lateral deviation at given distance after triggering of the intervention).

The proposed method includes setting up the car, designing the experiments, and fitting the test data over any driver behaviour model.

For the needs of this research, multiple scenarios of torque interventions have been tested with approximately 50 drivers in total. A driver behaviour model has been developed (consisted from 2 mass-mass-spring damper systems) and fitted on the data collected from the test track.

The evaluation of driver's interaction with the vehicle is vital as more driver support systems are being developed constantly. Incorporating the driver's admittance into the LKA tuning can improve efficiency.

# 5 REFERENCES

- [1] *S. Angelis and M. Tidlund, "Optimal steering control input generation for vehicle's entry speed maximization in a double-lane change manoeuvre," KTH Royal Institute of Technology, Stockholm, 2013.*
- [2] *W. B. Ribbens, Understanding Automotive Electronics, Woburn: Butterworth-Heinemann, 1998.*
- [3] *A. W. a. C. P. Marko Wolf, "Embedded Security in Cars," in Secure In-Vehicle Communication, Springer, 2006, pp. 95-109.*
- [4] *T. Gillespie, Fundamentals of vehicle dynamics, 1992.*
- [5] *D. P. J. Aisopoulos, "Suspension System," Department of Vehicles Alexander Technological Educational Institute of Thessaloniki, Greece, 2011.*
- [6] *R. N. Jazar, Vehicle Dynamics:Theory and Applications, Springer, 2008.*
- [7] *J. D. Halderman, Automotive Technology ,principles ,diagnosis, and service, Pearson, 2012.*
- [8] *J. Reimpell, H. Stoll and J. Betzler, The Automotive Chassis:Enginnering Principles, Butterworth Heinemann, 2001.*
- [9] *R. G. F. L. Stefan Resch, "Dynamic Kinematics and Compliance Analysis for Transient Vehicle Dynamics Behaviour on Intelligent test Bench concept," TÜV SÜD Automotive GmbH, Germany, 2008.*
- [10] *T. D. Gillespie , "Fundamentals of vehicle dynamics," Society of Automotive Engineers, 1992.*
- [11] *C. Constant, "Suspension design: definition and effects on vehicle behaviour," 28 1 2013. [Online]. Available: <http://www.car-engineer.com>. [Accessed 12 6 2014].*
- [12] *H. Heisler, Advanced Vehicle Technology, Butterworth Heinemann, 2002.*

- [13] Z. Lenksysteme, “Electric Power Steering System for Passenger Cars and Light Commercial Vehicles”.
- [14] H. B. Pacejka, *Tire and Vehicle Dynamics*, Society of Automotive Engineers, 2002.
- [15] Royal Institute of Technology, vehicle engineering department, “Vehicle Components KTH Course Compendium,” Lars Drugge, Stockholm, 2010.
- [16] W. F. Milliken and D. L. Milliken, “Race vehicle dynamics,” Society of Automotive Engineers International, 1995.
- [17] Royal Institute of Technology, vehicle engineering department, “Vehicle Dynamics Course Compendium,” Lars Drugge, Stockholm, 2011.
- [18] J. Jerrelind, J. Edrén, S. Li, M. M. Davari, L. Drugge and A. Stensson, “Exploring active camber to enhance vehicle performance and safety,” The International Association for Vehicle System Dynamics, 2013.
- [19] W. Milliken and D. Milliken, “Race vehicle dynamics,” Society of Automotive Engineers International, 1995.
- [20] R. Rajamani, “Vehicle Dynamics and Control,” New York, Springer Science+Business Media, Inc, 2006, pp. 221-256.
- [21] J. C. Dixon, *Tires, Suspension, and Handling, 2nd Edition*, Society of Automotive Engineers, 1996.
- [22] E. Bakker, L. Lidner and H. Pacejka, “A New Tire Model with an Application in Vehicle Dynamics Studies.,” Society of Automotive Engineers, no. 890087, 1989.
- [23] R.-V. R. i. TNO, “Modelling of tyres,” 1999.
- [24] E. Velenis, D. Katzourakis, E. Frazzoli, P. Tsiotras and R. Happee, “Steady state drifting stabilization of RWD vehicles.,” Control Engineering Practice, no. 19, pp. 1363-1376, 2011.
- [25] E. Bakker, L. Nyborg and H. Pacejka, “Tyre modelling for use in vehicle dynamics studies.,” Society for Automotive Engineers, no. 870421, 1987.
- [26] M. B. M. J. R. Messaoud Toumi, “Development of Analytical Model for Modular Tank Vehicle Carrying Liquid Cargo,” 2013.

- [27] B. Niessen, S. Jansen, I. Besselink, A. Schmeitz and H. Nijmeijer, "An enhanced generic single track vehicle model and its parameter identification for 15 different passenger cars. AVEC paper," in The 11th International Symposium on Advanced Vehicle Control, Seoul, 2012.
- [28] J. G. FERNÁNDEZ, "A Vehicle Dynamics Model for Driving Simulators," CHALMERS UNIVERSITY OF TECHNOLOGY, Göteborg, 2012.
- [29] Robert Bosch GmbH, Bosch Automotive Handbook 7th edition., Society of Automotive Engineers, 2007.
- [30] G. Rill, Road Vehicle Dynamics: Fundamentals and Modeling, Bosa Roca: CRC Press, 2011.
- [31] D. I. Katzourakis, Writer, Automotive Crash Safety; Active and Passive Safety Systems - Lecture 6: Electronic Stability Control. [Performance]. Delft University of Technology Biomechanical Engineering, 2009.
- [32] H. J. Forster, "Der Fahrzeugfuhrer als Bindeglied Zwischen Reifen," Fharwerk und Fahrbahn, VDI berichte, no. 916, 1991.
- [33] A. T. Van Zanten, R. Erhardt, G. Pfaff, F. Kost, H. Uwe and T. Ehret, "Control Aspects of the Bosch-VDC," Proceedings of the International Symposium on Advanced Vehicle Control, vol. 1, pp. 573-608, 1996.
- [34] S. V. Drakunov, B. Ashrafi and A. Rosiglioni, "Yaw Control Algorithm via Sliding Mode Control," Proceedings of the American Control Conference, pp. 580-583, 2000.
- [35] K. Uematsu and J. C. Gerdes, "A Comparison of Several Sliding Surfaces for Stability Control," Proceedings of the International Symposium on Advanced Vehicle Control (AVEC), 2002.
- [36] K. Yi, T. Chung, J. Kim and S. Yi, "An Investigation into Differential Braking Strategies for Vehicle Stability Control," Proceedings of the Institution of Mechanical Engineers, Part D: Journal of Automotive Engineering, vol. 217, pp. 1081-1093, 2003.
- [37] T. Yoshioka, T. Adachi, T. Butsuen, H. Okazaki and H. Mochizuki, "Application of Sliding Mode Control to Control Vehicle Stability," Proceedings of the International Symposium on Advanced Vehicle Control (AVEC), pp. 455-459, 1998.

- [38] J. J. E. Slotine and W. Li, *Applied Nonlinear Control*, Prentice Hall, 1991.
- [39] H. E. Tseng, B. Ashrafi, D. Madau, T. A. Brown and D. Recker, "The Development of Vehicle Stability Control at Ford," *IEEE/ASME Transactions on Mechatronics*, vol. 4, no. 3, pp. 223-234, 1999.
- [40] Y. Fukada, "Slip Angle Estimation for Vehicle Stability Control," *Vehicle Systems Dynamics*, vol. 32, pp. 375-388, 1999.
- [41] Y. A. Ghoneim, W. C. Lin, D. M. Sidlosky, H. H. Chen, Y. K. Chin and M. J. Tedrake, "Integrated Chassis Control System to Enhance Vehicle Stability," *International Journal of Vehicle Design*, vol. 23, no. 1/2, pp. 124-144, 2000.
- [42] U. Kiencke and L. Nielsen, *Automotive Control Systems*, Springer, 2005.
- [43] D. Katzourakis, *Driver steering support interfaces near the vehicle's handling limits.*, Delft: CPI Koninklijke Wöhrmann, 2012.
- [44] Euroncap, June 2014. [Online]. Available: <http://www.euroncap.com/Content-Web-Page/bf07c592-4f87-404e-bb06-56f77faee5a2/esc.aspx>.
- [45] G. Forkenbrock, W. Garrott and B. O'Harra, "An experimental examination of J-turn and fishhook maneuvers that may induce on-road, untripped, light vehicle rollover," in SAE paper, 2003-01-1009, 2003.
- [46] M. Nybacka, X. He, Z. Su, L. Drugge and E. Bakker, "Links between subjective assessments and objective metrics for steering, and evaluation of driver ratings," *Vehicle System Dynamics: International Journal of Vehicle Mechanics and Mobility*, March 2014.
- [47] J. Breuer, "Analysis of driver-vehicle-interaction in an evasive manoeuvre - results of moose test studies," in 16th ESV conference, Paper No: 98-S2-W-35, 1998.
- [48] D. Katzourakis, C. Droogendijk, D. Abbink, R. Happee and E. Holweg, "Force-feedback driver model for objective assessment of automotive steering systems," in 10th international symposium on advanced vehicle control, AVEC10, 2010.
- [49] Tomlab Optimization, "TOMLAB Optimization," Tomlab Optimization, 8 August 2012. [Online]. Available: <http://tomopt.com/tomlab/>. [Accessed 3 July 2013].

- [50] P. Rutquist and M. Edvall, "PROPT - Matlab Optimal Control Software," Tomlab optimization, Västerås, 2010.
- [51] P. Riekert and T. Schunck, Zur Fahrmechanik des gummibereiteten Kraftfahrzeugs., 1940, pp. 210-224.
- [52] R. Rajamani, "Vehicle Dynamics and Control," New York, Springer Science+Business Media, Inc, 2006, pp. 221-256.
- [53] H. Pacejka, Tire and Vehicle Dynamics, Society of Automotive Engineers, 2002.
- [54] E. Velenis, D. Katzourakis, E. Frazzoli, P. Tsiotras and R. Happee, "Steady state drifting stabilization of RWD vehicles," Control Engineering Practice, no. 19, pp. 1363-1376, 2011.
- [55] E. Bakker, L. Nyborg and H. Pacejka, "Tyre modelling for use in vehicle dynamics studies," Society for Automotive Engineers, no. 870421, 1987.
- [56] J. Dixon, Tires, Suspension, and Handling, 2:nd Edition, Society of Automotive Engineers, 1996.
- [57] M. Mitschke and H. Wallentowitz, Dynamik der Kraftfahrzeuge, 4. Auflage, Berlin and Heidelberg: Springer, 2004.
- [58] J. H. Yung-Hsiang and J. Gerdes., "The Predictive Nature of Pneumatic Trail: Tire Slip Angle and Peak Force Estimation using Steering Torque," Advanced Vehicle Control, 2008.
- [59] N. K. Z. R. Joly Antonin, "Relationship between Gripping Force and Mechanical Arm Admittance of a Driver under Perturbations," 2014.
- [60] H. Wang and D. Cole, "Identification and Validation of a Driver Model Including Neuromuscular System Dynamics," 2014.
- [61] M. Mitschke and H. Wallentowitz , Dynamik der Kraftfahrzeuge, 4. Auflage., Berlin and Heidelberg: Springer, 2004.
- [62] I. J. M. Besselink, A. J. C. Schmeitz and H. B. Pacejka. , "An improved Magic Formula/Swift tire model that can handle inflation pressure changes.," Vehicle System Dynamics, vol. 48, no. 1, pp. 337-352, 2010.
- [63] J. A. Snyman, Practical mathematical optimization, p.2-5, Springer Science+Business Media, inc, 2005.

- [64] K. L. Dmitrey, "OpenOpt," 15 June 2013. [Online]. Available: <http://openopt.org/Welcome>. [Accessed 17 June 2013].
- [65] P. E. Rutquist and M. M. Edvall, "PROPT - Matlab Optimal Control Software," Tomlab optimization, Västerås, 2010.
- [66] J. Nocedal and S. J. Wright, *Numerical Optimization*, New York: Springer Science+Business Media, Inc, 1999.
- [67] D. Katzourakis, "Optimal Steering Control Input Generation for Vehicle's Entry speed Maximization in a Double-Lane," Volvo car corporation PVV, Göteborg, 2013.
- [68] K. Holmström, "The TOMLAB Optimization Environment in Matlab," Mälardalen University, Västerås, 1999.
- [69] Mathworks, "MATLAB The Language of Technical Computing R2013a," Mathworks, 8 March 2013. [Online]. Available: <http://www.mathworks.se/products/matlab/>. [Accessed 3 July 2013].
- [70] Mathworks, "Documentation Center Optimization Toolbox," Mathworks, 8 March 2013. [Online]. Available: <http://www.mathworks.se/help/optim/>. [Accessed 3 July 2013].
- [71] Tomlab Optimization, "Matlab Symbolic Optimization Modeling," Tomlab Optimization, 8 August 2012. [Online]. Available: <http://tomsym.com/index.html>. [Accessed 3 July 2013].
- [72] P. E. Gill, W. Murray and M. A. Saunders, "User's Guide for SNOPT Version 7: Software for Large-Scale Nonlinear Programming," Stanford University, Stanford, 2008.
- [73] A. Nozad, M. Lidberg, T. Gordon and M. Klomp, "Optimal path recovery from terminal understeer," in *The International Association for Vehicle System Dynamics*, 2011.
- [74] P. Sundström, M. Jonasson, J. Andreasson, A. Stenson Trigell and B. Jacobson, "Path and control optimisation for over-actuated vehicles in two safety-critical maneuvers," in *Advanced Vehicle Control*, Loughborough, 2010.
- [75] H. B. Pacejka, "Tyre Models for Vehicle Dynamics Analysis," Delft, 1993.

- [76] Volvo Cars, “Volvo S60 vehicle Kinematics and Compliance Datasheet,” Volvo Cars, Gothenburg, 2009.
- [77] ISO Copyright Office, “International Standard, ISO 3888-2 manual,” Geneve, 2002.
- [78] H. B. Pacejka, *Tyre and Vehicle Dynamics, 2:nd edition*, Oxford: Society of Automotive Engineers International, 2005.
- [79] D. D. MacInnis, W. E. Cliff and K. W. Ising , “A Comparison of Moment of Inertia Estimation Techniques for Vehicle Dynamics Simulation,” Society of Automotive Engineers, no. 970951, 1997.
- [80] “How is ESC tested,” Euroncap, [Online]. Available: <http://www.euroncap.com/Content-Web-Page/bf07c592-4f87-404e-bb06-56f77face5a2/esc.aspx>. [Accessed 6 November 2013].
- [81] “RT3000 Family,” OXTS Inertial + GPS, [Online]. Available: <http://www.oxts.com/products/rt3000-family> . [Accessed 6 November 2013].
- [82] D. I. Katzourakis, E. Velenis, D. A. Abbink, R. Happee and E. Holweg, “Race-Car Instrumentation for Driving Behavior Studies,” IEEE Transactions on Instrumentation and Measurement, vol. 61, no. 2, 2012.
- [83] J. H. Yung-Hsiang and J. C. Gerdes. , “The Predictive Nature of Pneumatic Trail: Tire Slip Angle and Peak Force Estimation using Steering Torque.,” Advanced Vehicle Control, 2008.
- [84] W. F. Milliken, D. L. Milliken and M. Olley, “Chassis Design: Principles and Analysis,” Society of Automotive Engineers, 2002.
- [85] Modified, “Modified - Tech Articles - Performance Tire Buyers Guide - Photo 20,” [Online]. Available: [http://www.modified.com/tech/modp-0906-performance-tires-buyers-guide/photo\\_20.html](http://www.modified.com/tech/modp-0906-performance-tires-buyers-guide/photo_20.html). [Accessed 7 November 2013].
- [86] ISO Copyright Office, “ISO 3833:1977 Road vehicles -- Types -- Terms and definitions,” Geneve, 2002.
- [87] J. T. Betts, *Practical Methods for Optimal Control Using Nonlinear Programming*, Philadelphia: Society for Industrial and Applied Mathematics (SIAM), 2001.

[88] *J. Reimpell, H. Stoll and J. Betzler, The Automotive Chassis, Butterworth-Heinemann, 2001.*

[89] *“Collocation Method,” [Online]. Available: [http://en.wikipedia.org/wiki/Collocation\\_method](http://en.wikipedia.org/wiki/Collocation_method). [Accessed 23 5 2014].*

[90] *“Genetic Algorithms,” [Online]. Available: [http://en.wikipedia.org/wiki/Genetic\\_algorithm](http://en.wikipedia.org/wiki/Genetic_algorithm). [Accessed 24 7 2014].*





# 6 APPENDICES

## 6.1 ISO 3888 Description

The ISO 3888 Part 2-Obstacle avoidance is a dynamic process during which the vehicle is driven closed loop in a severe lane change manoeuvre such that high alternate lateral accelerations will be produced. It concerns passenger cars and light commercial vehicles up to 3500kg and involves rapidly driving from an initial lane to another parallel lane and then back to the initial one, so to recreate an obstacle avoidance scenario. During the manoeuvre no cone marking the track should be displaced for the pass to be considered as valid. The results of this test serve as a subjective evaluation of the vehicle's lateral dynamics and road holding ability. The test track that defines the manoeuvre can be seen below.

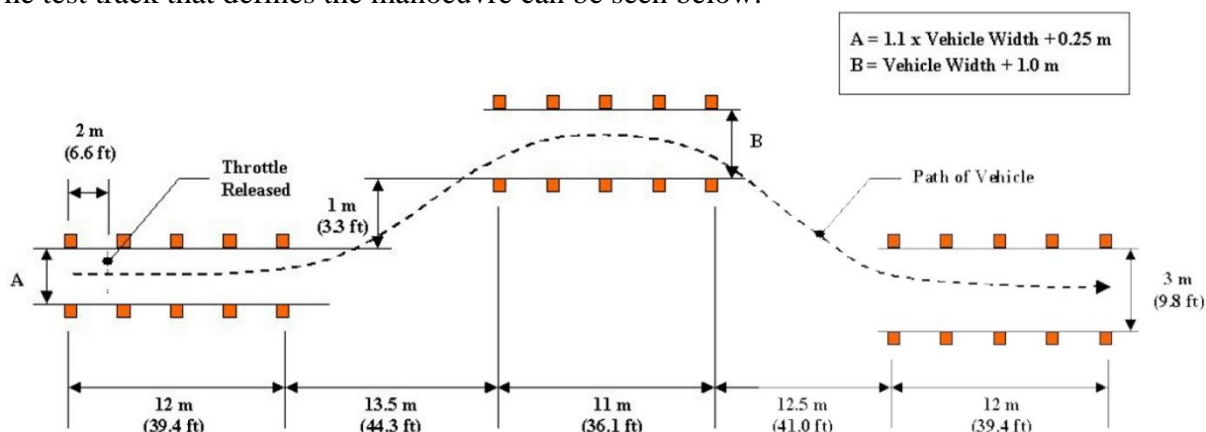


Figure App 1 - ISO 3888 part 2 double-lane change track illustration.

The track sizing is vehicle dependent as can be seen above where the width of the initial lane A and the second lane B is calculated, as noted in the figure's legend. The value of Vehicle Width is the tested vehicle's overall width without the rear-view mirrors. The geometry differs only in regards of the lane widths though, as the length of the lanes and their in-between spacing remains the same.

Driving should be performed with the highest gear that guarantees a minimum of 2000rpm of engine speed and vehicles with automatic gearbox should have the selector placed in the drive (D) position. The vehicle enters the track in lane A and after a distance of 2m the throttle is released<sup>33</sup> where after the remainder of the track is driven in the throttle release position, without any braking action. Only the steering wheel is being controlled by the driver and the vehicle's longitudinal speed is measured at the end of section A, that is at X = 12 m in the track.

It should be noted that this is a test that best suits subjective rather than objective evaluation of the vehicle's lateral dynamics characteristics. This is due to the fact that different

<sup>33</sup> While the ISO 3888 Part 2 document does not make any direct reference to whether the clutch should be disengaged or not, one may argue that since there is a reference to the engine speed at the entry point, it is implied that the clutch should remain engaged. In that case some engine braking is expected. In this thesis though, no such phenomenon is modelled, and the test is simulated as if the clutch is disengaged, i.e. no powertrain effects at all. This allows a clearer picture of the vehicle's dynamic behaviour that comes from its chassis and ESC setup since it isolates it from external (i.e. powertrain) influences.

drivers, with different skills, choose different paths and strategies to drive through the track so the measured speeds are considerably scattered, in spite of the velocity measurement taking place at the end of section A as a means of reducing this effect.

## 6.2 Test Vehicle Specifications

The vehicle used during all physical testing and as an example when performing the optimization of the steering angles is described below.

Table B 1. Test vehicle nominal parameters.

<i>Parameter description</i>	<i>Value</i>
<i>Model name</i>	<i>Volvo S60 T5 automat, year model 2009</i>
<i>Weight during testing (driver + equipment)</i>	<i>1823 kg</i>
<i>Curb weight (Standard equipment, full tank of fuel and no driver)</i>	<i>1635 kg</i>
<i>Gross weight</i>	<i>2060 kg</i>
<i>Yaw moment of inertia</i>	<i>2500 kgm<sup>2</sup></i>
<i>Width (excluding mirrors)</i>	<i>1865 mm</i>
<i>Length</i>	<i>4635 mm</i>
<i>Distance of front wheel from mass centre</i>	<i>1854 mm</i>
<i>Distance of rear wheel from mass centre</i>	<i>2781 mm</i>
<i>Distance to the right track from mass centre</i>	<i>793.5 mm (Estimated to mass in middle)</i>
<i>Body length in front of the front wheels</i>	<i>929.5 mm (Estimated to equal as in the rear)</i>
<i>Front wheels track width</i>	<i>1588 mm</i>
<i>Rear wheels track width</i>	<i>1586 mm</i>
<i>Height of centre of mass</i>	<i>500 mm</i>
<i>Front roll centre height</i>	<i>120 mm</i>
<i>Rear roll centre height</i>	<i>240 mm</i>
<i>Front roll stiffness</i>	<i>45 000 Nm/rad</i>
<i>Rear roll stiffness</i>	<i>37 500 Nm/rad</i>
<i>Rolling friction coefficient</i>	<i>0.013</i>
<i>Air drag coefficient</i>	<i>0.28</i>
<i>Frontal area</i>	<i>2.27 m<sup>2</sup></i>
<i>Maximum steering angle</i>	<i>31 °</i>
<i>Maximum steering angle rate</i>	<i>720 °/s</i>
<i>Steering ratio</i>	<i>14.95</i>
<i>Front roll steer coefficient</i>	<i>0.123</i>
<i>Rear roll steer coefficient</i>	<i>0.007</i>
<i>Pneumatic trail a linear range</i>	<i>1/30 m</i>
<i>Wheel radius</i>	<i>316 mm</i>
<i>Wheel width</i>	<i>200 mm</i>
<i>Magic formula, B</i>	<i>7.5418</i>
<i>Magic formula, C</i>	<i>1.4887</i>
<i>Magic formula, D</i>	<i>1.1233</i>
<i>Tire relaxation length</i>	<i>300 mm</i>

## 6.3 DLC Steering Robot Tests

In this appendix a figure for every test that has been conducted can be seen. The figures contain:

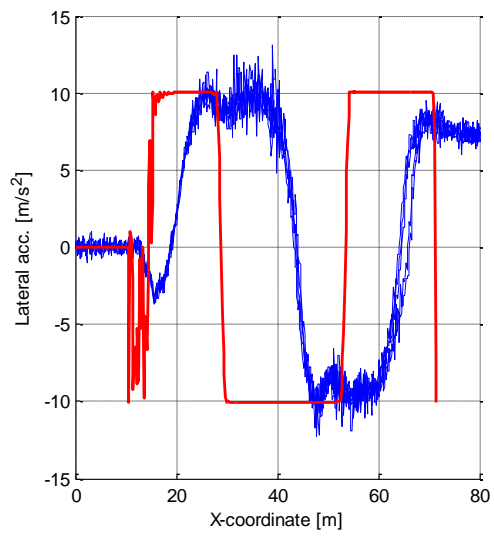
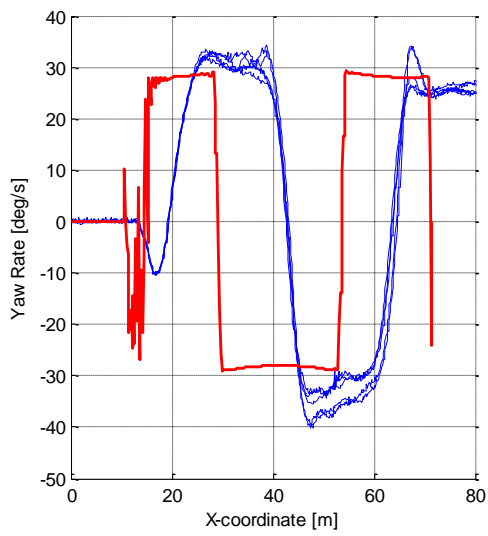
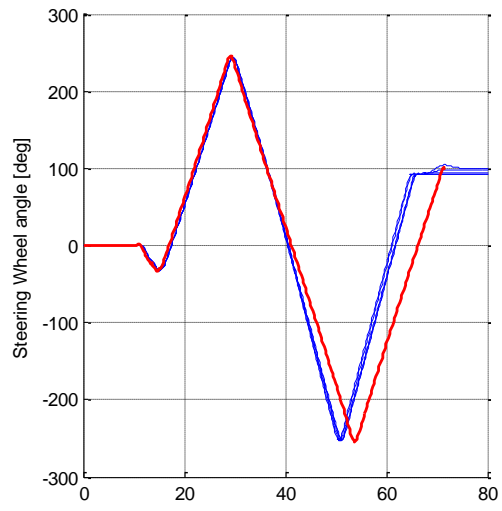
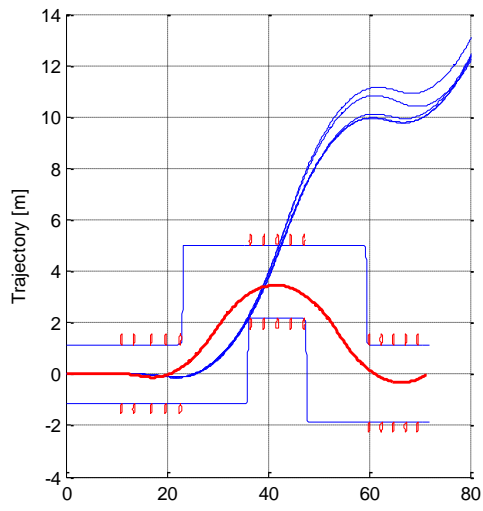
- the trajectory (top-left),
- the Steering wheel angle (top-right),
- the Yaw Rate (bottom-left)
- and the Lateral acceleration (bottom-right).

Table B 2. Steering Robot test scenarios

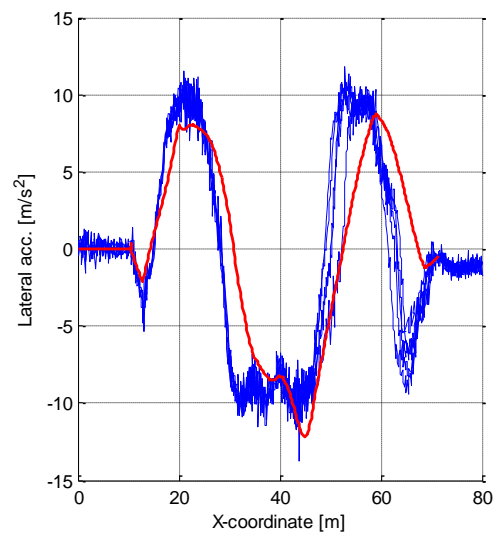
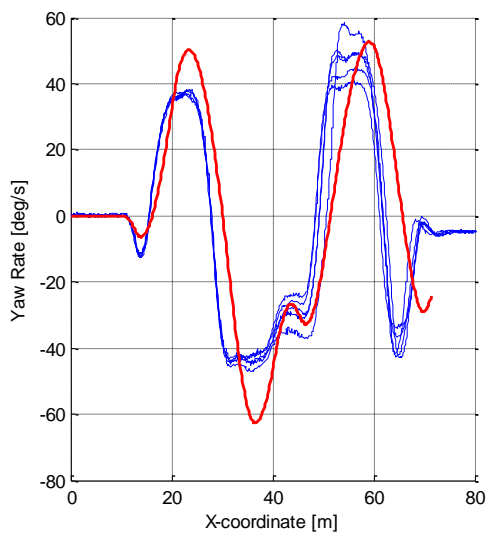
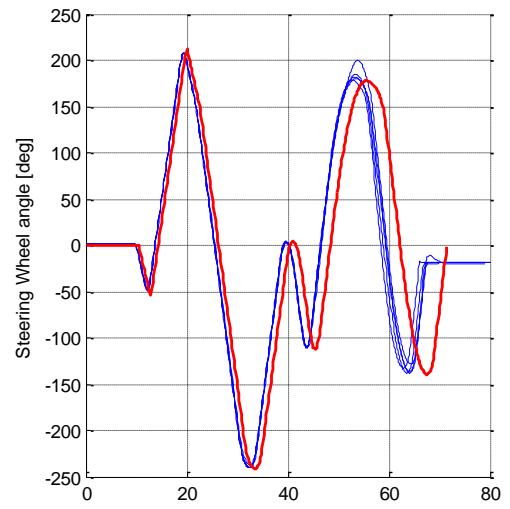
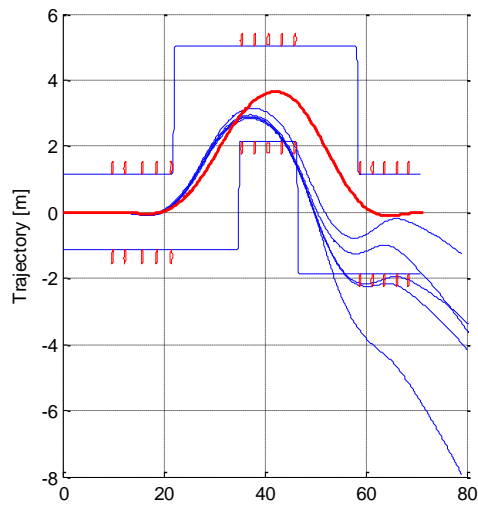
<i>Test #</i>	<i>Test Description</i>	<i>Vehicle Entry Speed</i>	<i>Vehicle ESC option</i>
<i>1</i>	<i>Point Mass Model</i>	<i>74.389</i>	<i>Disabled</i>
<i>2</i>	<i>Bicycle Model, Linear Tires</i>	<i>67.434</i>	<i>Disabled</i>
<i>3</i>	<i>Bicycle Model, MF Tires</i>	<i>67.339</i>	<i>Disabled</i>
<i>4</i>	<i>Two Track Model</i>	<i>68.342</i>	<i>Disabled</i>
<i>5</i>	<i>Two Track Model, Range Y position</i>	<i>70.686</i>	<i>Disabled</i>
<i>6</i>	<i>Two Track Model, Camber Thrust, Wheel Kinematics</i>	<i>69.890</i>	<i>Disabled</i>
<i>7</i>	<i>Two Track Model, Camber Thrust, Wheel Kinematics, ESC</i>	<i>72.649</i>	<i>Disabled</i>
<i>8</i>	<i>Two Track Model, Camber Thrust, Wheel Kinematics, Tire Relaxation</i>	<i>68.600</i>	<i>Disabled</i>
<i>9</i>	<i>Two Track Model, Opt ESC</i>	<i>77.002</i>	<i>Disabled</i>
<i>10</i>	<i>Two Track Model, Opt ESC</i>	<i>77.002</i>	<i>Enabled</i>
<i>11</i>	<i>Two Track Model, Camber Thrust, Wheel Kinematics, Tire Relaxation</i>	<i>72.649</i>	<i>Enabled</i>

Each scenario has been tested 5 times. With Red colour, result of the optimization can be seen. With Blue colour, measured data are depicted.

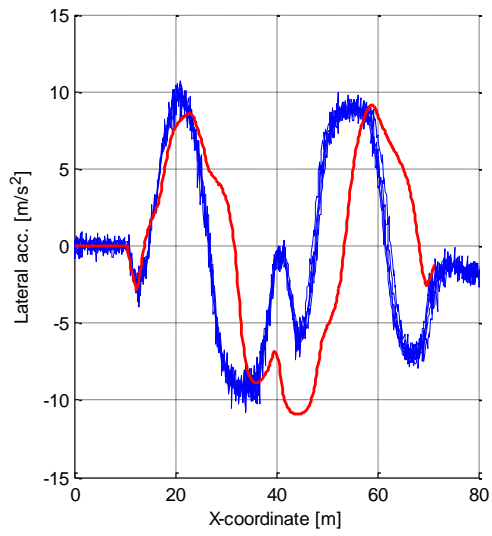
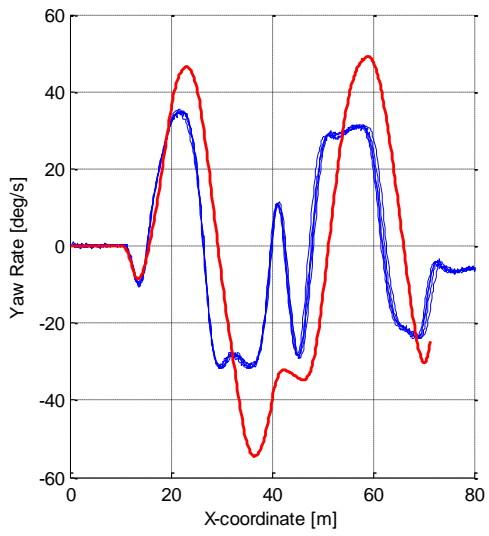
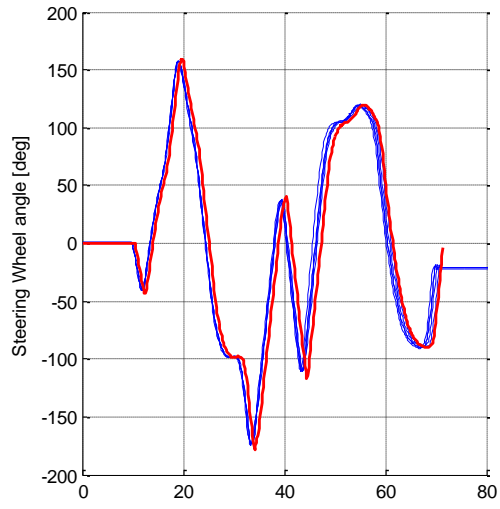
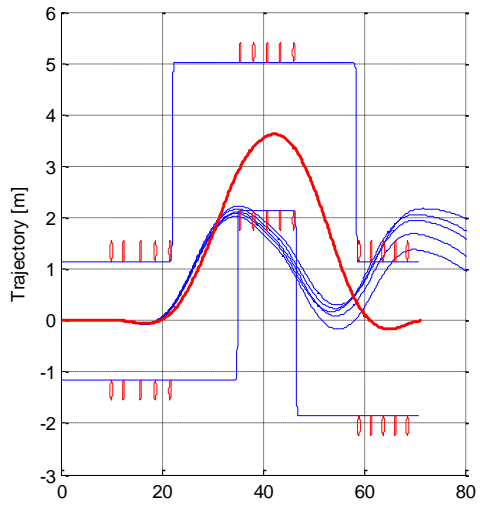
**Test 1: Point Mass Model**



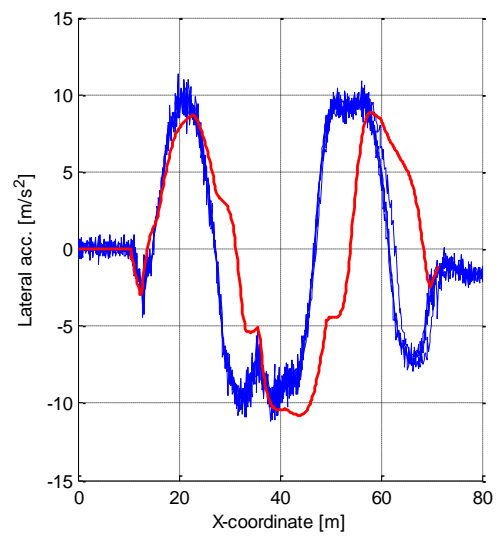
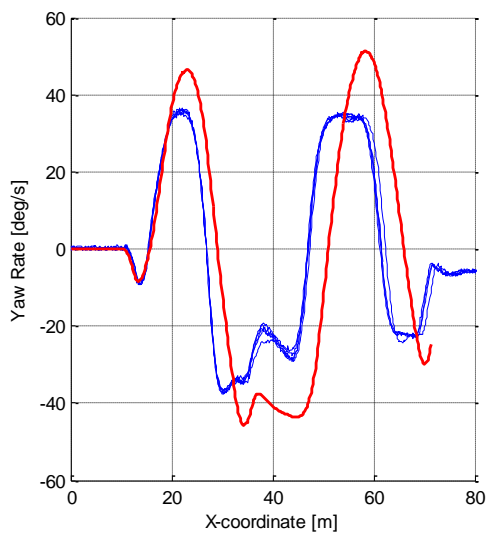
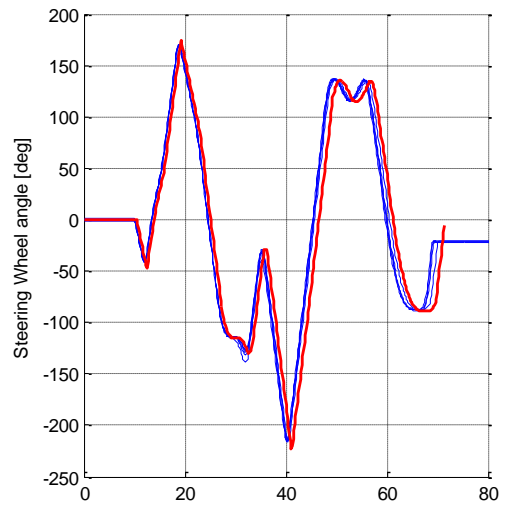
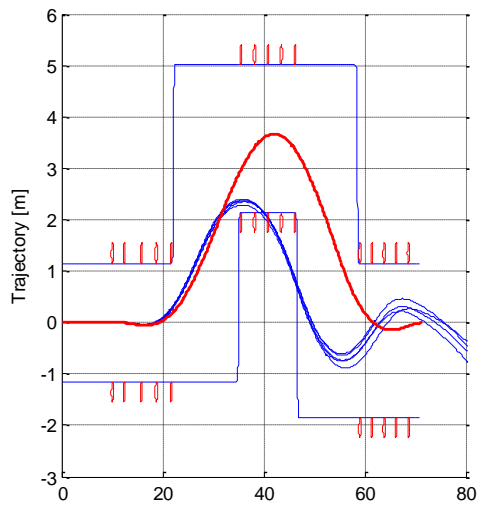
## Test 2: Bicycle Model, Linear Tires



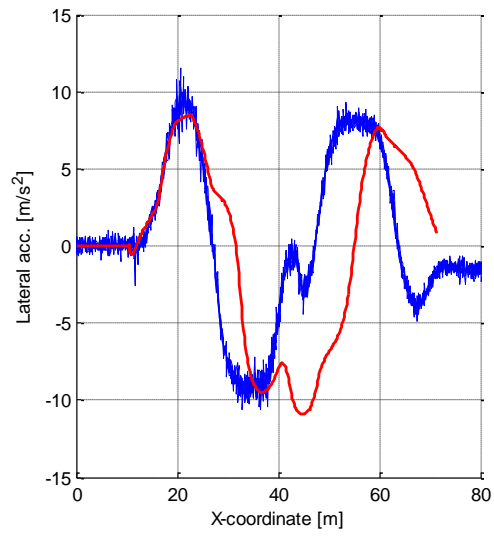
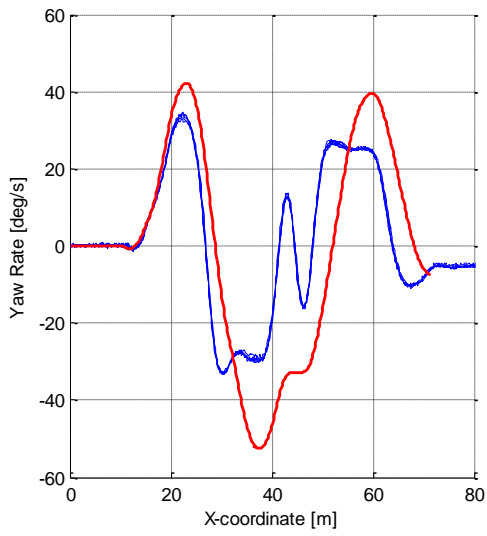
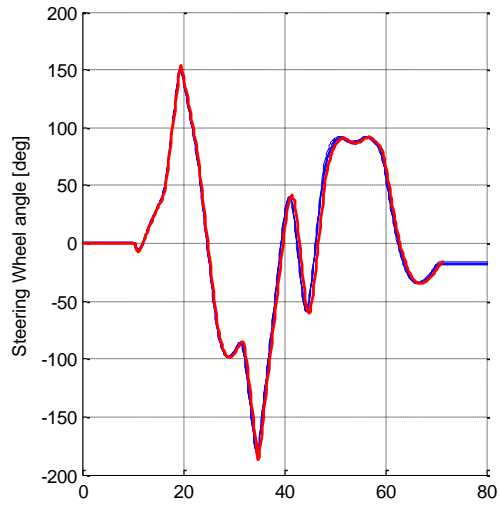
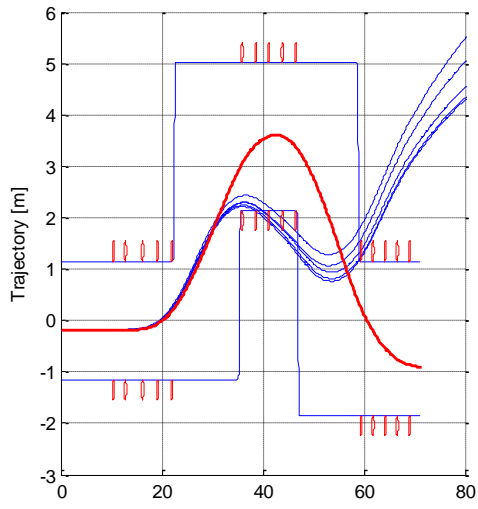
**Test 3: Bicycle Model, Magic Formula Tires**



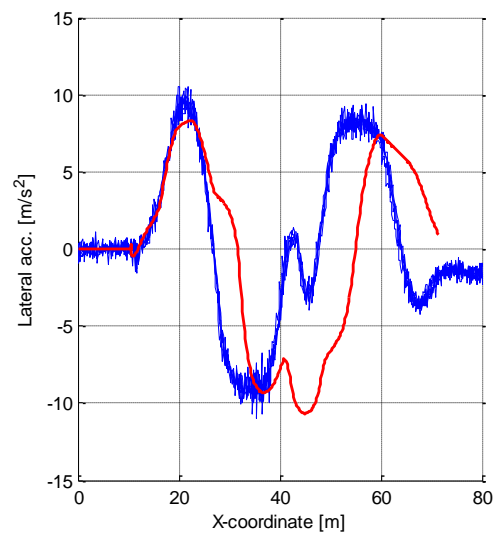
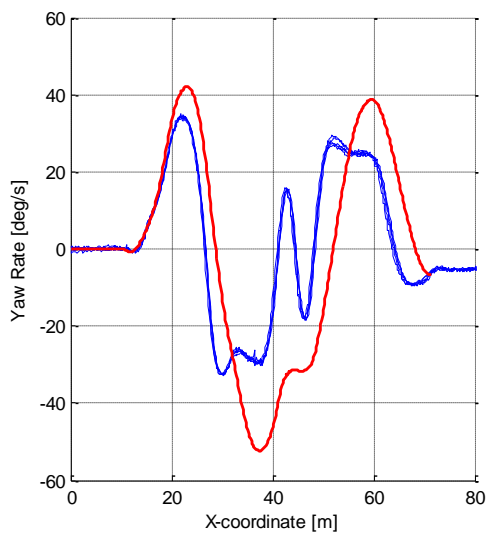
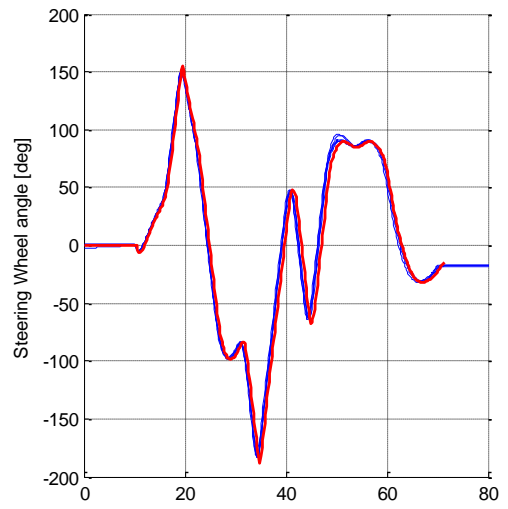
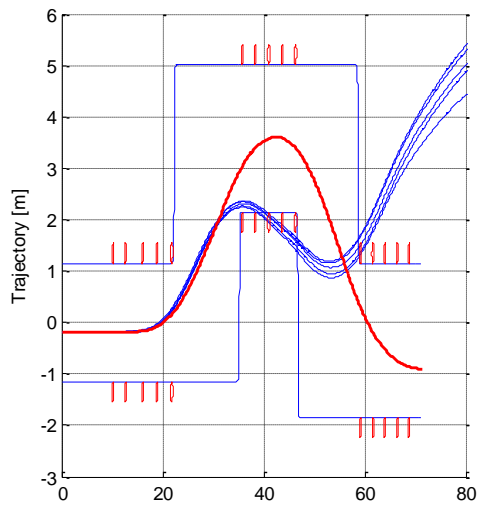
### Test 4: Two Track Model



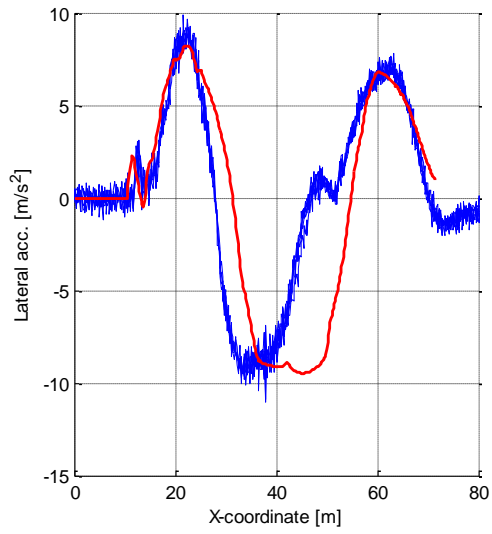
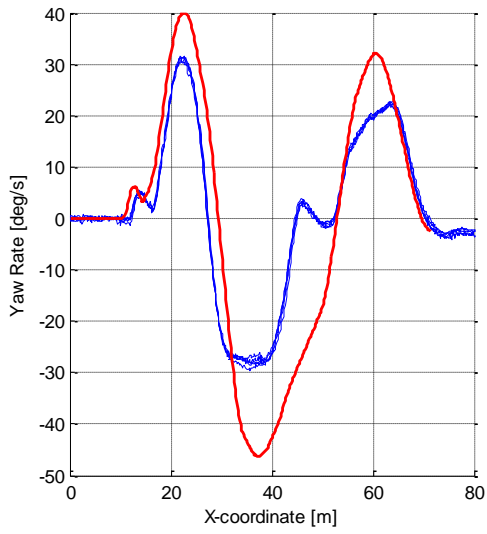
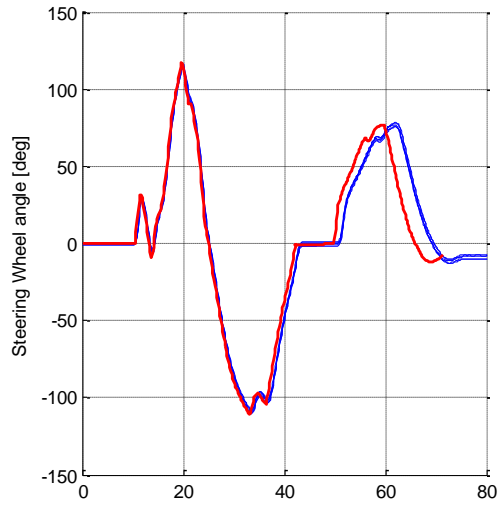
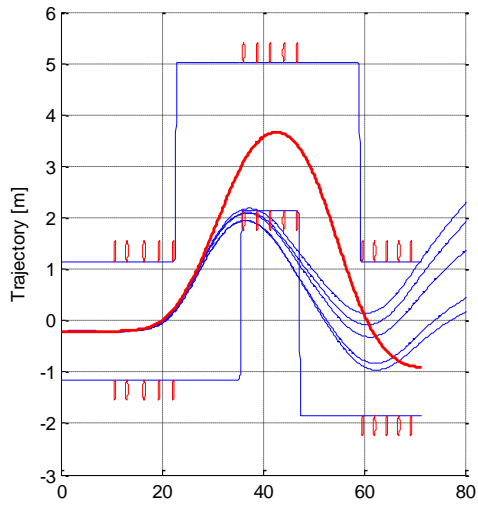
**Test 5: Two Track Model, Range Y position**



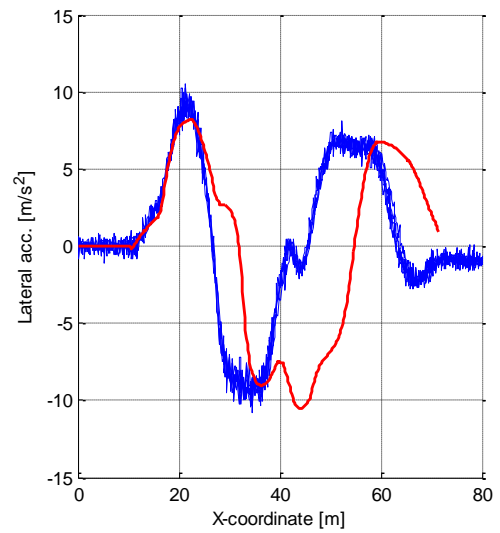
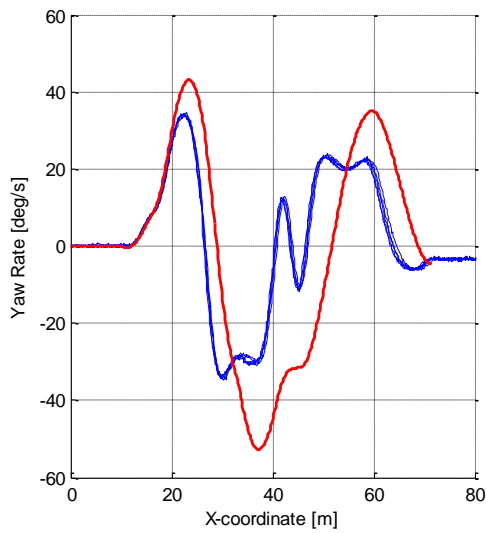
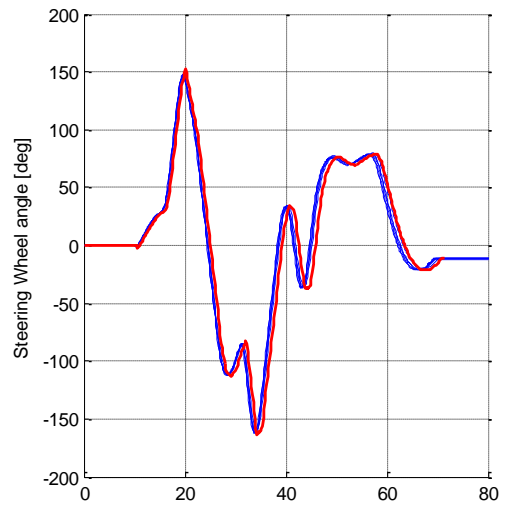
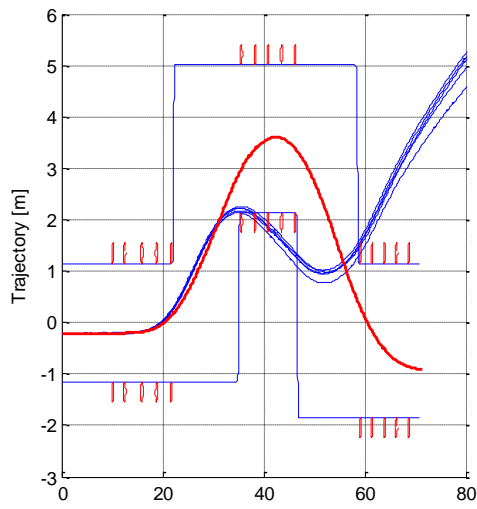
### Test 6: Two Track Model, Camber Thrust, Wheel Kinematics



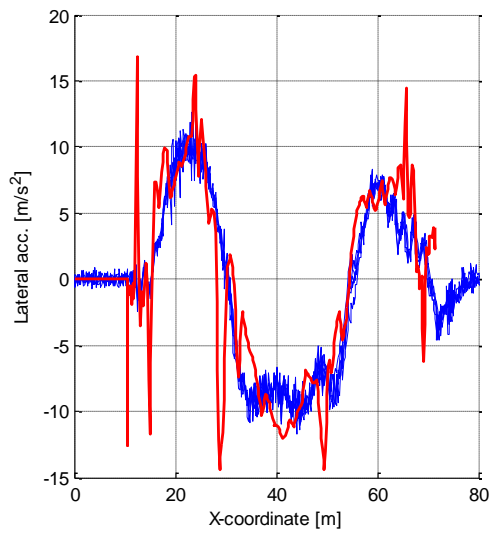
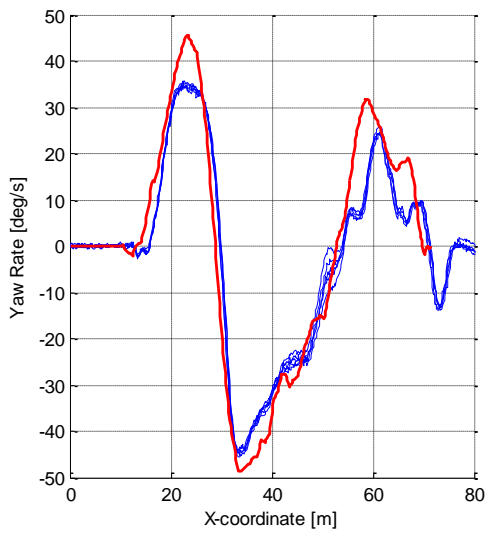
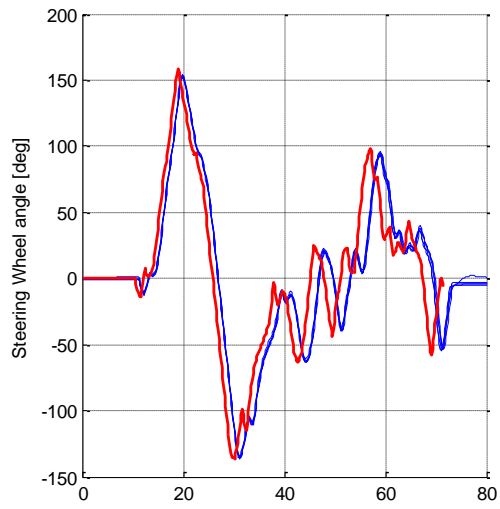
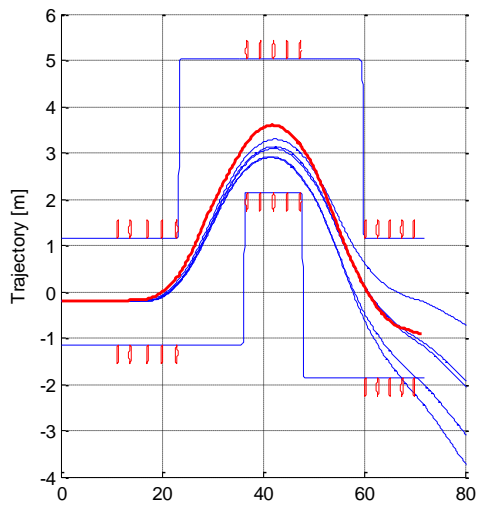
*Test 7: Two Track Model, Camber Thrust, Wheel Kinematics, ESC*



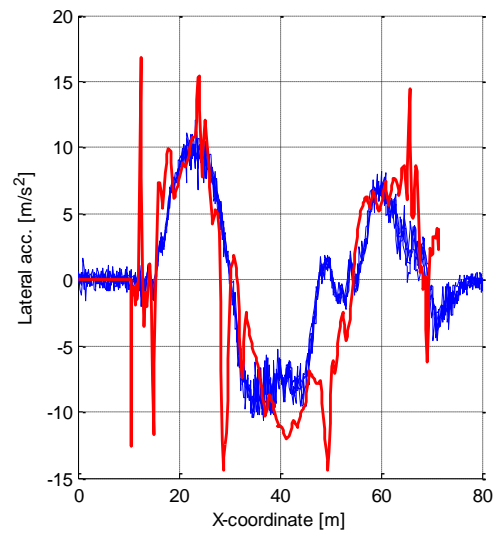
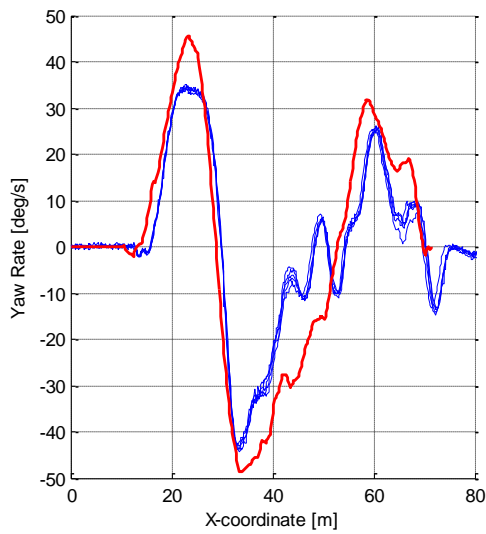
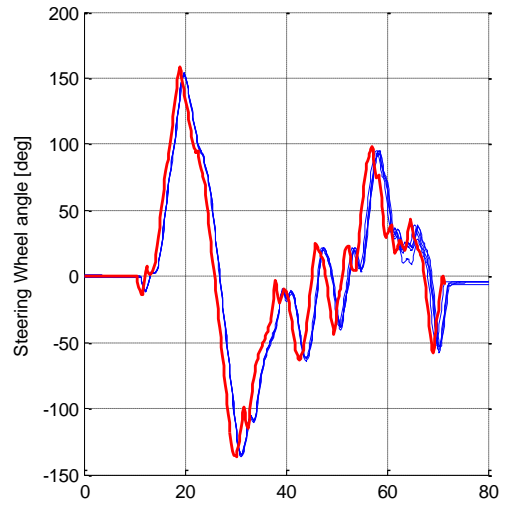
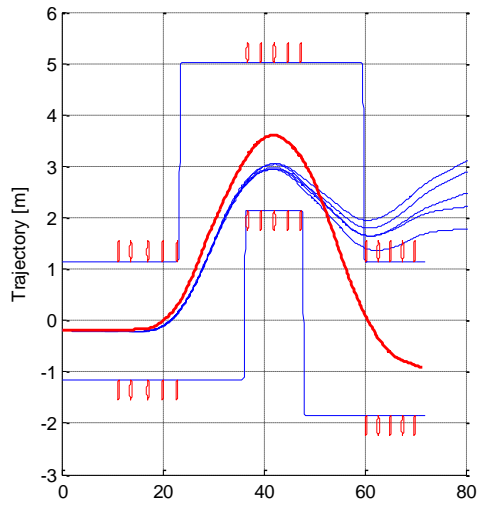
**Test 8: Two Track Model, Camber Thrust, Wheel Kinematics, Tire Relaxation**



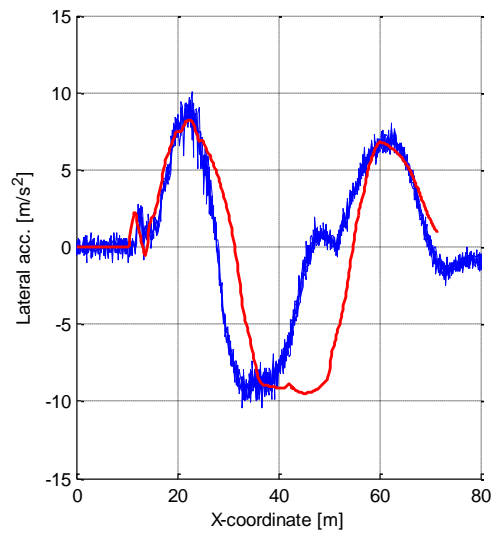
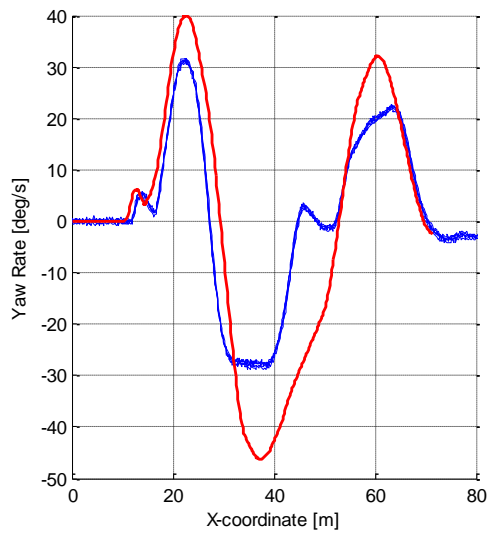
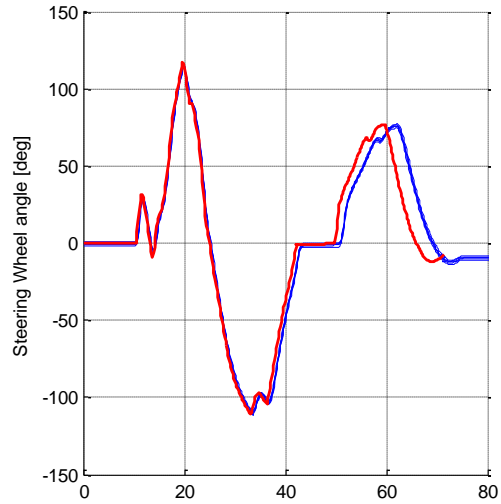
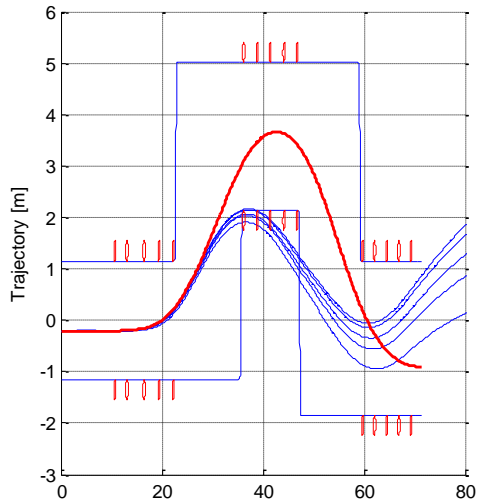
**Test 9: Two Track Model, Opt ESC**



**Test 10: Two Track Model, Opt ESC (Vehicle ESC: Enabled)**

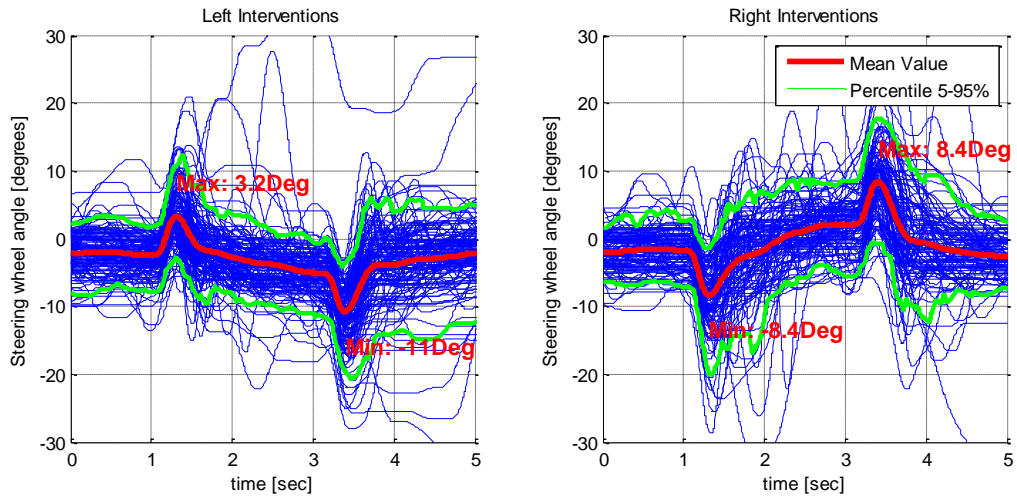


**Test 11: Two Track Model, Camber Thrust, Wheel Kinematics, and Tire Relaxation (Vehicle ESC: Enabled)**

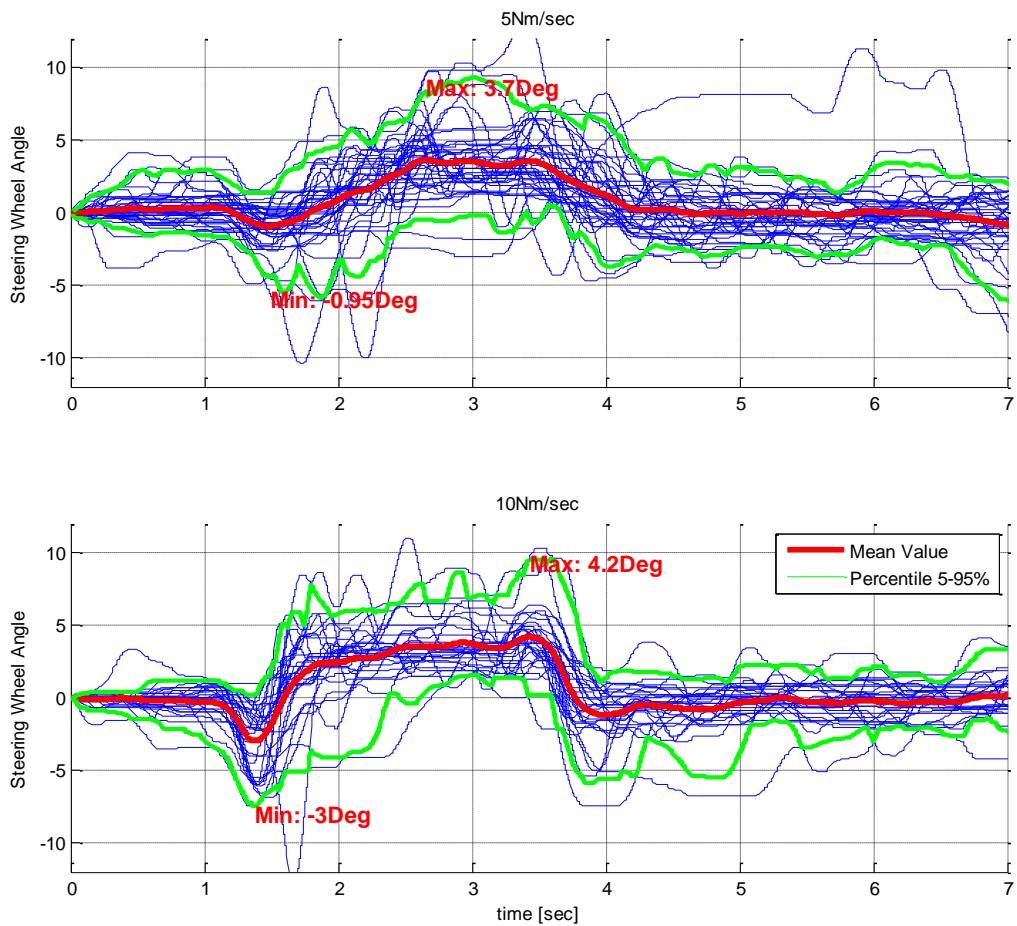


# 6.4 Lane Keeping Aid tests

*Data from track-testing: Driver's reaction to the steering wheel torque intervention have been categorized according to the direction<sup>34</sup>*

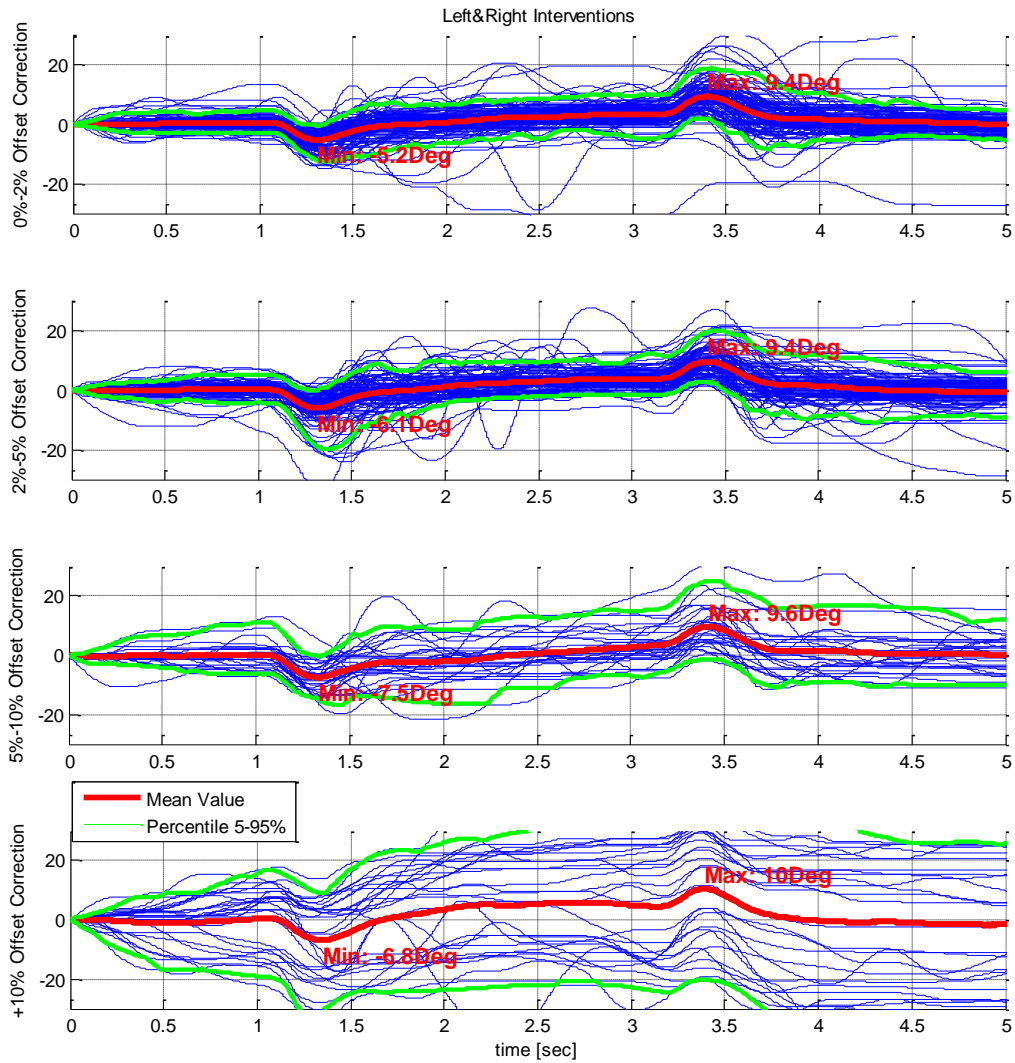


*Data from track-testing: Driver's reaction according to the rate of the intervention torque*



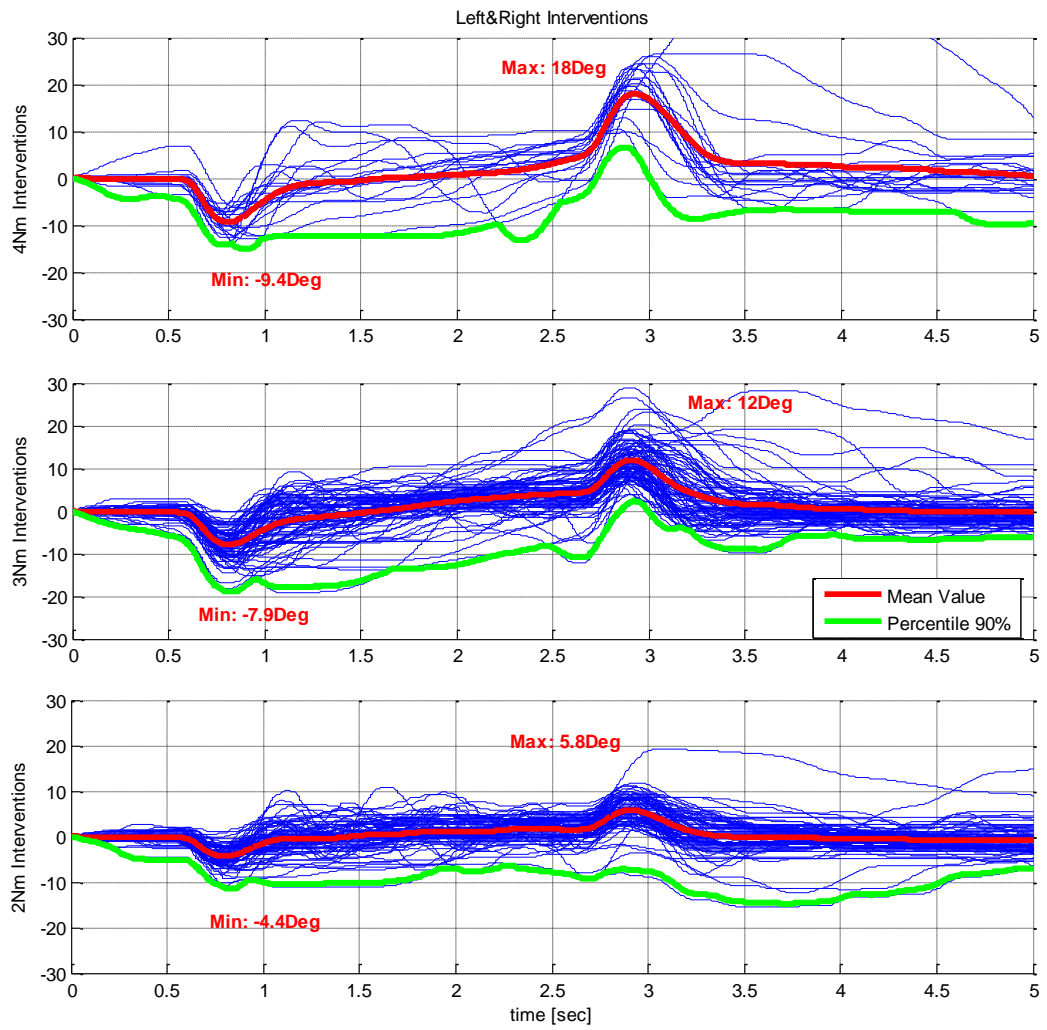
<sup>34</sup> The interventions were triggered in random direction.

*Data from track-testing: Driver's reaction according to the initial<sup>35</sup> steering wheel angle.*

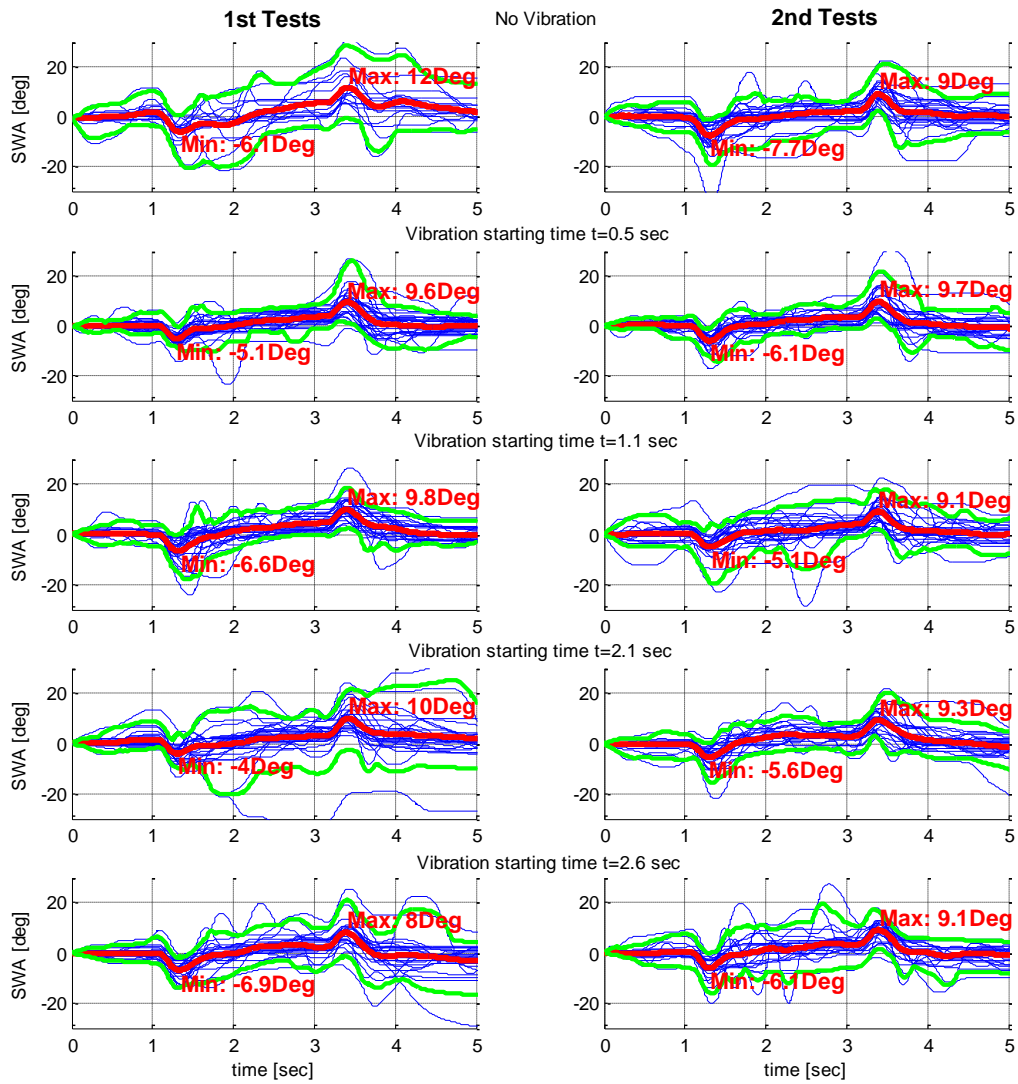


<sup>35</sup> The drivers who participated in the tests were driving in a close-track and were unaware about the time that the intervention would start. This meant that in some test, the drivers were actively steering the car to follow a desired path at the time the intervention started.

**Data from track-testing: Driver's reaction according to the amplitude of the torque intervention.**

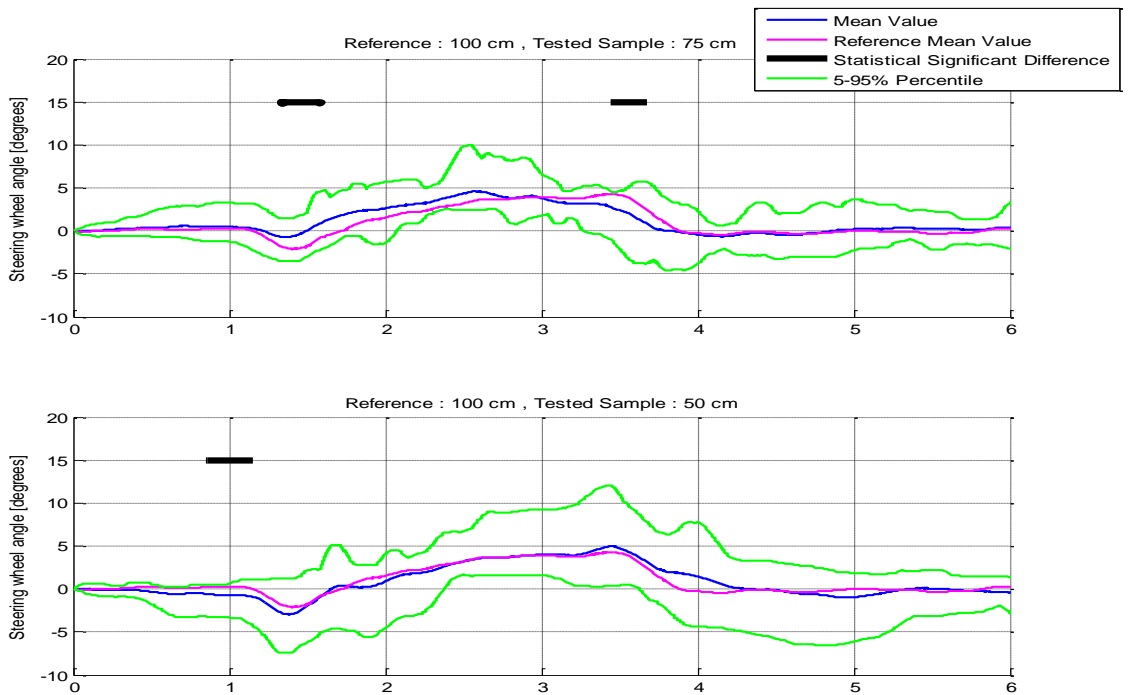
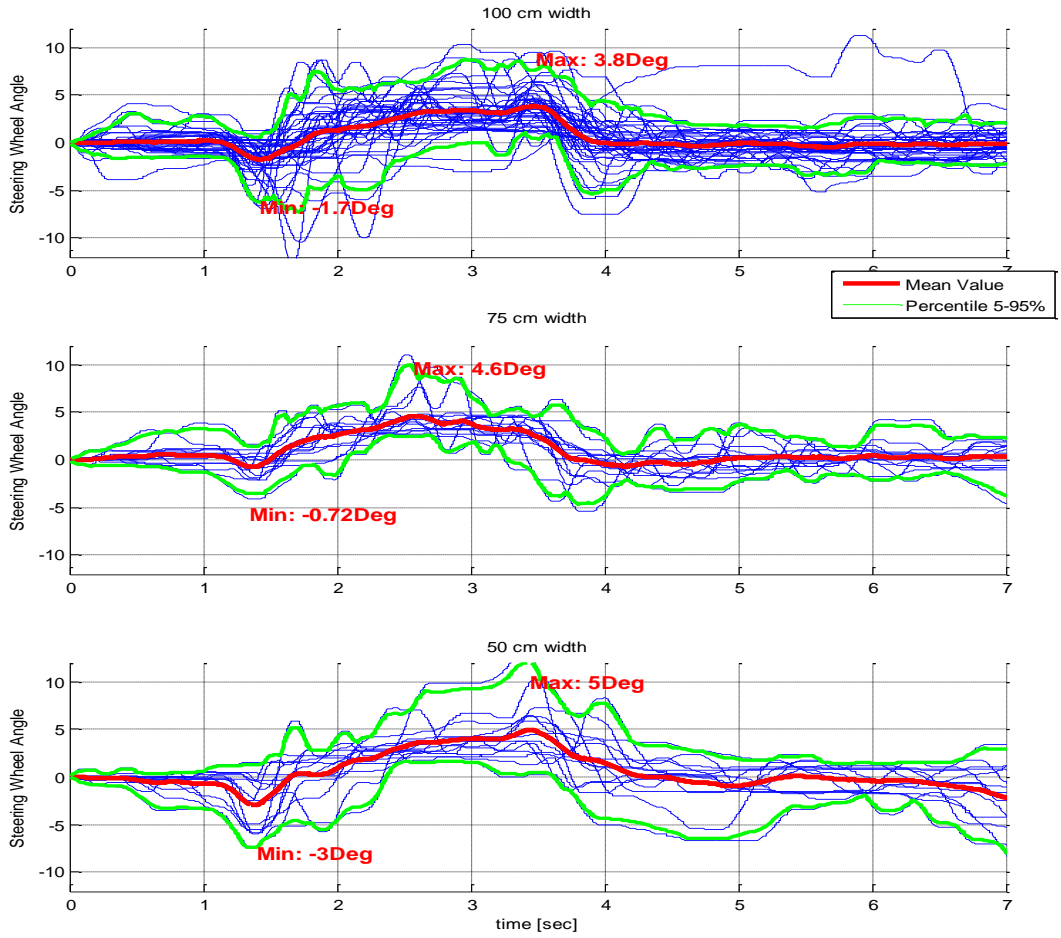


*Data from track-testing: Driver's reaction to the same<sup>36</sup> intervention often have significant differences. The 1<sup>st</sup> tests, when the driver is unaware usually gives the results needed.*

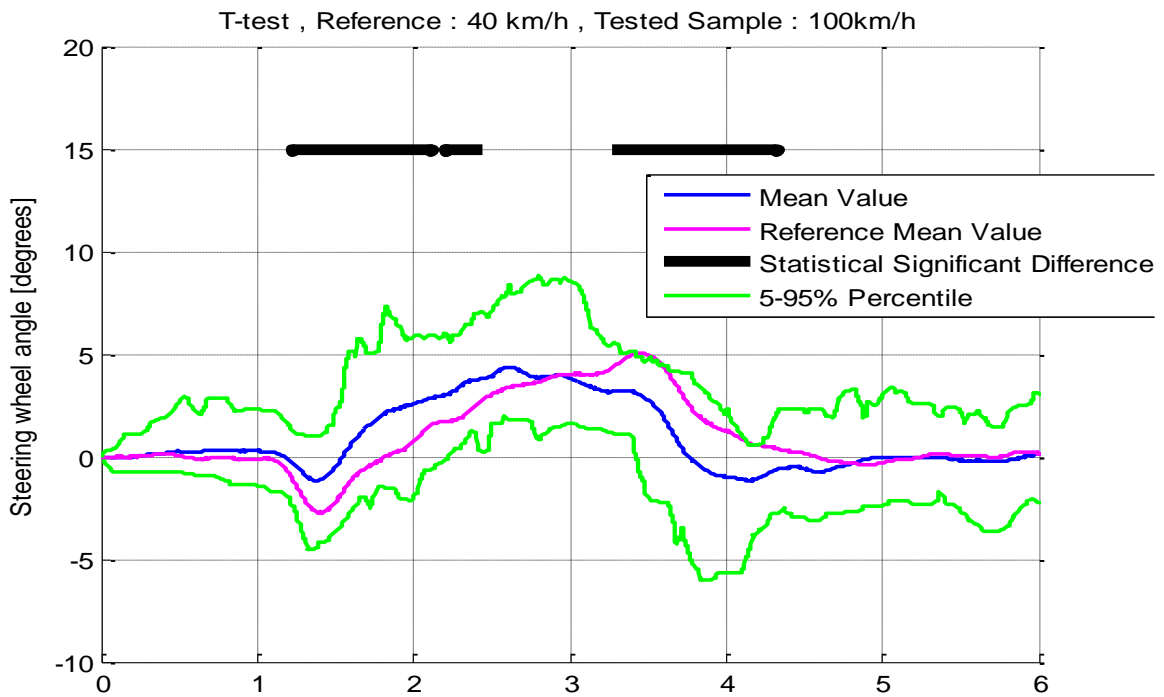
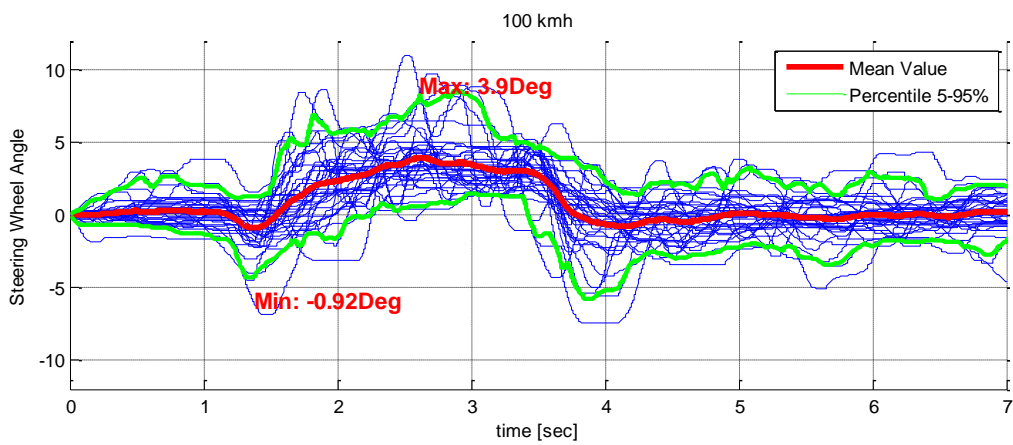
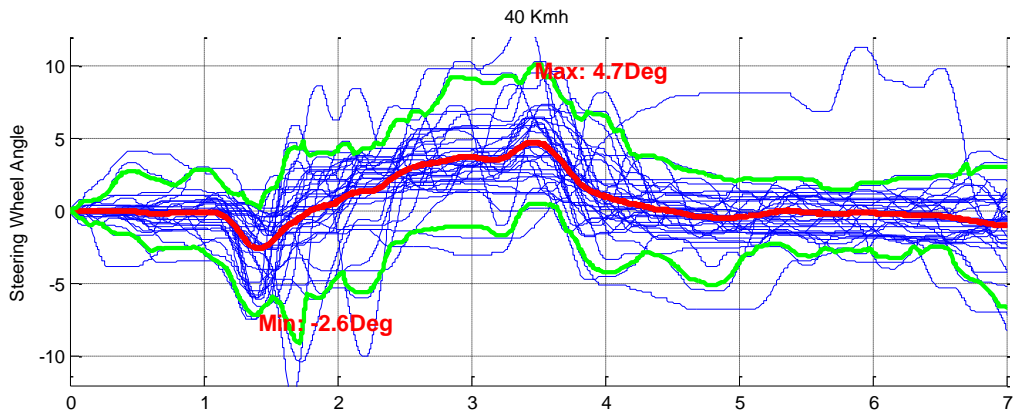


<sup>36</sup> Each test was performed at least 2 times, this helped us to evaluate the consistency of the drivers as well as have more test runs, which leads to better statistical results.

**Data from track-testing: Driver's reaction according to the width of the road**



**Data from track-testing: Driver's reaction according to the vehicle speed**



*Data from track-testing: this figure shows how different drivers react to the exact same torque intervention.*

